A MAJOR PROJECT REPORT ON

SIMULATION OF FLOW AND HEAT TRANSFER IN A CHANNEL WITH RECTANGULAR VORTEX GENERATORS AT DIFFERENT REYONALD NUMBERS AND BLADE ANGLES

Submitted in partial fulfillment of the requirement

For the award of the degree of

Master of Technology

In

Thermal Engineering

Submitted By

MANISH KUMAR

Roll No. 2K12/THR/27

Session 2012-15

Under the guidance of

Dr. RAJESH KUMAR

Associate professor

Department Of Mechanical Engineering

Delhi Technological University

BawanaRoad, Delhi-110042

CERTIFICATE

It is certified that Manish Kumar, Roll No. 2K12/THR/27, student of M.Tech. Mechanical Engineering, Delhi Technological University, has submitted the Minor Report on titled "**Simulation Of Flow And Heat Transfer In A Channel With Rectangular Vortex Generators At Different Reyonald Numbers And Blade Angles"** under our guidance towards the partial fulfillment of the requirements for the award of the degree of Master of Technology.

His work is found to be satisfactory and his discipline impeccable during the course of the project. His enthusiasm, attitude, towards the project is appreciated.

Dr.RAJESH KUMAR
Associate Professor
DEPARTMENT OF MECHANICAL ENGINEERING
DELHI TECHNOLOGICAL UNIVERSITY, DELHI

CANDIDATE'S DECLARATION

I hereby declare that the work which is being presented in this project report entitled**"Simulation Of Flow And Heat Transfer In A Channel With Rectangular Vortex Generators At Different Reyonald Numbers And Blade Angles"**submitted as minor project report towards the fulfilment of the requirements for the award of the degree of Master of Technology with specialization in Thermal Engineering, D.T.U. Delhi, is an authentic record of my own work carried out under the supervision of***Dr. Rajesh Kumar*** Mechanical Engineering Department, at Delhi technological university, Delhi.

The matter embodied in this dissertation report has not been submitted by me for the award of any other degree.

Manish Kumar

2K12/THR/27

ACKNOWLEDGEMENT

Generally, individuals set aims but more often than not, their conquest are by the efforts of not just one but many determined people. This complete project could be accomplished because of contribution of a number of people. I take it as a privilege to appreciate and acknowledge the efforts of all those who have, directly or indirectly, helped me achieving my aim.

I wish to express my deep sense of gratitude and veneration to my project guide, **Dr. Rajesh Kumar**, Department of Mechanical Engineering, Delhi Technological University, Delhi for their perpetual encouragement, constant guidance, valuable suggestions and continued motivation which has enabled me to complete this work.I also give my heartily thanks to **Prof. Naveen Kumar**,Head of Department of Mechanical Engineering, DTU and all the concerned faculty members of Department of Mechanical Engineering, Delhi Technological university for their kind help and valuable suggestions during the entire project

My special acknowledgement also goes to my family. They helped me in my project work and constantly encouraged me. Finally I pay my gratitude to all those who have directly or indirectly helped me in my project. Thank you all for your support.

Manish Kumar

2K12/THR/27

Contents

List of Figures

List of Tables

Nomenclature

a	=	Distance between the longitudinal vortex generators (m)
A	=	Cross section area of the channel (m^2)
B	=	Width of the channel (m)
c_p	=	Specific heat of the fluid (J/kg.K)
H	=	Height of the channel (m)
H_d	=	Hydraulic diameter of the channel (m)
h	=	Local heat transfer coefficient (W/m^2 K)
h_{avg}	=	Average heat transfer coefficient(W/m^2 K)
k	=	Thermal conductivity of the fluid (W/m.K)
L	=	Length of the channel (m)
LVG	=	Longitudinal vortex generator
$\dot{m}$	=	Mass flow rate of the fluid
Nu	=	Span wise averaged Nusselt number.
Pr	=	Prendtl number.
q_{avg}''	=	Average heat flux from the bottom wall(W/m^2)
Re	=	Reynolds number
T	=	Temperature of the fluid (K)
Ts	=	Local surface temperature of the bottom wall (K)
T_m	=	Bulk mean temperature of the fluid entering the cross section (K)
u_m	=	Mean velocity across the cross section.
V	=	Velocity of the fluid (m/s)
ρ	=	Density of the fluid (m^3/kg).
μ	=	Dynamic viscosity of the fluid (kg/ m.s).

α	=	Thermal diffusivity of the fluid ($k/ \rho.C_p$)
β	=	Angle between the axis of the rectangular channel and axis of the LVG (in degree)
υ	=	Kinematic viscosity of the fluid (m^2/s)
u	=	velocity in stream wise direction.
*	=	Non dimensional velocity in x direction
v	=	velocity in y direction
*	=	Non dimensional velocity in y direction
w	=	velocity in z direction
*	=	Non dimensional velocity in z direction

Chapter 1

Introduction

1.1 Introduction

The compact heat exchanger is widely used in fields such as automobile industry, heating and air conditioning, power system, chemical engineering, electronic chip cooling and aerospace, etc. The subject of heat transfer enhancement is of significant interest in developing compact heat exchanger to meet the desire of high efficiency and low cost with the volume as small as possible and the weight as light as possible.

The use of ribs/baffles placing in the cooling channels or channel heat exchangers is one of the commonly used passive heat transfer enhancement technique in single-phase internal flows. Periodically positioned ribs/baffles in the channels interrupt hydrodynamic and thermal boundary layers. Downstream of each rib/baffle the flow separates, recalculates, and impinges on the channel wall and these effects are the main reasons for heat transfer enhancement in such channels. The use of ribs/baffles increases not only the heat transfer rate but also substantial the pressure loss. The rib/baffle geometry and arrangement in the channel also alter the flow field resulting in different convective heat transfer distribution. In particular, the angled ribs, the rib cross-section, the rib-to-channel height ratio and the rib pitch-to-height ratio are all parameters that influence both the convective heat transfer coefficient and the overall thermal performance. It is, thus, difficult to realize the advantage of rib/baffle arrangements or geometry and the use of staggered ribs/ baffles with rib height and pitch spacing of 0.1 (0.5 for baffles) and 1 time of the channel height respectively is often recommended in most of the previous work.

The vortex generator (VG) can be regarded as a special kind of extended surface, which can be stamped on or punched out from the fin. A large amount of investigations have been carried out

in this area since 1960s .Although the heat transfer surface area may not be changed before and after the setup of VG, the fluid flow can be strongly disturbed because of the generation of vortex when fluid flows over it. In the conventional point of view, vortex generator not only disturbs the flow field, disrupts the growth of the boundary layer, but also makes fluid swirl and causes a heavy exchange of core and wall fluid, leading to the enhancement of heat transfer. The vortex may be divided into transverse vortex (TV) and longitudinal vortex (LV) according to its rotating axis direction. The axes of TVs lie perpendicular to the main flow direction, while LVs have their axes parallel to the main flow direction, thus they are also called stream wise vortices. In general, the LVs have been reported to be more efficient than TVs for heat transfer enhancement.

There are completely different strategies for heat exchange enhancement: active vortex methodology and passive vortex methodology. The active vortex methodology is employed to actively management the secondary flow and pressure drop therefore on meet the specified heat transfer rates even at the value of growing pumping power. There's very little far-famed use of this methodology in heat exchangers since the disbursement is incredibly high. some samples of active vortex methodology are the utilization of jets at completely different angles from the heat transfer surface into the physical phenomenon, and also the generation of a secondary flow through acoustic excitation, and Electro hydrokinetics (EHD) that is the method of manufacturing an electrical field to make electric body force within the flow. Passive vortex method is that where for heat exchange enhancement the longitudinal or latitudinal vortex generators are used. There are kinds of vortex generators are Delta wing, rectangular wing, delta winglet, rectangular winglet, quadrangle delta wing, mark surfaces, ribs, and fins. A good deal of analysis has been done mistreatment this methodology since it's economical and has maintenance

and disbursement in two heat exchangers. During this study, the utilization of passive vortex devices and it's in depth use in heat exchangers for warmth transfer improvement is delineated. Vortex generator is a kind of passive heat transfer enhancing device which is attached to the duct walls or fin surfaces and protrudes into the flow at an angle of attack to the flow direction. The basic principle of vortex generators (VGs) is to induce secondary flow, particularly longitudinal vortices, which disturb or cut off the thermal boundary layer developed along the wall and remove the heat from the wall to the core of the flow by means of large-scale turbulence. The use of ribs/baffles placing in the cooling channels or channel heat exchangers is one of the commonly used passive heat transfer enhancement technique in single-phase internal flows. The vortex generators in this study are placed at angle of 15°, 30° and 45° in a rectangular channel. Vortices are creating the down wash wave into the down face of the wall while up face wave is going in opposite direction from the wall, which we will found the outside of the vortices. Side by side the downstream direction, the velocity of the other vectors is decreasing as the distance is increasing in vortex core. In between the two vortexes thin layer of thermal boundary is occurring.

CFU stands for Common Flow Up. If we talking about the CFU Configuration we can see the distance between the leading edges of winglet pair is far more than if we compare it with trailing edges. The right winglet of vortex is always working as clockwise on the other hand the left one is rotates in anticlockwise. As we mentioned above "Vortices are creating the down wash wave into the bottom face of the wale while up face wave is going in opposite direction from the wall, which we will found the outside of the vortices. Side by side the downstream direction, the velocity of the other vectors is decreasing as the distance is increasing in vortex core" so we can say that interaction between the anticlockwise vortex is increasing regularly.

When the flow goes downwards then in CFU core of vortex also goes to upper level from lower level. We can find a thin layer of thermal boundary is available on the outer region of vortices. It makes two prominent vortexes as some form of patterns, those patterns are created because the pressure on top wings surface is much less compared to the bottom to top. So, therefore the flow adjacent to the leading edge gives rise to curls around the leading edge from bottom to top. This is also known as Primary Vortex, it is running throughout the length if and only if the leading edges are sharp enough, and it separates the flow.

1.2 Layout of the thesis

The subsequent chapters of the dissertation have been organized in the following manner. Chapter-2 of the thesis provides an extensive review of the literature in the field of heat transfer enhancement and flow analysis by the application of vortex generators. Chapter-3 provides the basic information of CFD like introduction, pre & post processing, meshing, setup, governing equations, method of solution, SIMPLE algorithm and turbulence models. The problem definition is explained in Chapter-4 with complete details regarding the geometry, mesh generation, fluent set up and boundary conditions used to obtain the numerical solution is given here. Chapter-5 provides the results for the case of rectangular vortex generators for the four Reynolds number based upon channel height at 3 different blade angles. Finally Chapter-6 contains the conclusions of the present work besides scope for future work in this area.

Chapter 2

Literature review

An important mechanism is in steady flow by swirl or vortex generation is heat exchange enhancement. In addition to differentiate the both effects from each other the flow must be steady otherwise we can't separate swirl effect from the destabilization effect. Because of separation of flow, the vortices are generated. Schuauer and Spangenberg are the first one who told the first what is the use of longitudinal vortex in 1960 and from then research on LVG's has been increased day by day. In 1992 Triggelback et al was established a rectangular channel and he proved that a set of delta winglet was always performed better than set of rectangular winglets at much higher angle of attack and Reynolds number. In 1996 Feibig et al is the first person that showed the performance of delta pair wings and winglets and rectangular wings and winglets in a flat plate and channel flow. In 1997 two friends namely Gentry and Jacobi showed about the characteristics of heat transfer enhancement of delta wing vortex generator in a flat plate channel flow. In this view they proved by showed result that average of heat enhanced by 50-60 percent foe a laminar flow. In 2007 Sohankar proved that if we increased the no of Reynolds that will automatically increasing vortex strength. In 2009. In 2009 Tian et al was successfully compared delta winglet pair with rectangular winglet pair for common flow up and down configuration and also proved that the delta winglet pair in common flow down configuration is better that any other configuration that are using that time. They conjointly mentioned that the Nusselt range for rectangular winglet pairs affects more than delta winglet pairs for various configurations and also conjointly showed that the friction issue for RWP is above that of DWP.

Wu et al.[2005] numerically studied the impact of punched delta winglet pairs at totally different attack angles in a very rectangular channel. They showed the typical heat transfer of either side of the channel will increase with a rise in Sir Joshua Reynolds range and angle of attack. For overall thickness for a RWP with or while not punched holes, shows a lower average Nusselt range than within the case of zero thickness. They showed that the upper Nusselt range is found in a very rectangular channel with holes and without holes however the friction issue is higher, too. They also showed that an attack angle of 45˚ is more effective than 15˚, 30˚, 60˚, and 90˚ and the pressure drop also increases with the increase in angle of attack. Another study, each experimental and numerical, by Shanghai dialect et al. [2008] shows that heat transfer sweetening in a very rectangular channel decreases with the rise of LVG's location from the channel recess and with the decrease in cross area between the LVG combine. They conjointly showed that with a rise in space, each heat transfer sweetening and pressure loss can increase, at a hard and fast space of LVG. Properly increasing the length and decreasing the peak could be a sensible plan to induce additional heat transfer sweetening and to stop important flow loss. it had been all over that DWP, that is 0.5 the channel height, offers higher results than DWP with height capable channel height. Hiravennavar et al. [2007] established that a DWP of finite thickness performs higher than a DWP with zero thickness. Ferrouillat et al. [2006] showed that the delta winglet combine and rectangular winglet combine of finite thickness each facilitate in heat transfer however the delta winglet combine is additional economical. They conjointly showed that the gap between 2 vortex generator rows ought to be seven to 10 times the channel height. Wang et al. [2007] by experimentation showed that LVG's on aspect each side either side} is best than on only 1 side in a very rectangular channel. Deb et al. Also, flow uses less procedure time and storage than low Re close to wall models.

Yang et al. [2001] accurately for seen the vortex characteristics and given results that were fairly near the experimental results for a combine of DWP in a very rectangular channel for a flow. Kim and Patel [1994] conducted experimental and numerical studies on the interaction between the vortices. They conjointly showed that the circulation of each CFD and CFU vortices will increase with downstream flow in a very biconcave channel whereas it's not an equivalent on a flat plate or hogged surface. Zhu et al. [1995] showed that a mix of LVG's on one wall and roughness components on the opposite wall shows higher heat transfer enhancement for turbulent flows. Torii et al. [2002] showed that in a fin-tube heat exchanger, typical flow up configuration is additional effective than a typical flow down configuration. Chen et al. [2000] showed that in a finned oval tube heat exchanger, performance enhancement with increasing Re while it is less dependent with growing number of punched winglets. Chen et al. [2000] also observed that in line arrangement of punched DWP at low Re is less efficient than a staggered arrangement. Mahmood et al. [2002] by experimentation showed the flow in a channel of staggered arrays of dimples. An active vortex methodology of mistreatment jets was mentioned by Zhang et al. [1993], and therefore the methodology has been for studied as a method of active boundary layer management. The jets typically circular in form and injected with a specific skew angle, pitch, and rate equal the free stream rate. Another active vortex methodology, called EHD, depends on associate outwardly provided electric field to an electrical body force nearer to the heat transfer surface whereas directly increasing the heat transfer coefficients and, thus, increasing the performance of the system.

Zohir studied the influence of pulsation on heat transfer enrichment and all over that heat transfer improvement for counter flow is far above that of a parallel flow in homocentric double pipe heat exchangers.

Chapter 3

Computational Fluid Dynamics

3.1 Introduction

CFD is usually known as Computational Fluid Dynamics and it is a vital branch of mechanics, uses numerical strategies and algorithms to investigate and solve fluid flow problems. There are many advantages of CFD over the previous methods, it is inexpensive and involve not so much of effort. Computers are used to solve algorithms which analyze the fluid flow and define fluid nature. Now a days CFD is commonly used as there is increase in computational capabilities over time and better numerical solving methods. In a fluid flow CFD is used to solve the partial differential equation of any order. It also used in analyzing the complex flow in heat exchanger, furnace, reactors etc. It is used in many branches of engineering, like designer of vehicles to improve the aerodynamics, forecast the weather by meteorologists, to develop weapons and estimate the damage by military organization. For CFD analysis few simple steps must be followed

3.1.1 Pre-Processing and Geometry Modeling

Knowing the problem is the first step to any problem to solve. A well stated problem is give well resolved data. Pre-processing step consist of defining a geometry, which define over domain of interest. There are some geometry modeling tools like Creo Parametric, AutoCAD, Pro/ENGINEER, and Solid Works are used to create the geometry. To model the geometry in this study Creo Parametric 2.0 was used.

3.1.2 Meshing

In this step our domain of interest or (geometry) is divided into segments or elements called meshing. These segments are made up of triangles for 2D geometry and for 3D geometry. They are made up of tetrahedral or hexahedral. These are the elements over which the governing equations are approximated. The governing equation is approximated on every single element and if the mesh is not sufficiently refined then there is limited accuracy in the solution. Gambit or ANSYS workbench used for generation of elements. For getting CFD simulation FEM (Finite Element Method) is used commonly. As the governing equations are solved over separate control volume and for structural analysis of solid the FEM method is generally used. In this matter is divided into tiny element which related to each other. More memory is required by FEM, as it is more stable than FVM (Finite Volume Method). For driving the discrete equation by using Taylors series expansion is known as FDM (Finite Difference Method). For complex geometries we normally use FEM. ANSYS also used FEM (Finite Element Method).

3.1.3 Setup

When the meshing is completed the problem is setup defining the boundary condition. For a well defined problem we have to specify the proper boundary condition. Even a single wrong boundary condition gives a wrong result. So we have to define the fluid property, viscosity, operating condition at inlet and outlet. FLUENT 14.0, the most commonly used Commercial software is used to set up and solve the flow in this study.

3.1.4 Post-Processing

Once the governing equations are solved at every element various properties such as temperature, velocity, Mach number, and pressure are extracted from the results as values. we analyze them by color plots, contour plots, graphical representation and generate reports also. By improving the mesh quality we can increase the accuracy of result. Para view, ANSYS CFD-Post etc. are some post processing software used.

3.2 Governing Equations

For a viscous, heat conducting fluid the **Navier-Stokes equations** are the basic governing **equations,** for simulation of CFD problems it plays a very important role. When Newton's second law is applied to fluid motion these equation comes. These Partial differential equations based on the conservation law which define mass, momentum, and energy flow conservation. The flow in the rectangular channel is considered laminar, incompressible, and steady state. The N-S equations are shown in the simplest form. The following assumptions were made,

1. It is a steady flow. Thus, this study does not depend on the time.
2. The fluid has constant density and viscosity which means it is incompressible ρ = constant. Thus, the thermal changes that occur in the fluid because of constant density are neglected in this study.
3. The only velocity component at inlet is in the direction of the flow, u = V. Thus, v = w = 0.
4. Gravity is neglected in this study and the thermal changes due to gravity are very small which are also neglected, and

5. The wall has non slip conditions. The velocity is zero at contact with the wall, thus u = 0 at the wall.

The following scales and non-dimensional variables are used,

$$u^* = \frac{u}{U}$$

$$v^* = \frac{v}{U}$$

$$p^* = \frac{p}{\rho U^2}$$

$$x^* = \frac{x}{L}$$

$$y^* = \frac{y}{L}$$

$$t^* = \frac{t}{L/U}$$

$$Re = \frac{\rho U L}{\mu}$$

The continuity equation in a non-dimensional form for a steady state flow is given by,

$$\frac{\partial u^*}{\partial x^*} + \frac{\partial v^*}{\partial y^*} = 0$$

The momentum equation in a non-dimensional form for a steady state flow is given by,

$$u^* \frac{\partial u^*}{\partial x^*} + v^* \frac{\partial u^*}{\partial y^*} + \frac{\partial p^*}{\partial x^*} = \frac{1}{Re}\left(\frac{\partial^2 u^*}{\partial x^{*2}} + \frac{\partial^2 u^*}{\partial y^{*2}}\right)$$

$$u^* \frac{\partial v^*}{\partial x^*} + v^* \frac{\partial v^*}{\partial y^*} + \frac{\partial p^*}{\partial y^*} = \frac{1}{Re}\left(\frac{\partial^2 v^*}{\partial x^{*2}} + \frac{\partial^2 v^*}{\partial y^{*2}}\right)$$

$$* \frac{*}{*} + \frac{*}{*} + * \frac{*}{*} + \frac{*}{*} = \frac{1}{*^2}\left(\frac{2*}{*} + \frac{2*}{*} + \frac{2*}{*}\right)$$

The energy equation in a non-dimensional form for a steady state flow is given by,

$$\frac{(**)}{*} + \frac{(**)}{*} + \frac{(**)}{*} + \frac{*}{*} = \frac{1}{(*^2 + *^2 + *^2)}\left(\frac{2*}{} + \frac{2*}{} + \frac{2*}{}\right)$$

3.3 Finite volume method

The Finite Volume Method (FVM) is one of the most versatile discretization techniques used in CFD. Based on the control volume formulation of analytical fluid dynamics, the first step in the FVM is to divide the domain into a number of control volumes (cells, elements) where the variable of interest is located at the centroid of the control volume. The next step is to integrate the differential form of the governing equations (very similar to the control volume approach) over each control volume. Interpolation profiles are then assumed in order to describe the variation of the concerned variable between cell centroids. The resulting equation is called the discretized equation. In this manner, the discretized equation expresses the conservation principle for the variable inside the control volume.

The most compelling feature of the FVM is that the resulting solution satisfies the conservation of quantities such as mass, momentum, energy, and species. This is exactly satisfied for any control volume as well as for the whole computational domain and for any number of control volumes. Even a coarse grid solution exhibits exact integral balances.

3.4 Second-Order Upwind Scheme

When second-order accuracy is desired, quantities at cell faces are computed using a multi dimensional linear reconstruction approach. In this approach, higher-order accuracy is achieved at cell faces through a Taylor series expansion of the cell-centered solution about the cell centroid. Thus when second-order unwinding is selected, the face value φ_f is computed using the following expression:

$$, \quad = \quad + \quad . \vec{}$$

Where and are the cell-centered value and its gradient in the upstream cell, and $\vec{}$ is the displacement vector from the upstream cell centroid to the face centroid. This formulation requires the determination of the gradient in each cell.

3.5 Discretised Equations for Solution Algorithm

It is common practice to subdivide the computational domain into number of sub domains or elements such that separate profile assumption can be made with each sub domain. In order to solve the non- linearity associated with fluid flow and energy equations the pressure-velocity linkage can be resolved by adopting an iterative solution strategy such as SIMPLE / SIMPLEC algorithm. A guessed pressure field is used to solve the momentum equation and pressure correction equation field which is in turn used to update the velocity and pressure field. To start the iteration process we use initial guess for velocity and pressure fields. As the algorithm proceeds our aim is to progressively to improve these guessed fields. The process is iterated until the convergence of velocity and pressure fields are obtained**.**

The discretised momentum equations in x direction:

$$a_{i,J}\, u_{i,J} = \sum a_{nb}\, u_{nb} + \left(P_{I-1,J} - P_{I,J}\right) A_{i,J} + b_{i,J} \qquad (3.1)$$

The discretised momentum equation for y direction

$$a_{I,j} v_{I,j} = \sum a_{nb} v_{nb} + (P_{I,J-1} - P_{I,J}) A_{I,j} + b_{I,j} \tag{3.2}$$

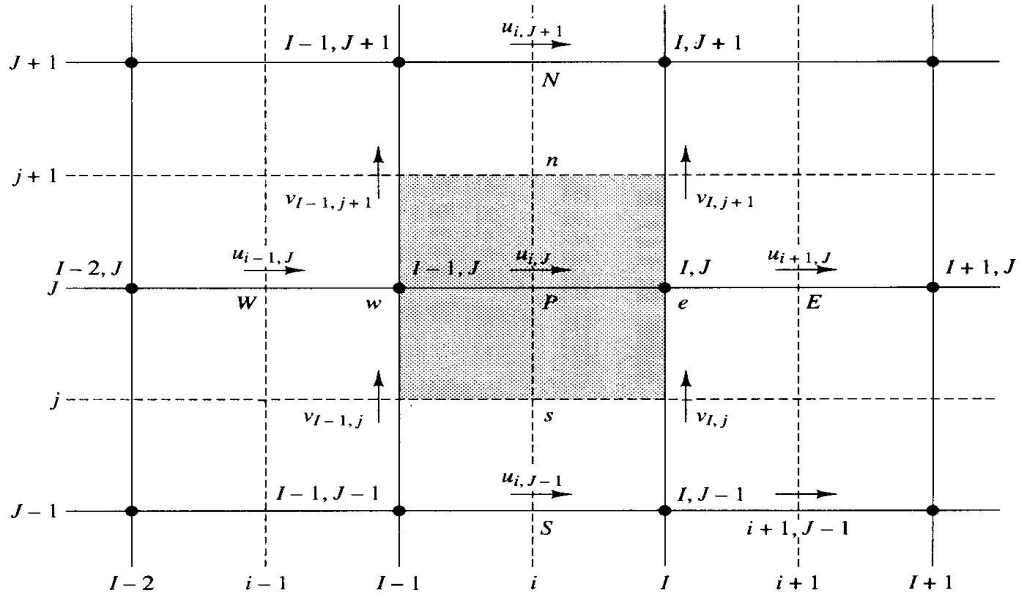

Fig 3.1 Grid Arrangement for Flow Calculation in Two Dimensions

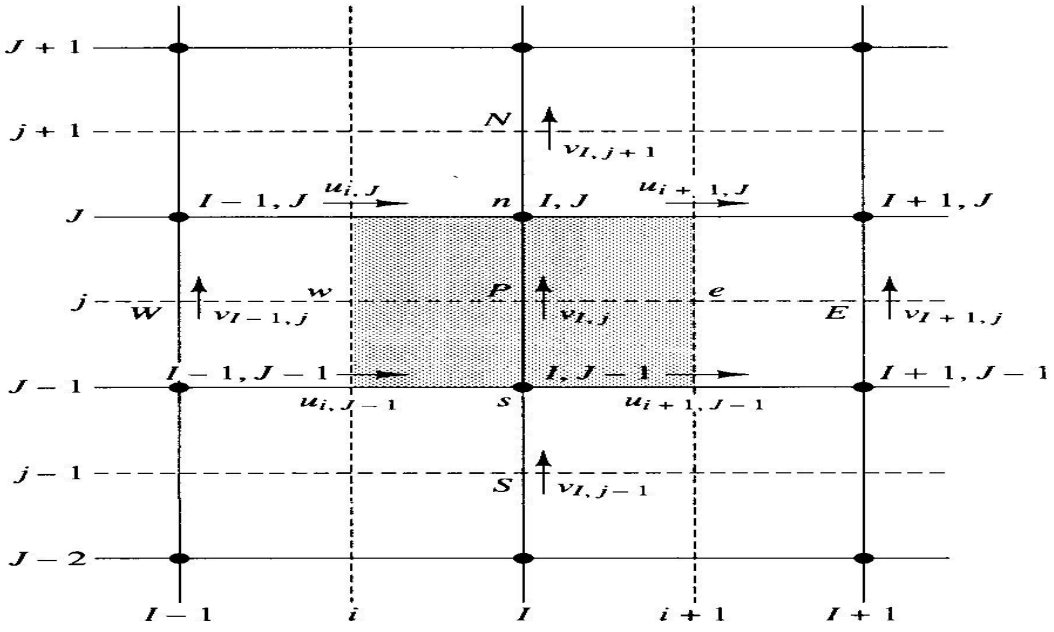

Fig 3.2 Control Volume and Its Neighbouring Velocity Components

3.6 The SIMPLE Algorithm

The SIMPLE algorithm stands for Semi–implicit Method for Pressure Linked Equations. This is essentially a guess and correct procedure for the calculation of pressure on staggered grid for the discretised momentum equations. This pressure-velocity Coupling algorithm uses a relationship between velocity and pressure corrections to enforce mass conservation and to obtain the pressure field.

$$a_{i,J}\,u_{i,J} = \sum a_{nb}\,u_{nb} + \left(P_{I-1,J} - P_{I,J}\right)A_{i,J} + b_{i,J}$$

This method can be explained with the two dimensional steady state laminar flow equations. The guessed pressure for the above equations is p* while the velocities are u* and v* as follows.

$$a_{i,J}\,u^*_{i,J} = \sum a_{nb}u^*_{nb} + \left(P^*_{I-1,J} - P^*_{I,J}\right)A_{i,J} + b_{i,J}$$

(3.3)

$$a_{I,j}\,v^*_{I,j} = \sum a_{nb}v^*_{nb} + \left(P^*_{I,J-1} - P^*_{I,J}\right)A_{I,j} + b_{I,j} \qquad (3.4)$$

Now the correction $'$, $'$ and $'$ may be introduced as (correction formulae)

$$p = p^* + p' \qquad (3.5)$$

$$u = u^* + u' \qquad (3.6)$$

$$v = v^* + v' \qquad (3.7)$$

Where P=correct pressure field and * is =guessed pressure field.

substitution of correct pressure field p into momentum equations yield correct velocity field.

Subtraction of equations (3.1) and (3.2) from (3.3) and (3.4) respectively would give us

$$a_{i,J}\left(u_{i,J} - u^*_{i,J}\right) = \sum a_{nb}\left(u_{nb} - u_{nb}^*\right) + \left[\left(p_{I-1,J} - p^*_{I-1,J}\right) - \left(p_{I,J} - p^*_{I,J}\right)\right]A_{i,J} \qquad (3.8)$$

$$a_{i,J}\left(v_{i,J}-v^{*}_{i,J}\right)=\sum a_{nb}\left(v_{nb}-v^{*}_{nb}\right)+\left[\left(p_{I,J-1}-p^{*}_{I,J-1}\right)-\left(p_{I,J}-p^{*}_{I,J}\right)\right]A_{I,j} \quad (3.9)$$

Using correction formulas the equation (4.8) and (4.9) may be written as:

$$a_{i,J}\,u'_{i,J}=\sum a_{nb}u'_{nb}+\left(p'_{I-1,J}-p'_{I,J}\right)A_{i,J} \quad (3.10)$$

$$a_{i,j}\,v'_{i,j}=\sum a_{nb}\,v'_{nb}+\left(p'_{I,J-1}-p'_{I,J}\right)A_{I,j} \quad (3.11)$$

In order to simplify the above equations the two approximations

$$\sum a_{nb}u'_{nb} \quad and \quad \sum a_{nb}v'_{nb}$$

are dropped. The omissions of these terms are the main approximations of SIMPLE algorithm. We obtained

$$u'_{i,J}=d_{i,J}\left(p'_{I-1,J}-p'_{I,J}\right) \quad (3.12)$$

$$v'_{I,j}=d_{I,j}\left(p'_{I,J-1}-p'_{I,J}\right) \quad (3.13)$$

Where , = —— and , = ——

So far we have considered momentum equations but velocity field also subjected to constraint that it should also satisfy continuity equations. The continuity equation for the control volume is

$$(\rho uA)_{i+1,J}-(\rho uA)_{i,J}+(\rho vA)_{I,j+1}-(\rho vA)_{I,j}=0 \quad (3.14)$$

Substitution of corrected velocities of equations into discretised continuity equations gives:

$$\left[\rho_{i+1,J}A_{i+1,J}\left(u^{*}_{i+1,J}+d_{i+1,J}\left(p'_{I,J}-p'_{I+1,J}\right)\right)-\rho_{i,J}A_{i,J}\left(u^{*}_{i,J}+d_{i,J}\left(p'_{I-1,J}-p'_{I,J}\right)\right)\right]+\left[\rho_{I,j+1}A_{i,J+1}\left(v^{*}_{I,j+1}+d_{I,j+1}\left(p'_{I,J}-p'_{I,J+1}\right)\right)-\rho_{I,j}A^{*}_{I,j}\left(v^{*}_{I,j}+d_{I,j}\left(p'_{I,J-1}-p'_{I,J}\right)\right)\right]=0$$

(3.15)

Identifying the coefficient of p' it may be written as

$$a_{I,J}\,p'_{I,J} = a_{I+1,J}\,p'_{I+1,J} + a_{I-1,J}\,p'_{I-1,J} + a_{I,J+1}\,p'_{I,J+1} + a_{I,J-1}\,p'_{I,J-1} + b'_{I,J} \tag{3.16}$$

Where

$a_{I+1,J}$	$a_{I-1,J}$	$a_{I,J+1}$	$a_{I,J-1}$	$b'_{I,J}$
$(\rho dA)_{i+1,J}$	$(\rho dA)_{i,J}$	$(\rho dA)_{I,\,j+1}$	$(\rho dA)_{i,J}$	$(\rho u^* A)_{i,J} - (\rho u^* A)_{i+1,J} + (\rho v^* A)_{I,j} - (\rho v^* A)_{I,j+1}$

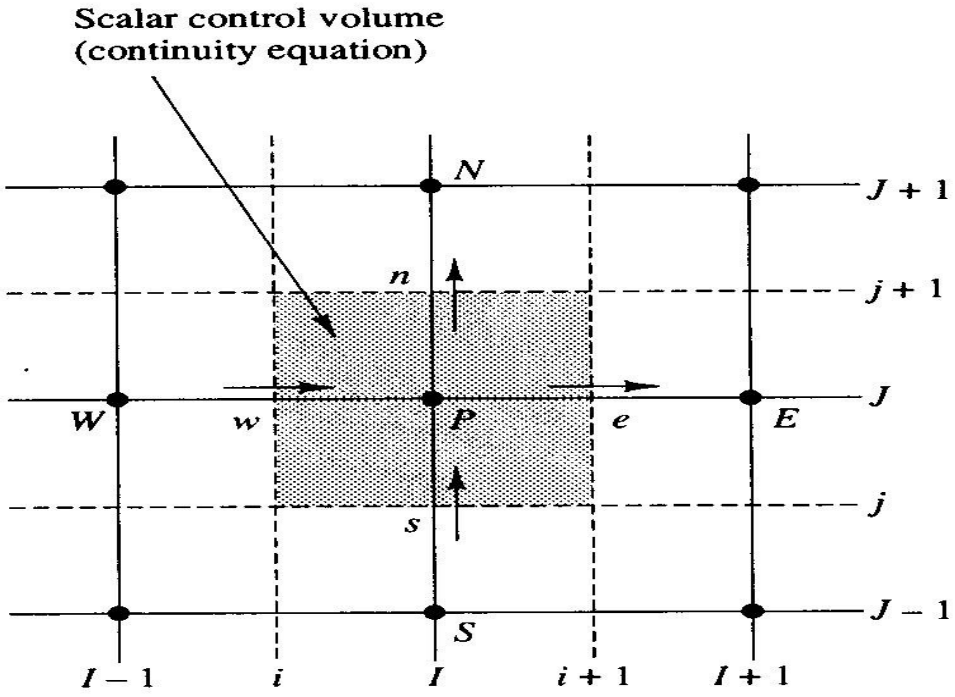

Fig 3.3 Scaler Control Volume Used For Discretisation of Continuity equation

The above equation (3.16) represents the descretised continuity equation as an equation for pressure correction p'. By solving above pressure correction equation the correct pressure field

may be known and correspondingly substitute pressure field into continuity equation would give us the correct velocity field. The omission of the terms such as $\sum a_{nb}u_{nb}'$ in the derivation does not affect much the final results. Because the pressure correction and velocity corrections will be zero in a converged solution giving p*=p and u*=u.

3.7 Sequence of Operation for the SIMPLE Algorithm

1: Guess the pressure filed p*

2: Solve the momentum equations to obtain u* and v*

3: Solve the p' equation

4: Calculate the p by adding p' to p*

5: Calculate the u and v from velocity correction formula.

6: Treat the corrected pressure p as new guessed pressure p*.return to

Step 2 and repeat the whole procedure until a converged solution is obtained.

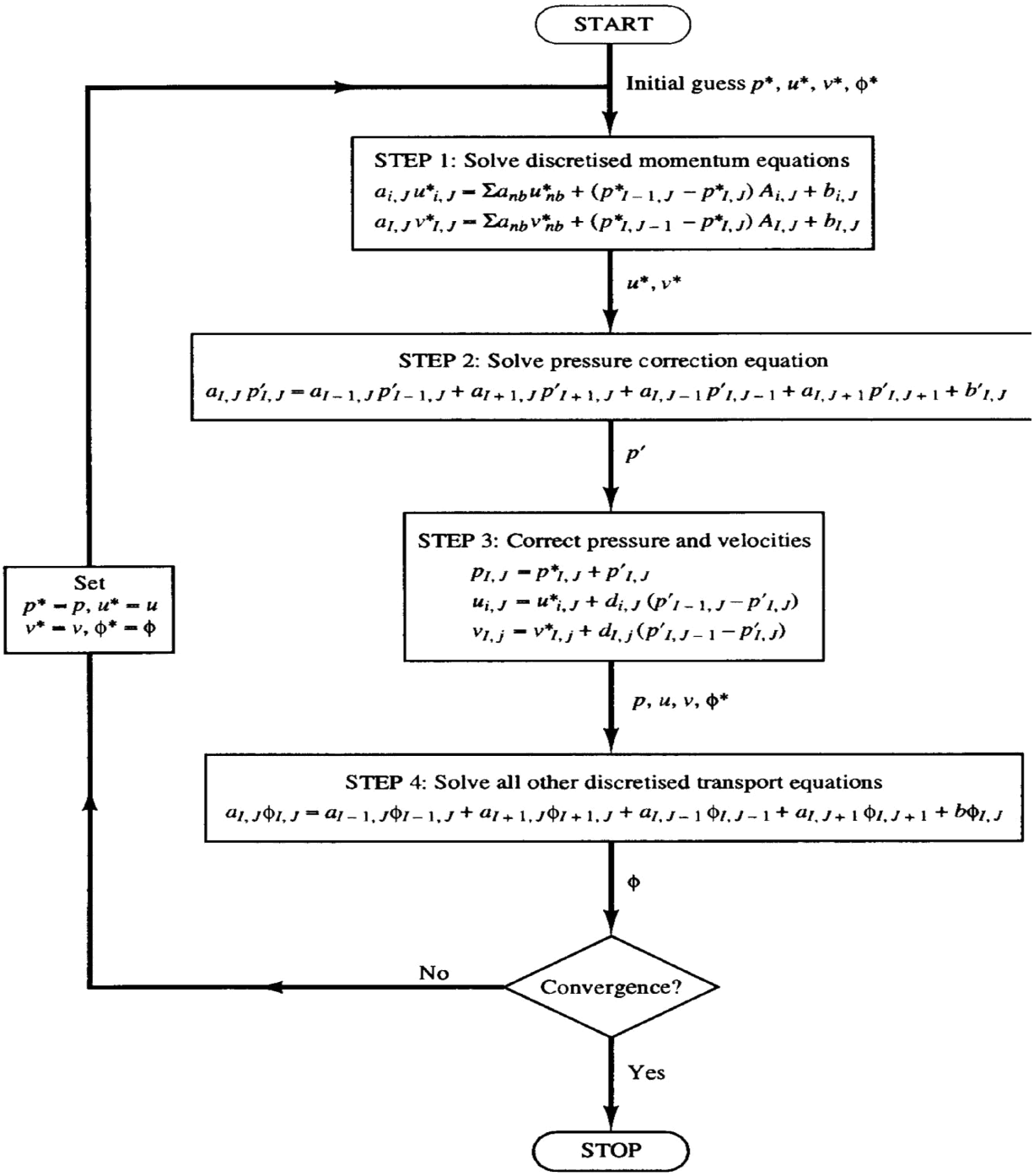

3.8 Turbulence Models

There are many models to solve the turbulent nature flow but it is an unfortunate fact that no single turbulence model is universally accepted as being superior for all classes of problems. The

choice of turbulence model will depend on considerations such as the physics encompassed in the flow, the established practice for a specific class of problem, the level of accuracy required, the available computational resources, and the amount of time available for the simulation. To make the most appropriate choice of model for your application, one needs to understand the capabilities and limitations of the various models. The turbulence model used in this simulation is Realizable *k*- Models with enhanced wall treatment.

3.9 The Reynolds- Averaged Navier Strokes Equations

For a fluid flow the RANS equations(Reynolds Averaged Naviers Strokes equations) are known as time-averaged equations. Reynolds decomposition is the major objective for this equation, in this an instantaneous quantity is decomposed into fluctuating and time averaged quantity. For turbulent flow RANS equations are commonly used by scientists. For giving approximate time-averaged solutions to the Navier-Strokes equations, we use RANS Equations and the approximation depends upon the information of properties of flow turbulence. RANS equations written in Einstein notation for stationary, incompressible Newtonian fluid:

$$\rho\bar{u}_j\frac{\partial\bar{u}_i}{\partial x_j} = \rho\bar{f}_i + \frac{\partial}{\partial x_j}\left[-\bar{p}\delta_{ij} + \mu\left(\frac{\partial\bar{u}_i}{\partial x_j} + \frac{\partial\bar{u}_j}{\partial x_i}\right) - \rho\overline{u_i'u_j'}\right].$$

The change in momentum of fluid element result unsteadiness and convection by mean flow, it is symbolized by the left hand side of equation.Reynold stress is caused by the fluctuating velocity field due to the viscous stress and apparent stress $\left(-\rho\overline{u_i'u_j'}\right)$. The mean pressure field produced by isotropic stress. There is generation of abundant turbulence model, as the non linear Reynolds stress need extra modeling so it comes near to RANS equations.

The true time average ($\bar{X}$) of a variable (x) is defined by

$$\bar{X} = \lim_{T \to \infty} \frac{1}{T} \int_{t_0}^{t_0+T} x \, dt.$$

For a study of disorder dynamical system where the equations are under turbulent condition this show that the system has one strange attractor, the Navier-Stroke equation are used to prove the result. The limit ($\bar{X}$) must be independent of the initial condition at t_0. However, assuming the limit exists (which it does for any bounded system, which fluid velocities certainly are), there exists some T such that integration from t_0 to T is arbitrarily close to the average. This means that given transient data over a sufficiently large time, the average can be numerically computed within some small error. However, there is no analytical way to obtain an upper bound on T.

The solution of the RANS equations is now used in engineering applications to predict the flow in fairly complex configurations. This approach, however, suffers from one principal shortcoming, the fact that this model must represent a very wide range of scales. While the small scales tend to depend only on viscosity, and may be somewhat universal, the large ones are affected very strongly by the boundary conditions. Thus, it does not seem possible to model the effect of the large scales of turbulence in the same way in flows that are very different.

3.10 Standard, RNG, and Realizable *k*- Models

It is a two equation model means, it includes two extra transport equations to represent the turbulent properties of the flow and consider the effects like convection and diffusion of

turbulent energy. The first transported variable is turbulent kinetic energy, *k*. The second transported variable in this case is the turbulent dissipation (ϵ). It is the variable that determines the scale of the turbulence, whereas the first variable (k) determines the energy in the turbulence. The difference in these model is based on the

(a) The method of calculating turbulent viscosity.

(b) The turbulent Prandtl numbers governing the turbulent diffusion of k and ε.

(c) The generation and destruction terms in the ε equation

It is a two equation model means, it includes two extra transport equations to represent the turbulent properties of the flow and consider the effects like convection and diffusion of turbulent energy. The first transported variable is turbulent kinetic energy, *k*. The second transported variable in this case is the turbulent dissipation (ϵ). It is the variable that determines the scale of the turbulence, whereas the first variable (k) determines the energy in the turbulence. The difference in these model is based on the

(a) The method of calculating turbulent viscosity.

(b) The turbulent Prandtl numbers governing the turbulent diffusion of k and ε.

(c) The generation and destruction terms in the ε equation

Chapter 4

Problem Definition

4.1 Introduction

This chapter, gives a complete description of the provided numerical simulation. For this model Geometric modeling, computational grid, and setup are explained. With turbulent intensity of 3 percent the calculation for flow velocity is,

$$= \frac{}{\mu}$$

where,

Re = Reynolds number, (dimensionless)

ρ = density of the fluid, (kg/m3)

V = mean velocity of fluid flow, (m/s)

H = characteristic length or Channel Height (m)

μ = dynamic viscosity of the fluid, (kg / (m·s))

Density of the water is 998.2 kg/m3 and the dynamic viscosity of water is .0010003 kg / (m·s). Ratio of kinematic viscosity to thermal diffusivity is called Prandtl number. Higher Prandtl number shows that the convective heat transfer is powerful. Prandtl number is a dimensionless number. The Prandtl number for water in this study is taken as 6.99.

$$\overline{\upsilon}$$

$$Pr = \alpha$$

Where

υ = kinematic viscosity of the fluid = μ/ρ, (m^2/s)

α = thermal diffusivity of the fluid = K/ρCp, (m2/s)

K = thermal conductivity of the fluid, (W / (m·K))

Cp = specific heat of the fluid, (J / (kg·K))

Ratio of convective heat transfer coefficient to the conductive heat transfer coefficient is called Nusselt Number. Generally in a laminar flow Nusselt Number is close to one when the magnitude of convection and conduction are similar. The Nusselt number have a constant value for completely grown internal laminar flow. The values rely upon the height of the channel.

$$= \frac{}{}$$

where,

h = heat transfer coefficient, (W / (m2·K))

H = Height of the Channel

The span wise averaged Nusselt number was calculated as follows:

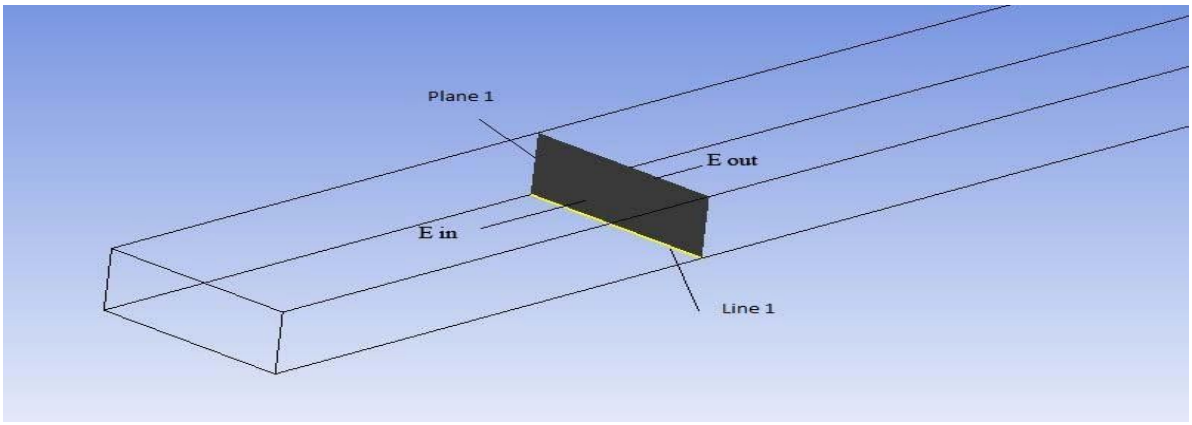

Fig. 4.1 Plane 1 and Line 1 in the channel

Total mass flow rate entering the Plane 1 shown in the fig. 4.1 is,

$\dot{} = \int$

If we assume the fluid entering the Plane 1 with some constant velocity , so

$\dot{} =$

Equating these to equations for Plane 1

$= \int$

$= \int$

Now equating the energy entering the Plane 1

$= \int$

We calculate the mean temperatureas

$= \quad \frac{\int \quad}{} \quad$

The Span wise Averaged Nusselt number at Line 1 shown in the Fig 4.1 is= $\frac{h}{}$

h , the averaged convection coefficient at Line 1 is calculated as

$''$

$= h \; (\quad - \quad)$

Where,

Ts = Bottom wall Surface Temperature.

T_m = mean temperature of fluid entering the Plane 1

So by knowing the □ along the Line 1 we can calculate the Span wise averaged Nusselt Number.

As in this study, the flow is going through a rectangular channel, the hydraulic diameter is

$$= \frac{4 * *}{\frac{}{}}$$

$$= 0.0571 \quad 4 * * = 2(+)$$

The turbulent intensity of the fluid entering the rectangular channel is taken as 3% .

Boundary conditions specify the flow and thermal variables on the boundaries of the physical model. . The computational domain uses following boundary conditions. Table 4.1 shows the boundary conditions assigned in FLUENT.

Table 4.1 Boundary Conditions

Zone	**Assigned Boundary Type**
INLET	Velocity Inlet, Inlet fluid temperature = 300K
Outlet	Pressure Outlet, 0 Pa gauge
Bottom wall	Wall (No Slip), Constant Temperature = 373 K
Top wall	Wall (No Slip), Constant Heat Flux = 0 W/m^2
Side walls	Wall (No Slip), Constant Heat Flux = 0 W/m^2
Vortex Generators	Wall (No Slip), Constant Temperature = 373 K

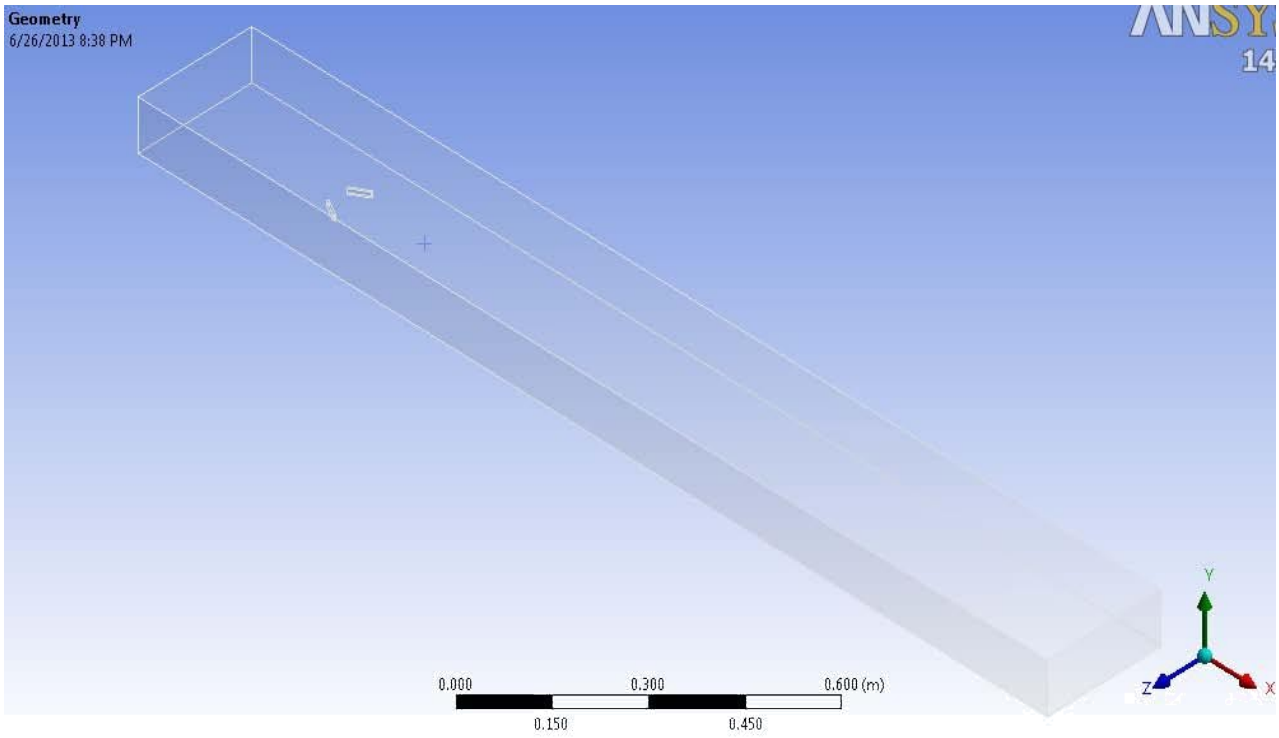

Fig. 4.2 Isometric view of the entire channel, blade angle 30°

4.2 Geometric Model

The rectangular channel has cross section dimensions of 25 cm x 10 cm. Length of the channel is 200 cm. The vortex generators have the dimensions length x breadth x height of 1cm x .4 cm x 1 cm. The blade angle for the rectangular vortex generators are taken 15°, 30°, and 45°. The bottom wall material is taken as Aluminium and the fluid flowing is water. The flow in the channel is with 3 % turbulent intensity and enters the channel with uniform constant velocity across the cross section. The backflow turbulent intensity at outlet is also taken as 3 %. The Reynolds numbers are chosen as 800, 1600, 2400 and 3200. Shown in Figure 4.2 is the isometric view of the channel along with vortex generators.

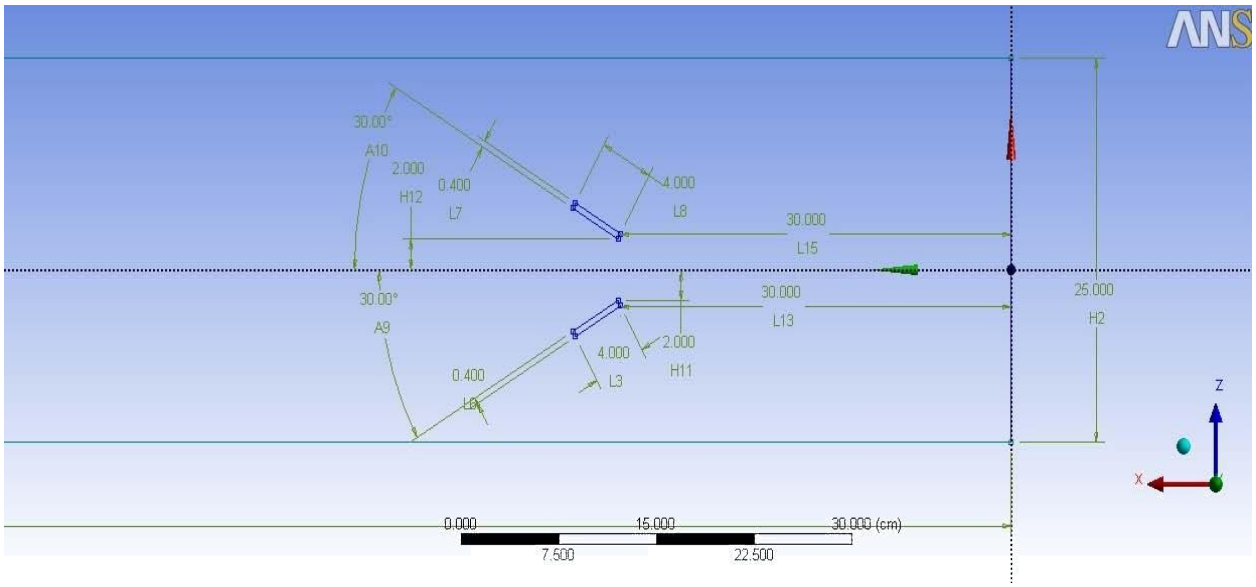

Fig. 4.3 Geometric model with blade angle 30° (dimensions in cm)

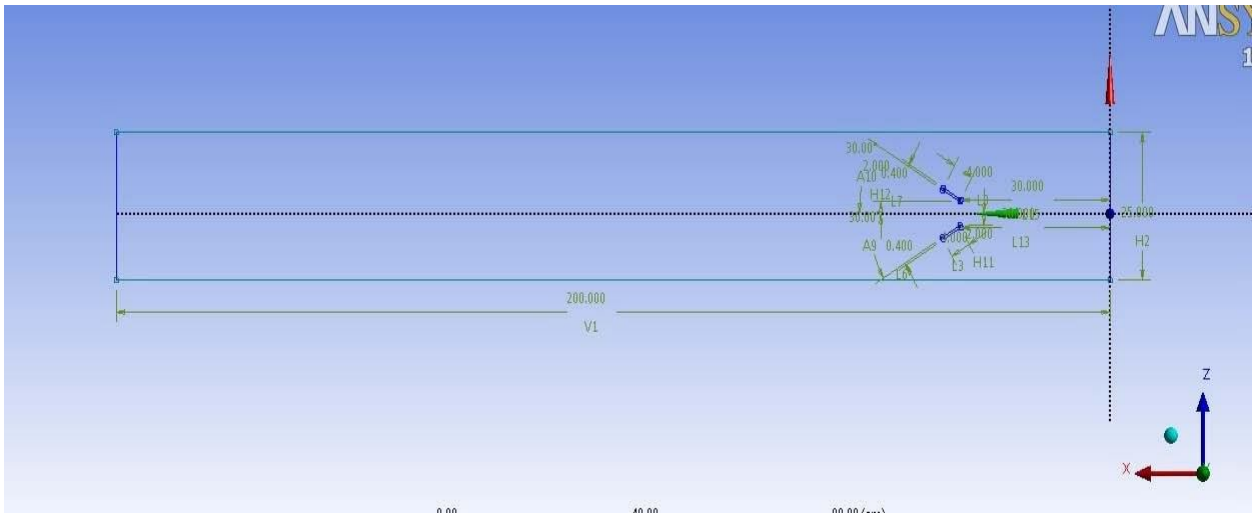

Fig. 4.4 Geometric model with blade angle 30°, complete view (dimensions in cm)

4.3 Grid Generation

In this study ANSYS Workbench was used as a meshing tool. The structured non uniform grid was generated. The fig. 4.5 shows the fine meshing near the vortex generators. Fine meshing is needed near the wall region to capture the boundary layer on the wall. The whole fluid domain

has all the elements as hexa elements. Mapped Face Meshing option from the ANSYS Workbench meshing tool was used to generate this kind of structured non uniform meshing. Bias factor of 10 was used to make the grids near the wall and the vortex generators fine to capture the boundary layer effects.

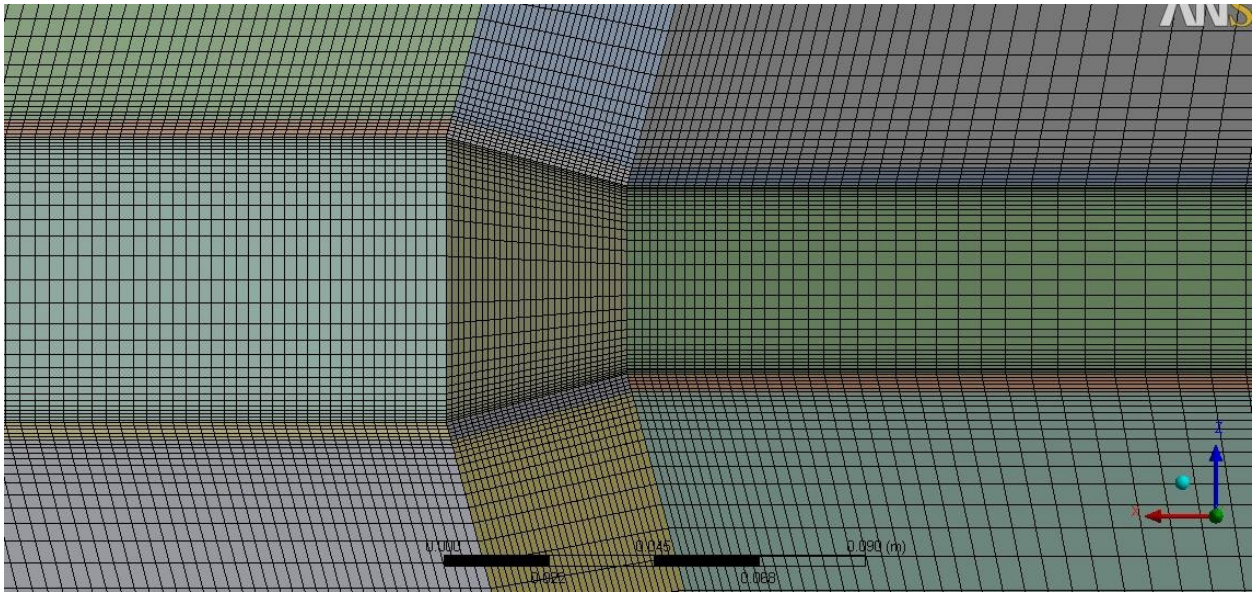

Fig. 4.5 Structured non uniform grid around the vortex generators (top wall shown)

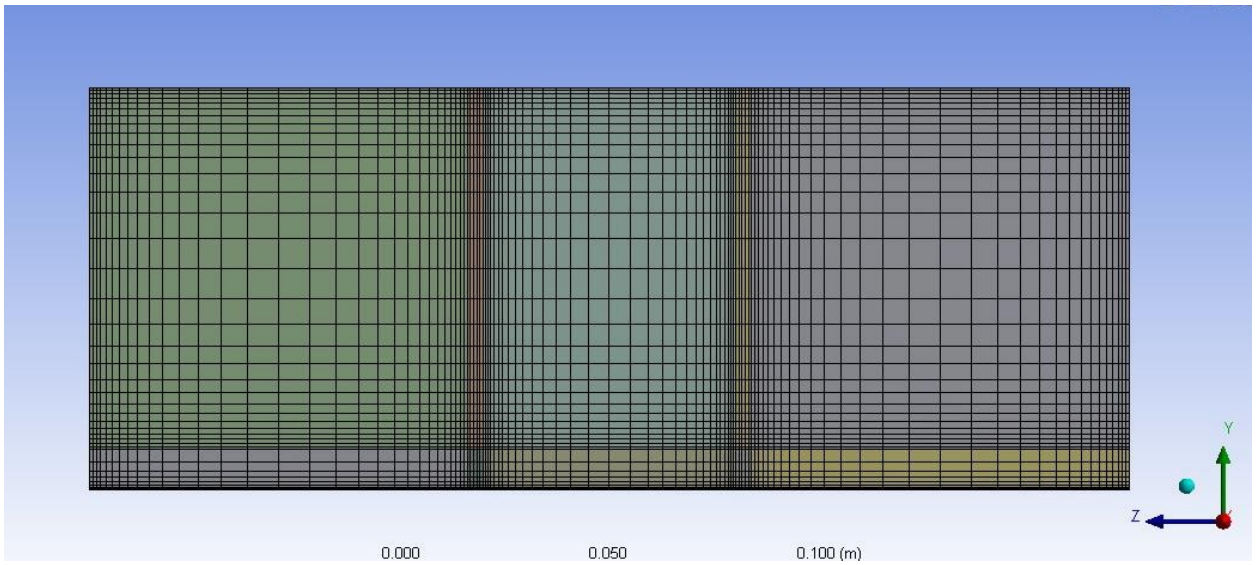

Fig. 4.6 Meshing shown at the fluid domain's rectangular cross section

Fig. 4.6 and fig. 4.7 below show the cross sectional and isometric view of the meshing. The isometric view shows the very fine meshing in the region near the vortex generators to capture the effects near the vortex generators properly.

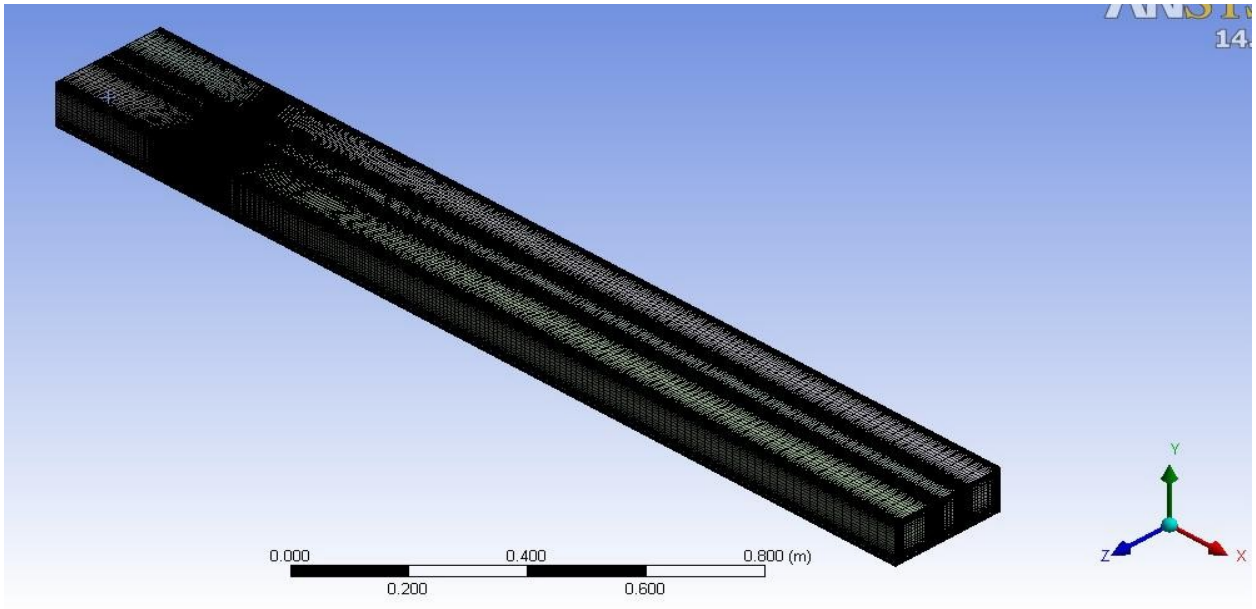

Fig. 4.7 Isometric view of the fluid domain meshing.

4.4 FLUENT Setup

For CFD analysis FLUENT 14.0 was used in study. Importing the mesh files which are created in ANSYS Workbench, the model is setup to allow energy equation in a Realizable k-Ɛ model with enhanced wall treatment. In this study the fluid used was water with thermal conductivity 0.6 W/m.K, constant density of 998.2 kg/m^3, dynamic viscosity of 0.001003 kg/m.s, and the constant pressure specific heat is 4182 J/Kg-K. On the rectangular channel including the inlet and outlet channel previously mentioned boundary conditions are applied and The operating condition on the interior of the channel is fluid. The bottom surface of the rectangular channel and all the surface of the vortex generator is the heated section to which 373 k temperature is applied. A specific velocity based on the Reynolds number corresponding to the chosen

Reynolds number and an inlet temperature of 300 K has been given to the inlet. The ambient condition is shown by outlet which has zero pressure. The no slip boundary condition given by the walls of the whole channel and surfaces of the vortex generator. For energy and momentum a second order upwind discretization method has been used. The absolute criteria of continuity, x velocity, y velocity and z velocity equal to 10^{-4} and energy equal to 10^{-8} are all the factors on which convergence is based on. This shows that once the residuals reach the above mentioned mark, the solution will converge. From the inlet surface the model is computed and for the solutions to converge 1000 iterations were given.

4.5 Grid Independency Validation

For different geometries, different sets of grids were considered. At Re = 800, 1600, 2400 and 3200 by simulating the channel with or without vortex generators, the grid independence was conducted. The number of elements, ranging from 1.1 million to 1.5 million, were taken for different geometries and compared with the span wise averaged Nusselt number. This helped in deciding the element number for different geometry. The final element numbers for each of the geometries is shown in Table 4-2.

Table 4.2 No. of elements in the fluid domain meshing.

Geometry	Element Numbers
β= 15°	1061600
β= 30°	1024400
β= 45°	1061600

CHAPTER 5

Results and Discussion

Numerical simulation of the flow in the channel with heated bottom wall has been carried out. In this chapter feature of the flow at different blade angle and different Re are discussed in detail.

5.1 Analysis of performance of vortex generators with 15° blade angle at Reynolds number 800, 1600, 2400, and 3200.

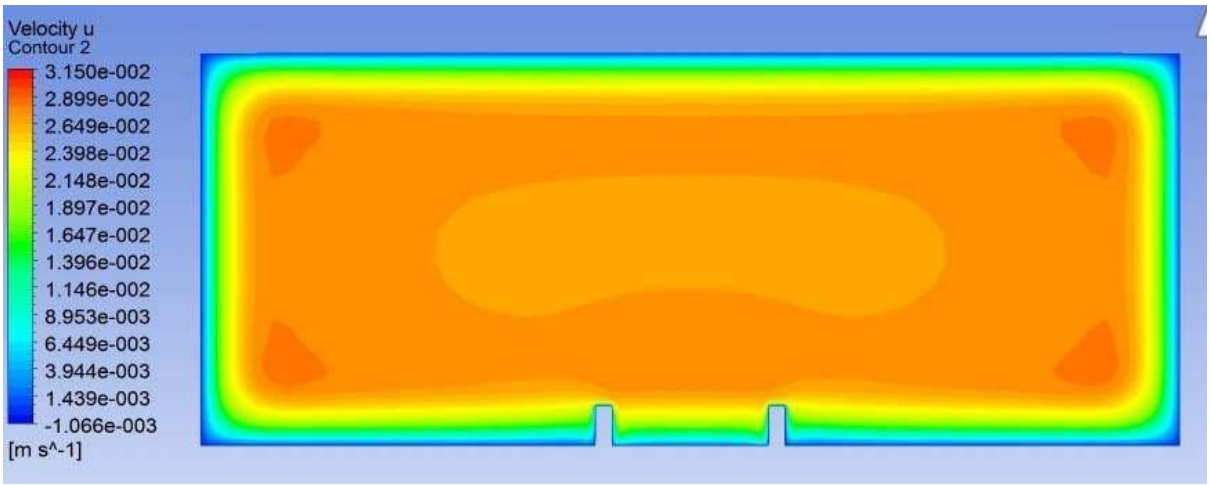

Fig. 5.1 Contours **of u velocity, Re 2400, β = 15°** (yz plane, x=30 cm)

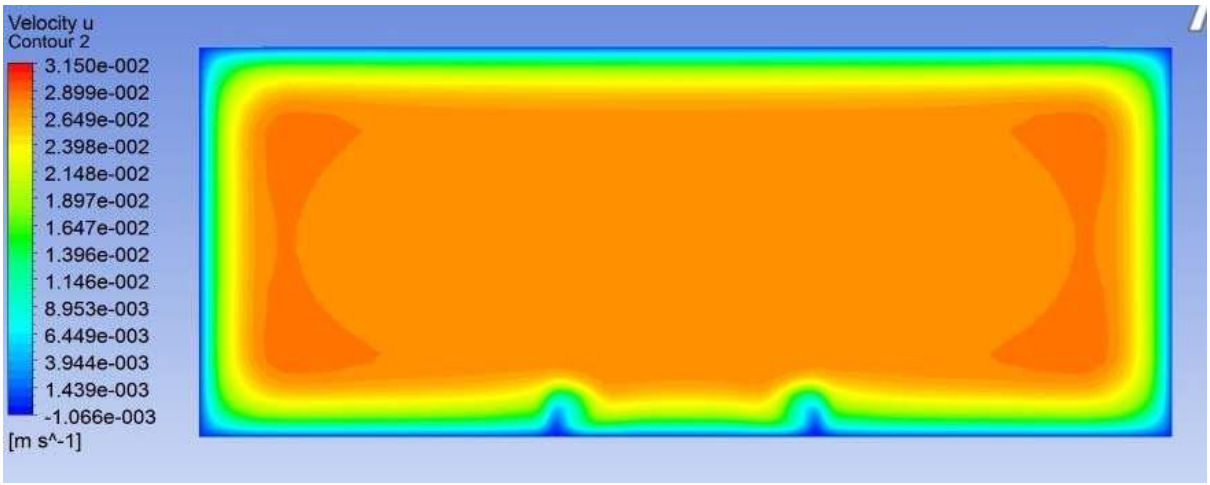

Fig. 5.2 Contours **of u velocity, Re 2400, β = 15°** (yz plane, x=35 cm)

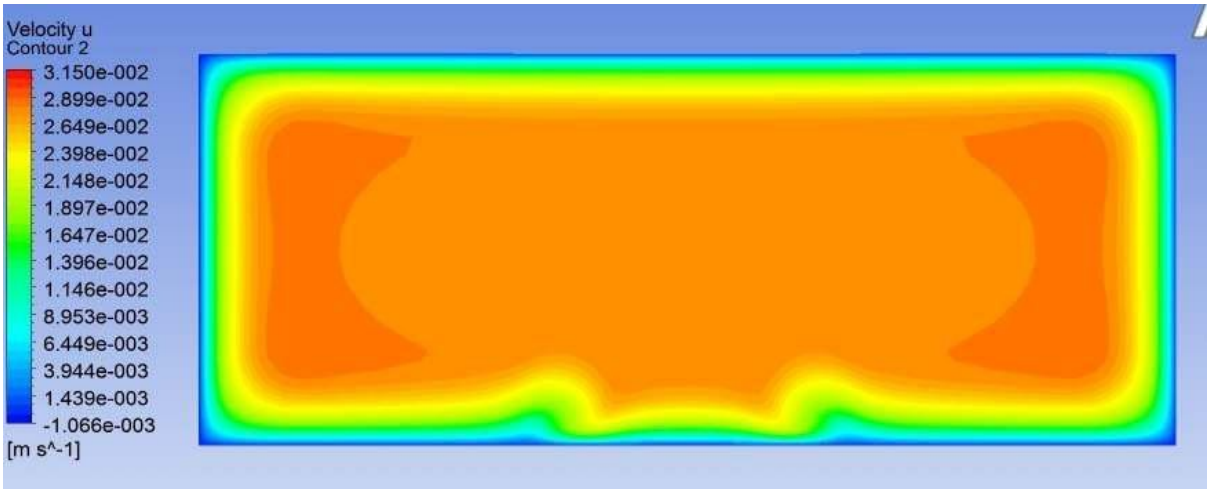

Fig. 5.3 Contours **of u velocity, Re 2400, β = 15°** (yz plane, x=40 cm)

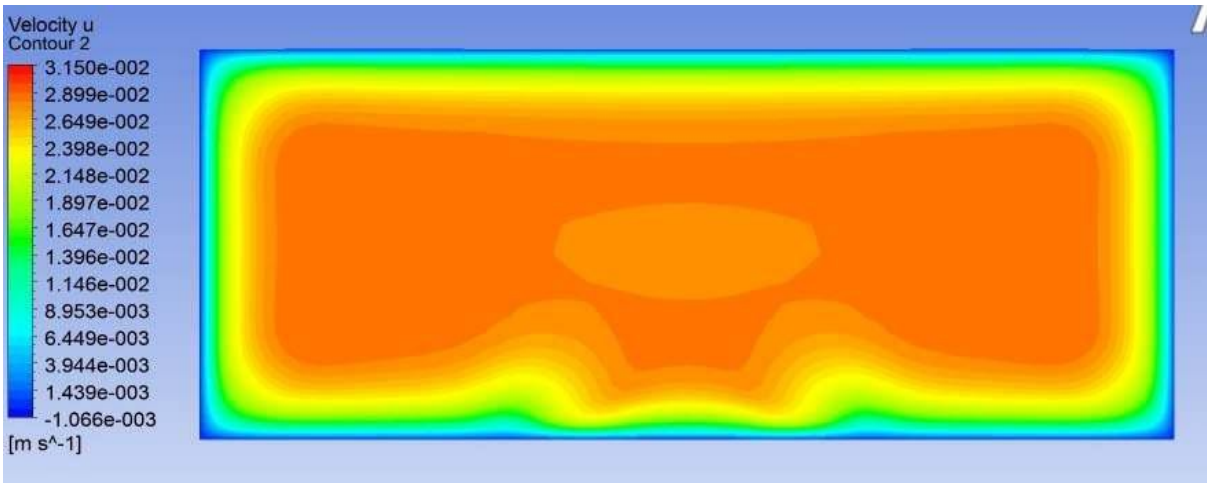

Fig. 5.4 Contours **of u velocity, Re 2400, β = 15°** (yz plane, x=50 cm)

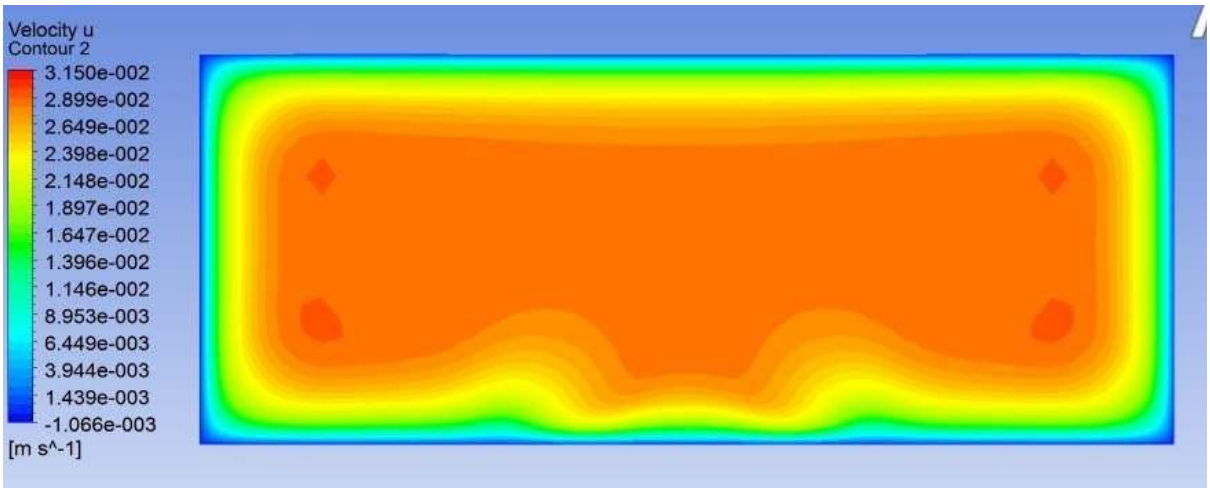

Fig. 5.5 Contours **of u velocity, Re 2400, β = 15°** (yz plane, x=55 cm)

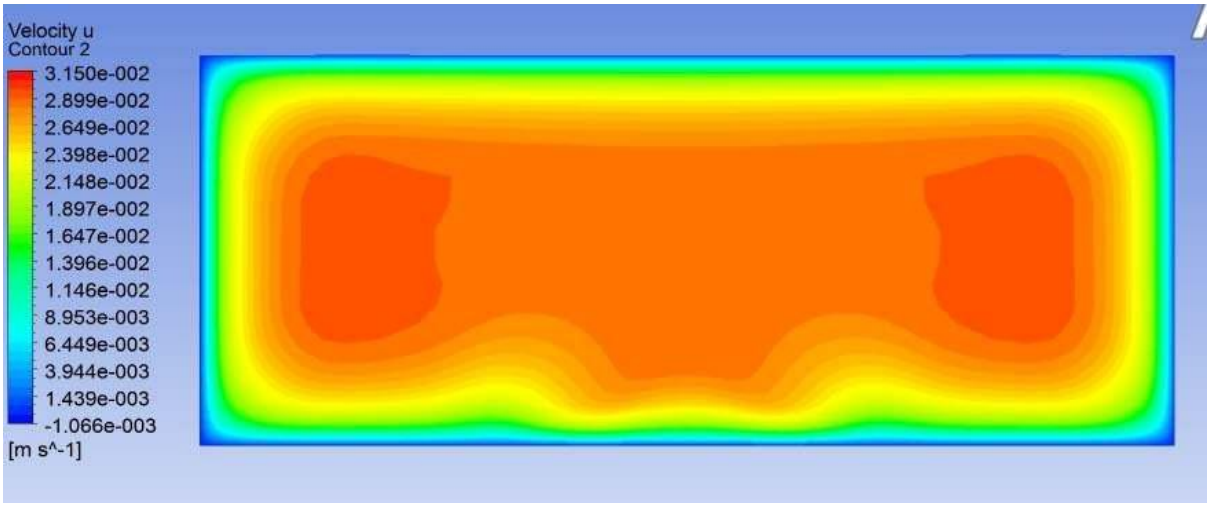

Fig. 5.6 Contours **of u velocity, Re 2400, β = 15°** (yz plane, x=65 cm)

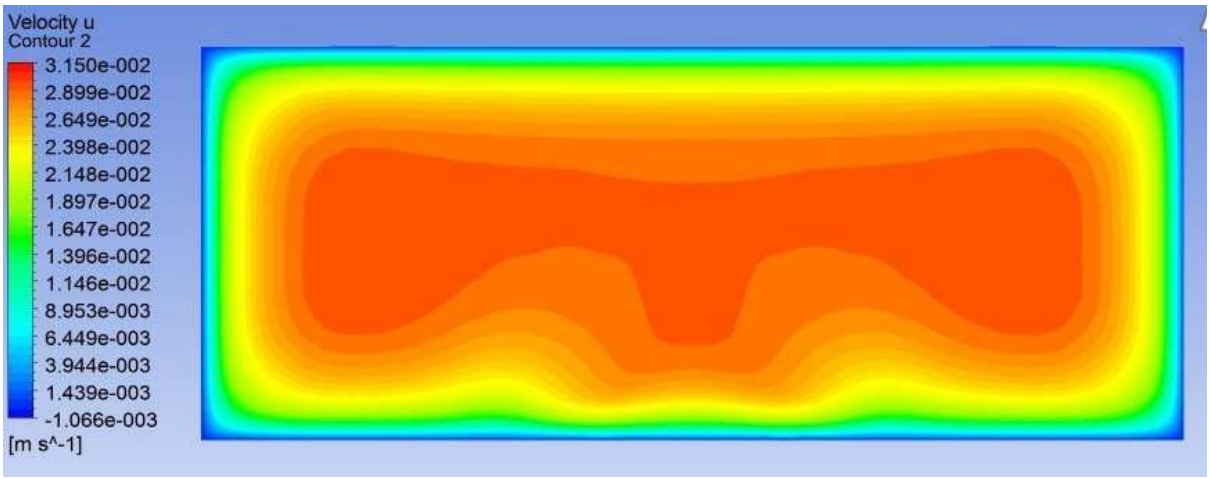

Fig. 5.7 Contours **of u velocity, Re 2400, β = 15°** (yz plane, x=70 cm)

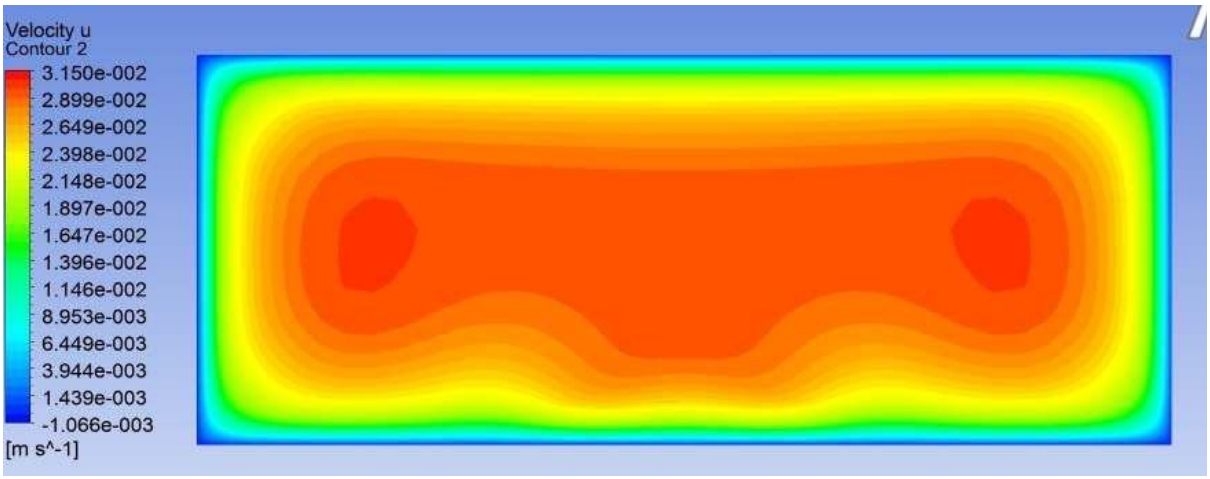

Fig. 5.8 Contours **of u velocity, Re 2400, β = 15°** (yz plane, x=85 cm)

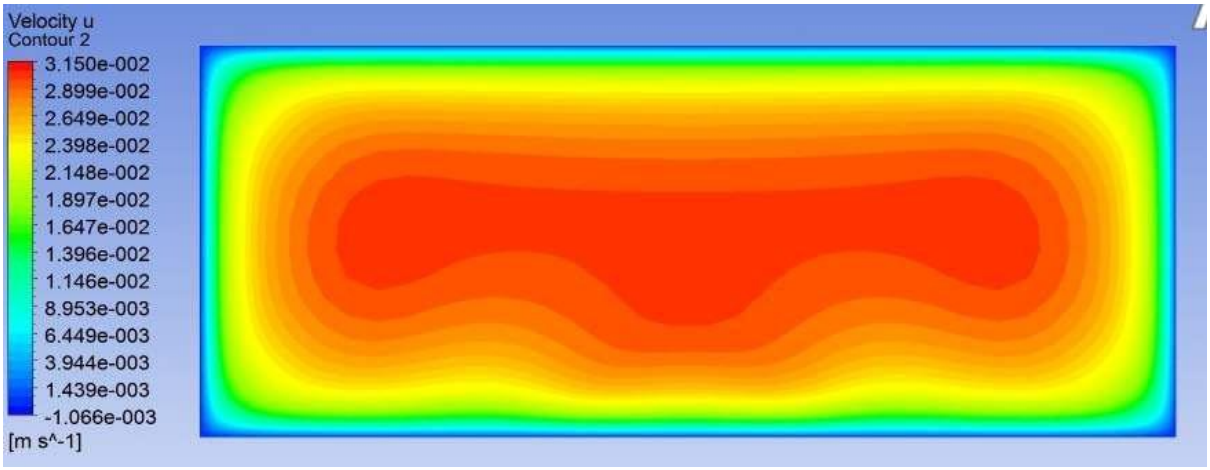

Fig. 5.9 Contours **of u velocity, Re 2400, β = 15°** (yz plane, x=100 cm)

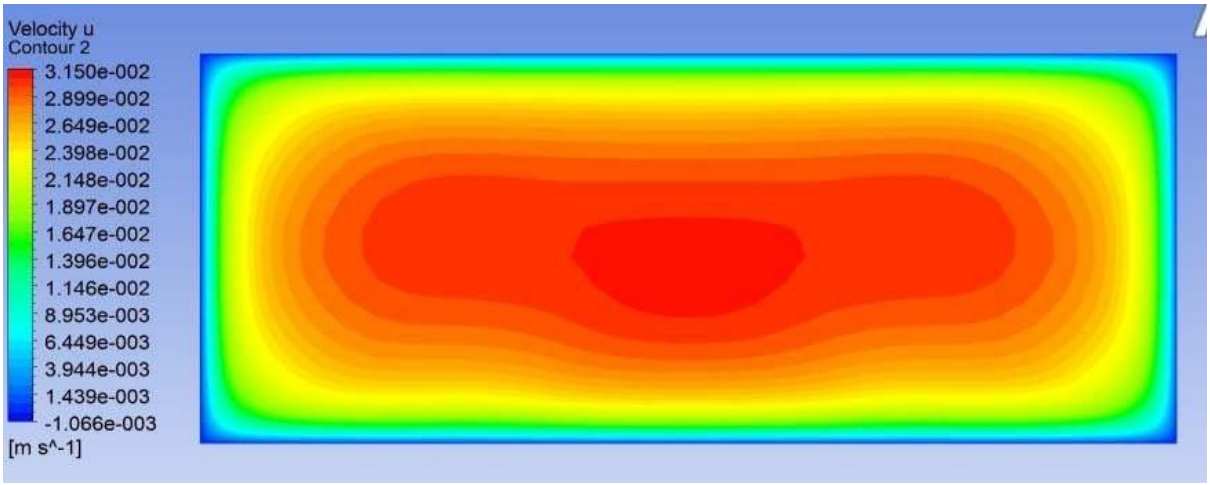

Fig. 5.10 Contours **of u velocity, Re 2400, β = 15°** (yz plane, x=140 cm)

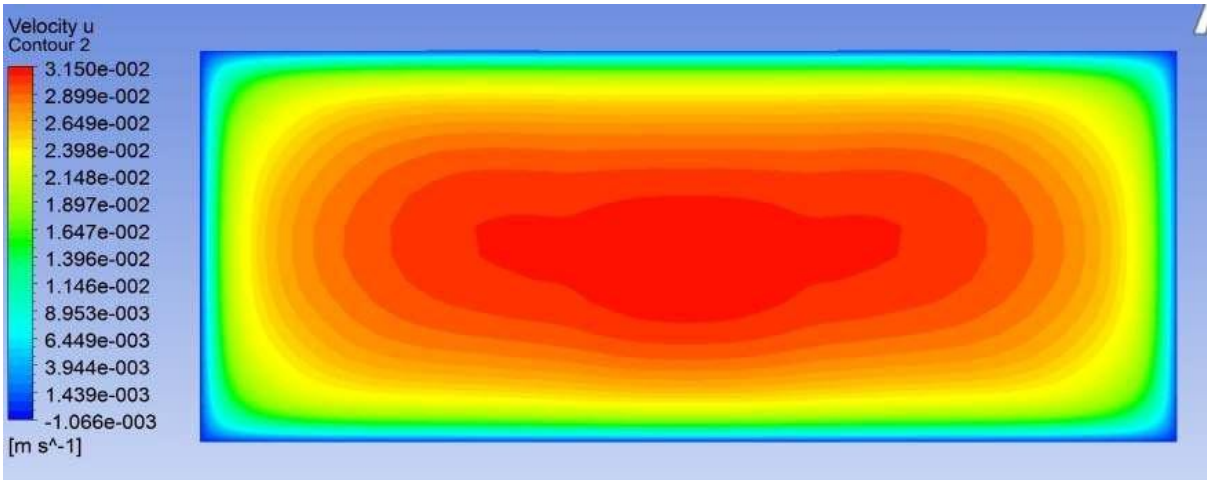

Fig. 5.11 Contours **of u velocity, Re 2400, β = 15°** (yz plane, x=180 cm)

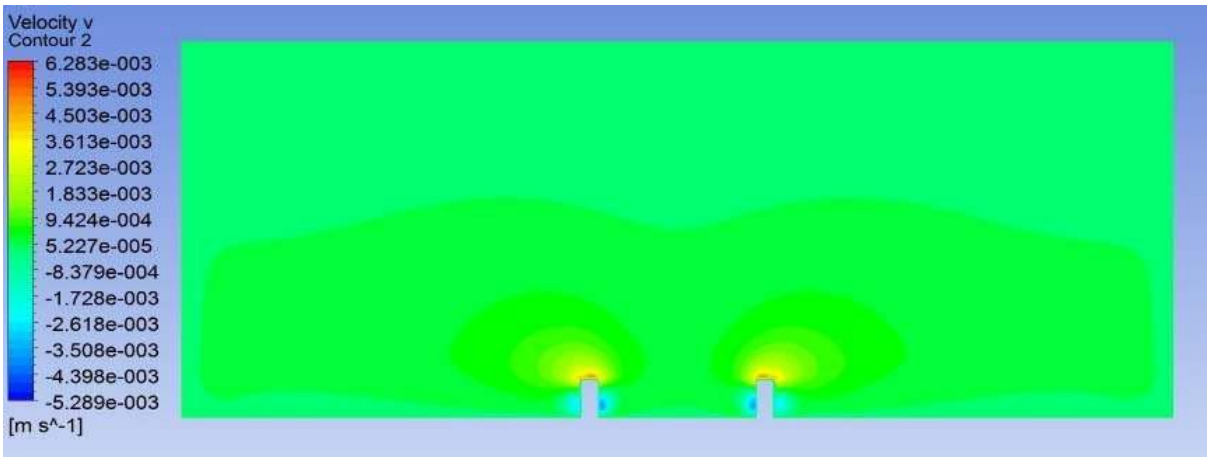

Fig. 5.12 Contours **of v velocity, Re 2400, β = 15°** (yz plane, x=30 cm)

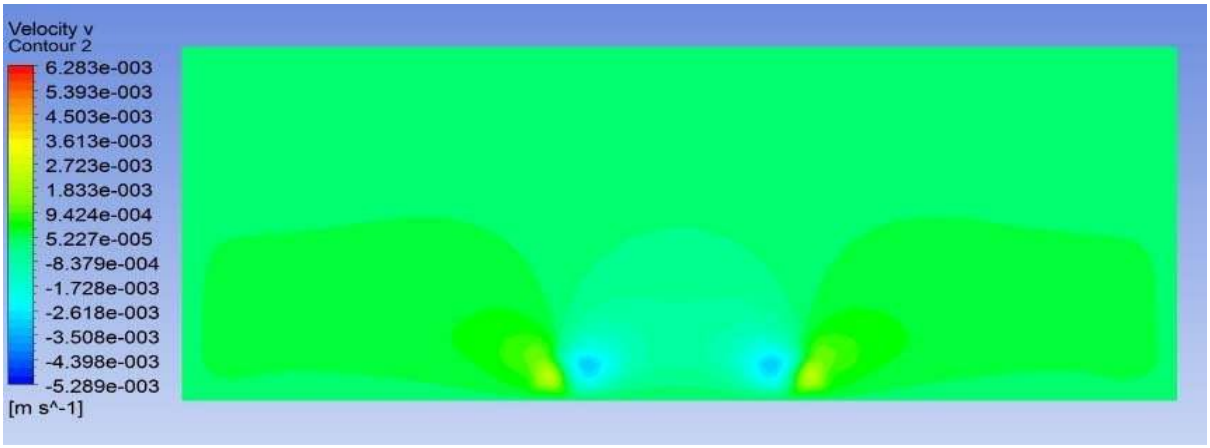

Fig. 5.13 Contours **of v velocity, Re 2400, β = 15°** (yz plane, x=35 cm)

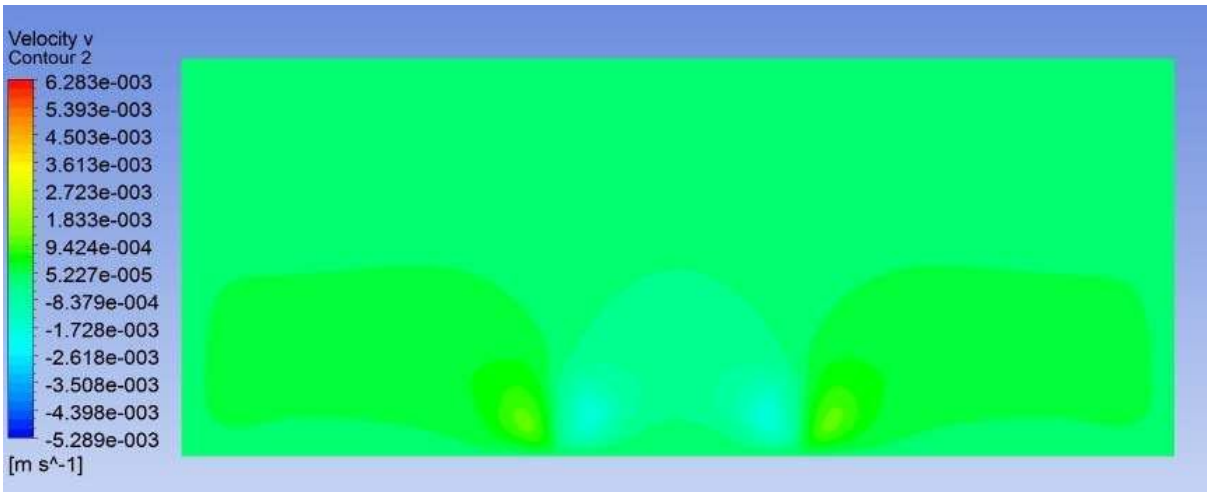

Fig.5. 14 Contours **of v velocity, Re 2400, β = 15°** (yz plane, x=40 cm)

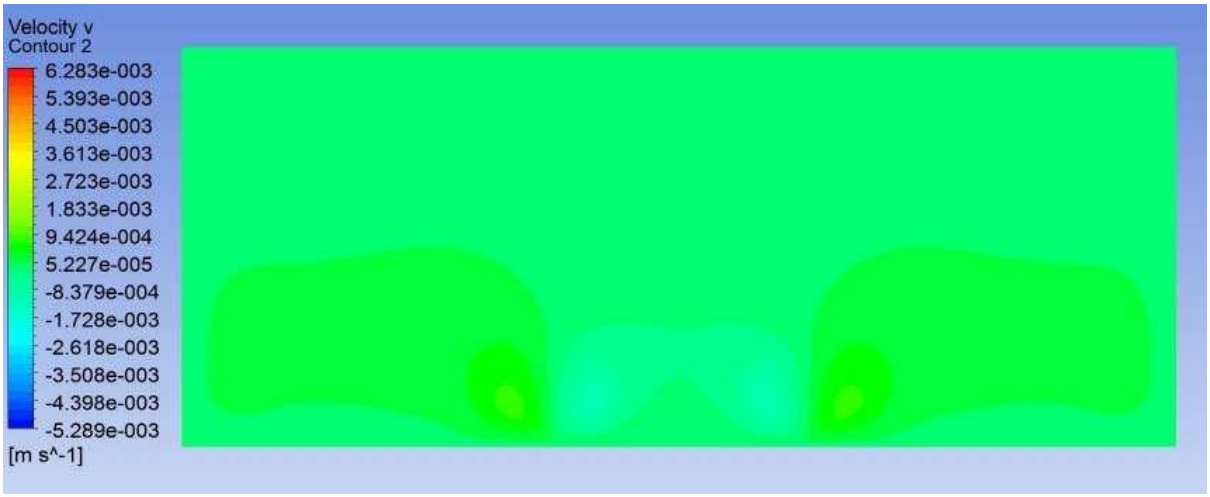

Fig. 5.15 Contours **of v velocity, Re 2400, β = 15°** (yz plane, x=45 cm)

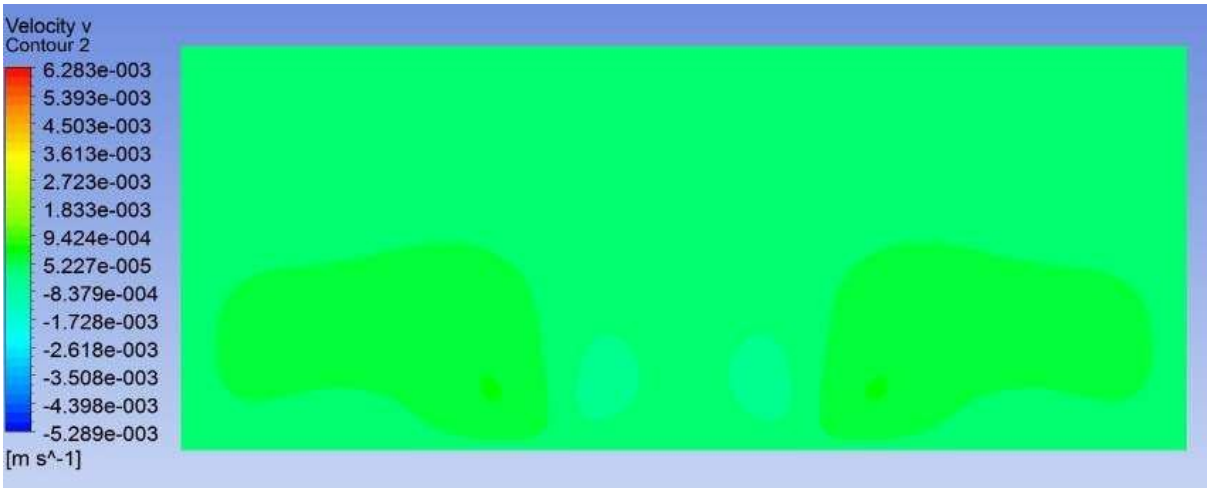

Fig. 5.16 Contours **of v velocity, Re 2400, β = 15°** (yz plane, x=60 cm)

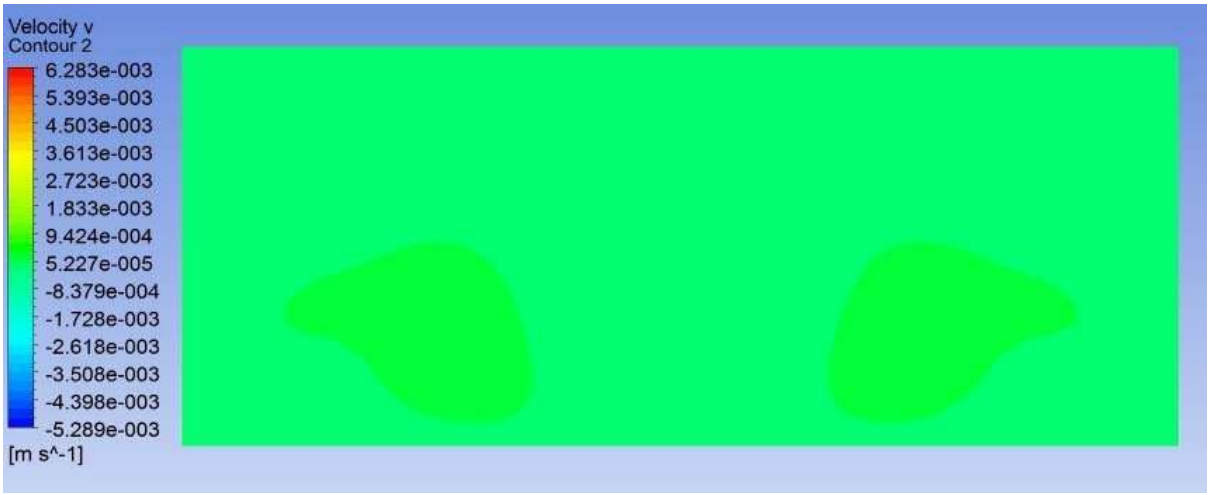

Fig. 5.17 Contours **of v velocity, Re 2400, β = 15°** (yz plane, x=90 cm)

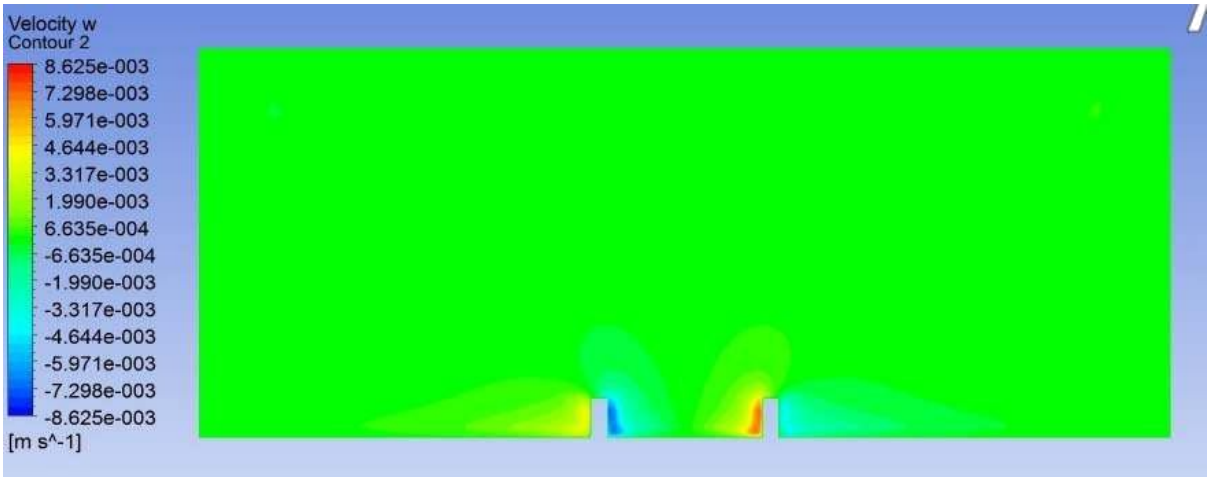

Fig. 5.18 Contours **of w velocity, Re 2400, β = 15°(** yz plane, x=30 cm)

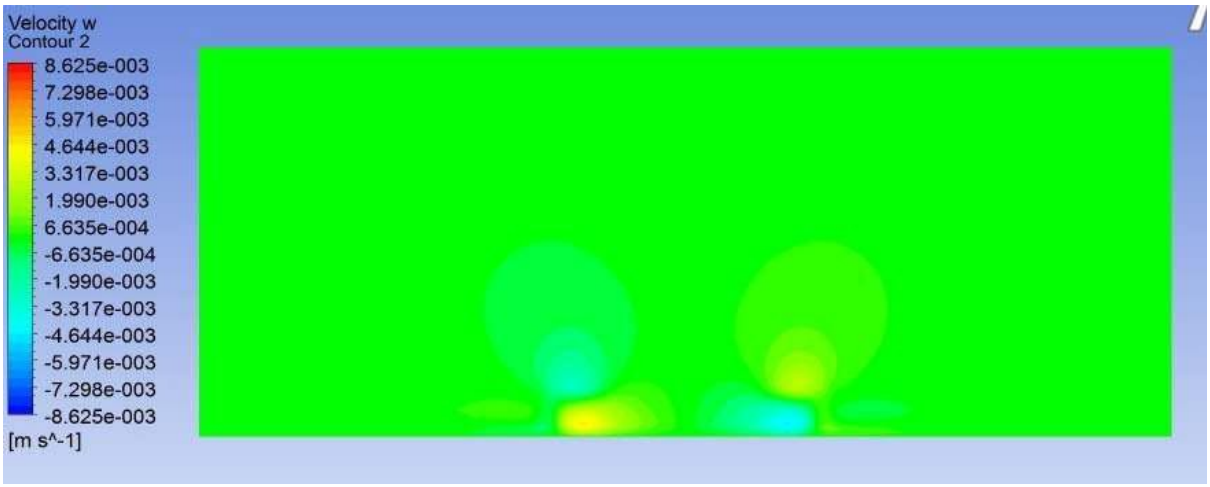

Fig. 5.19 Contours **of w velocity, Re 2400, β = 15°** (yz plane, x=35 cm)

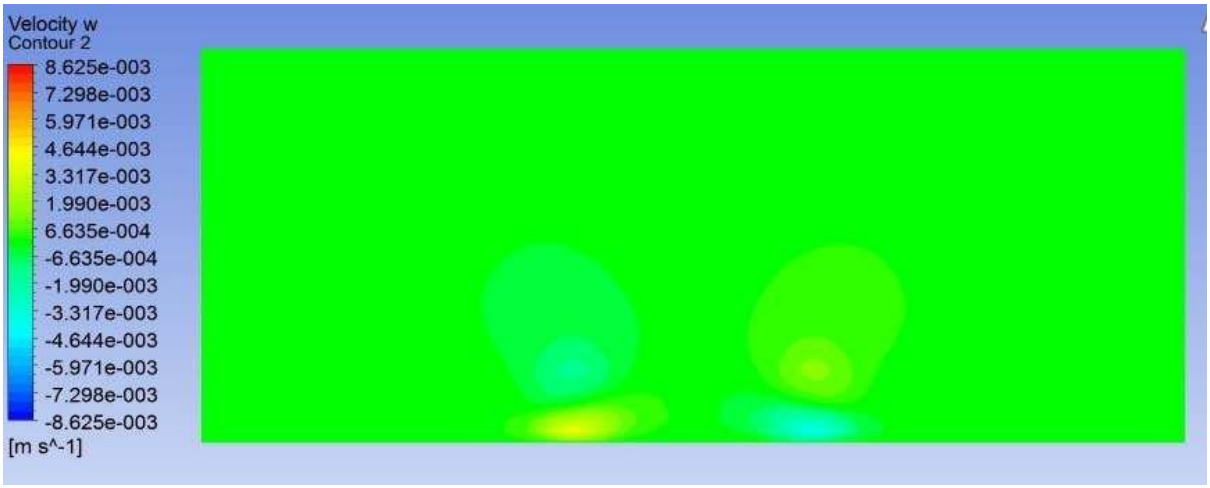

Fig. 5.20 Contours **of w velocity, Re 2400, β = 15°** (yz plane, x=40 cm)

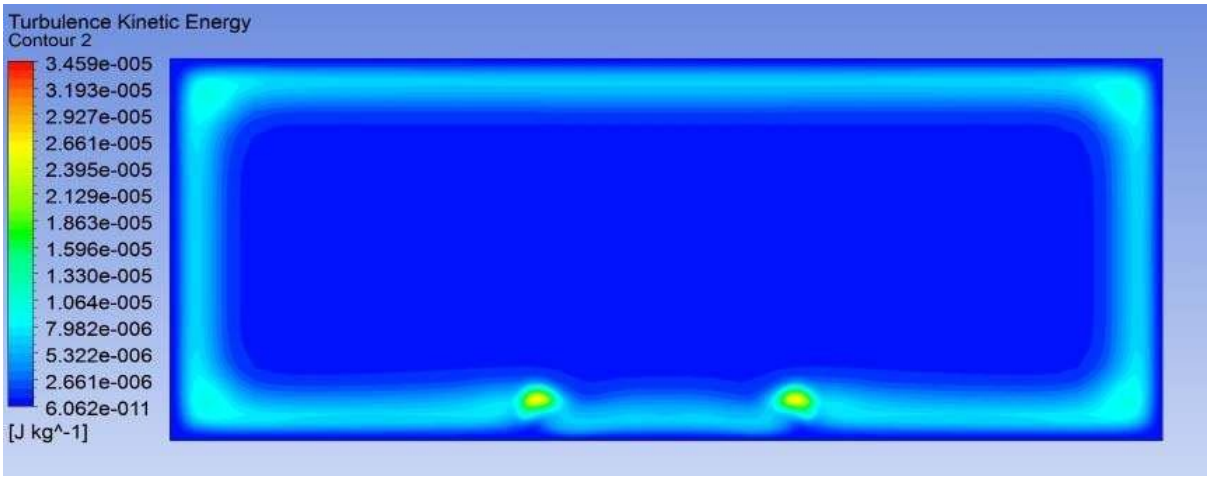

Fig 5.21 Contours of turbulent kinetic energy at Re 2400, **β = 15°** (yz plane, x=35 cm)

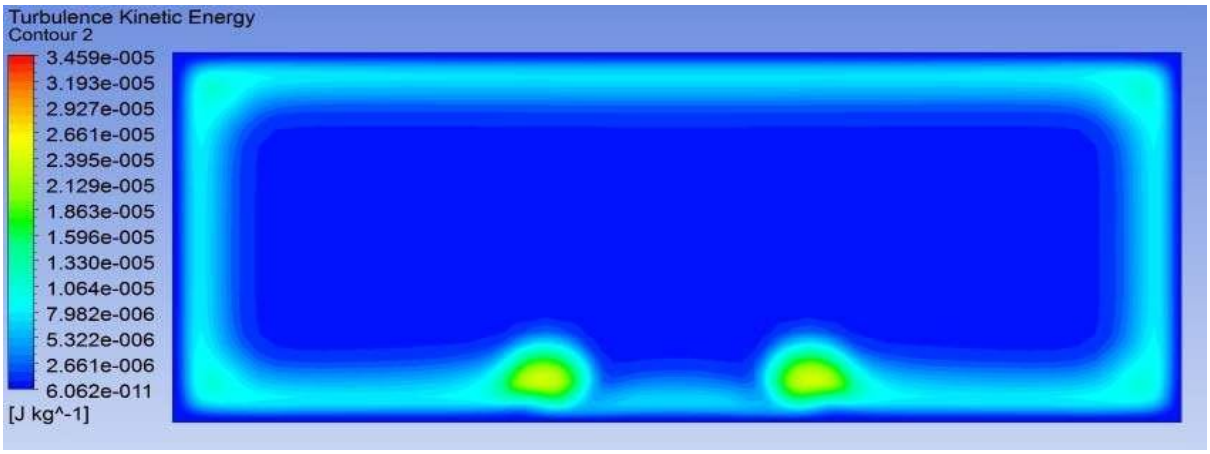

Fig. 5.22 Contours of turbulent kinetic energy at Re 2400, **β = 15°(yz plane, x=40 cm)**

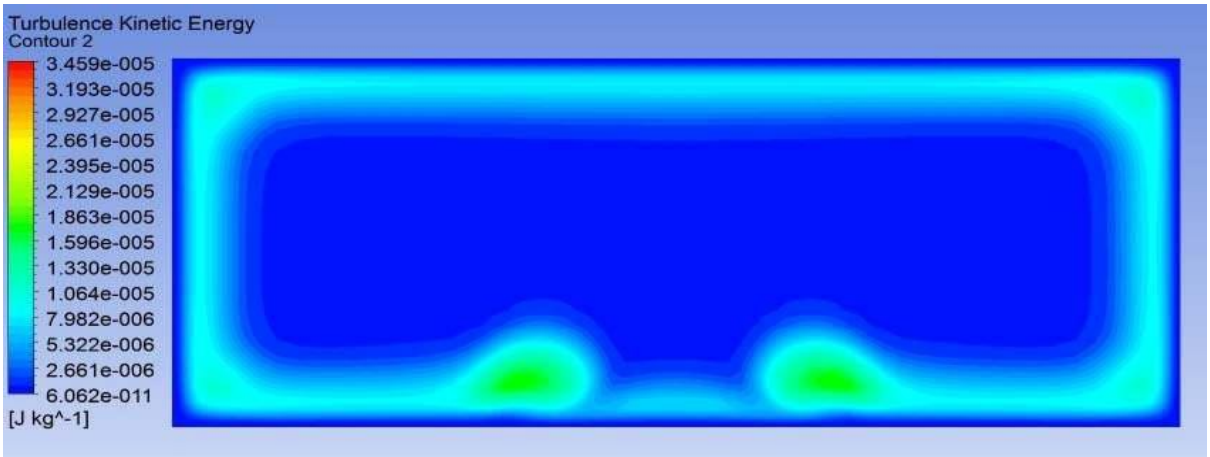

Fig. 5.23 Contours of turbulent kinetic energy at Re 2400, **β = 15°** (yz plane, x=45 cm)

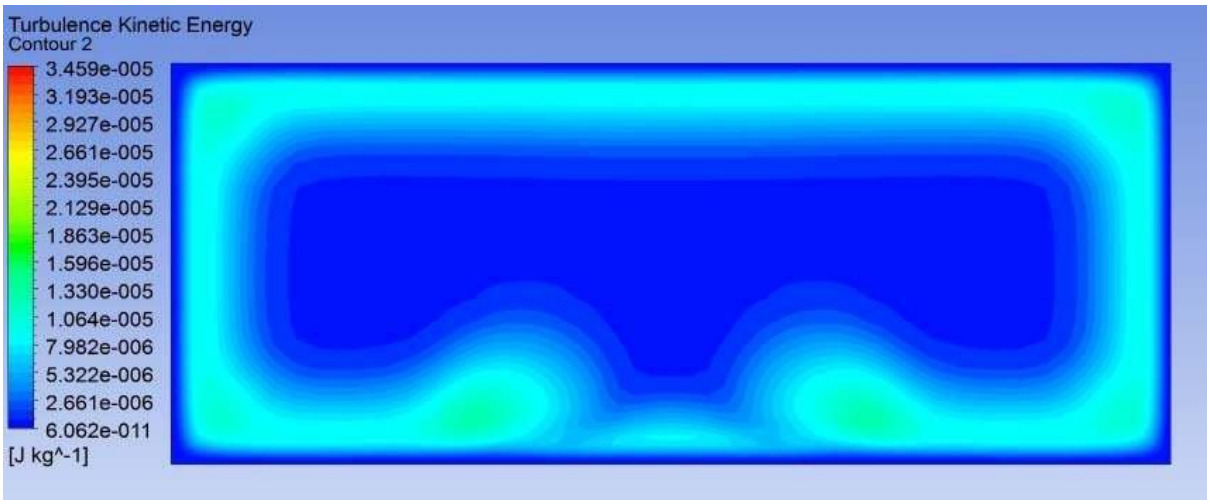

Fig. 5.24 Contours of turbulent kinetic energy at Re 2400, **β = 15°** (yz plane, x=60 cm)

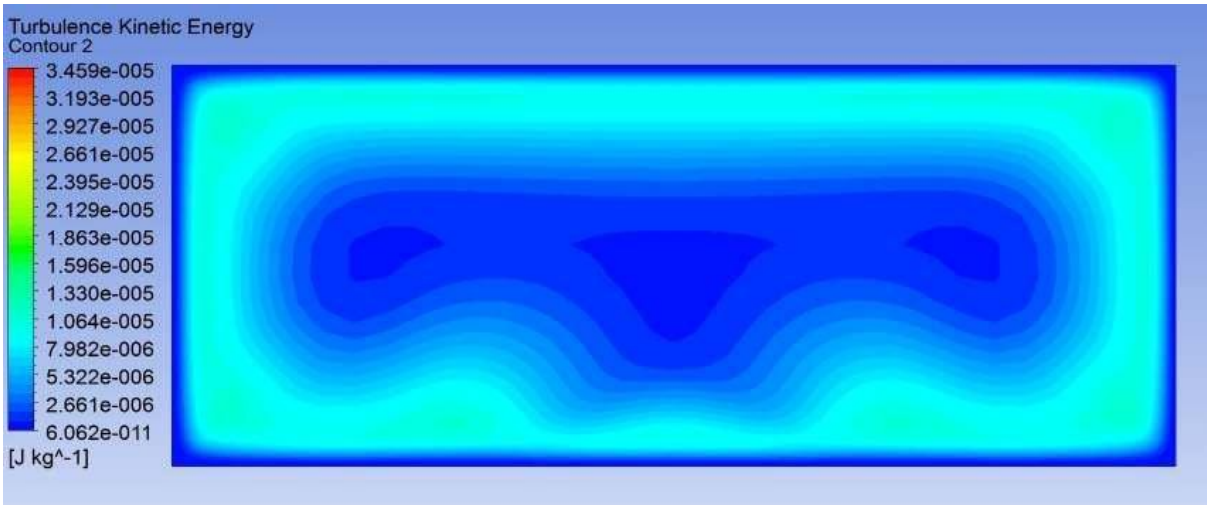

Fig 5.25 Contours of turbulent kinetic energy at Re 2400, **β = 15°(yz plane, x=90 cm)**

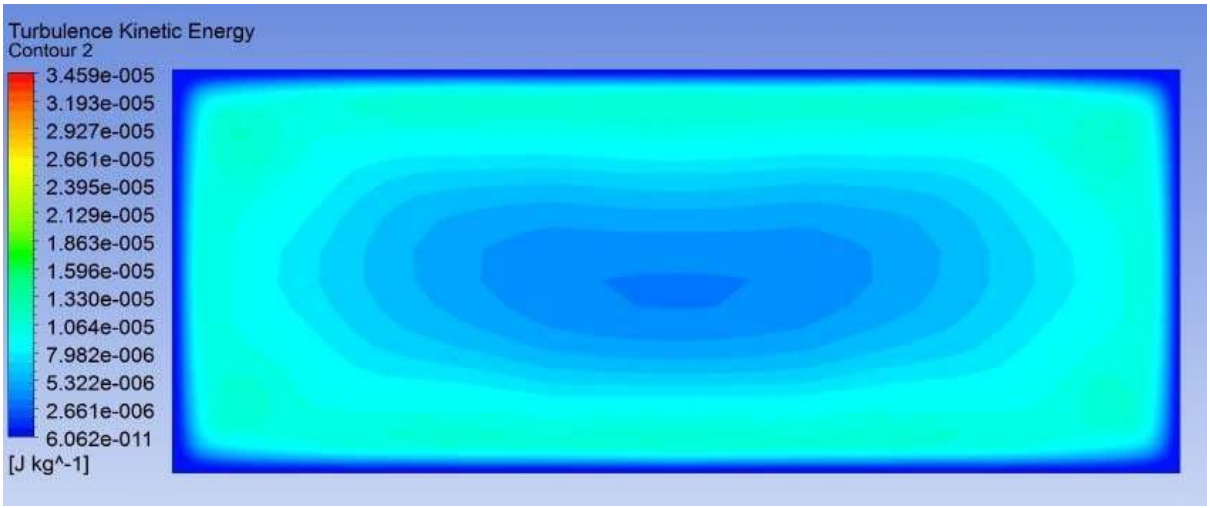

Fig. 5.26 Contours of turbulent kinetic energy at Re 2400, **β = 15°** (yz plane, x=190 cm)

The variation of span wise averaged Nusselt number was calculated at different values of x/H at Reynolds no of 800, 1600, 2400, and 3200. It shows that the span wise averaged Nusselt no. increase with the increase in Reynolds number at a particular x/H. Fig. 5.27 to fig. 5.30 show the behavior at these Reynolds no with angle 15° blade angle. The increment in the span wise averaged Nusselt no. can be observed from these figures. Observation also shows that with the increase in Reynolds no for same particular blade angle (at 15°) the increasing effect of the Nusselt no. penetrate through the much greater value of x/H.

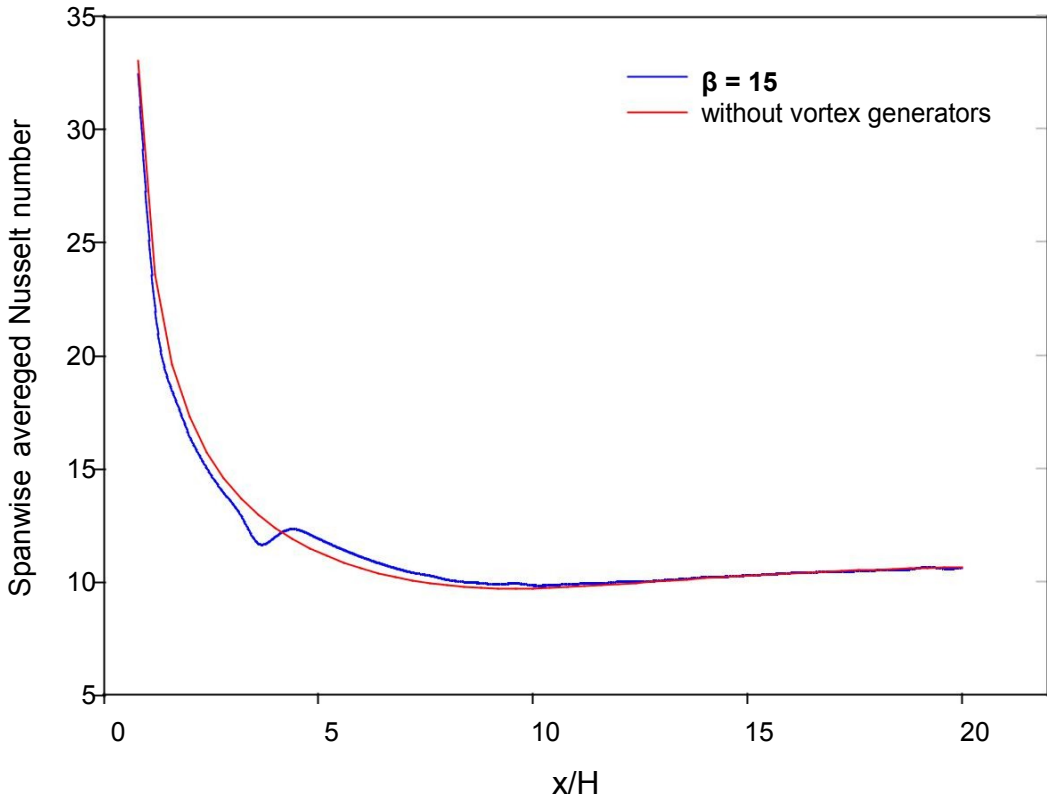

Fig. 5.27 Variation of spanwise avereged Nusselt number at Re 800, **β = 15**

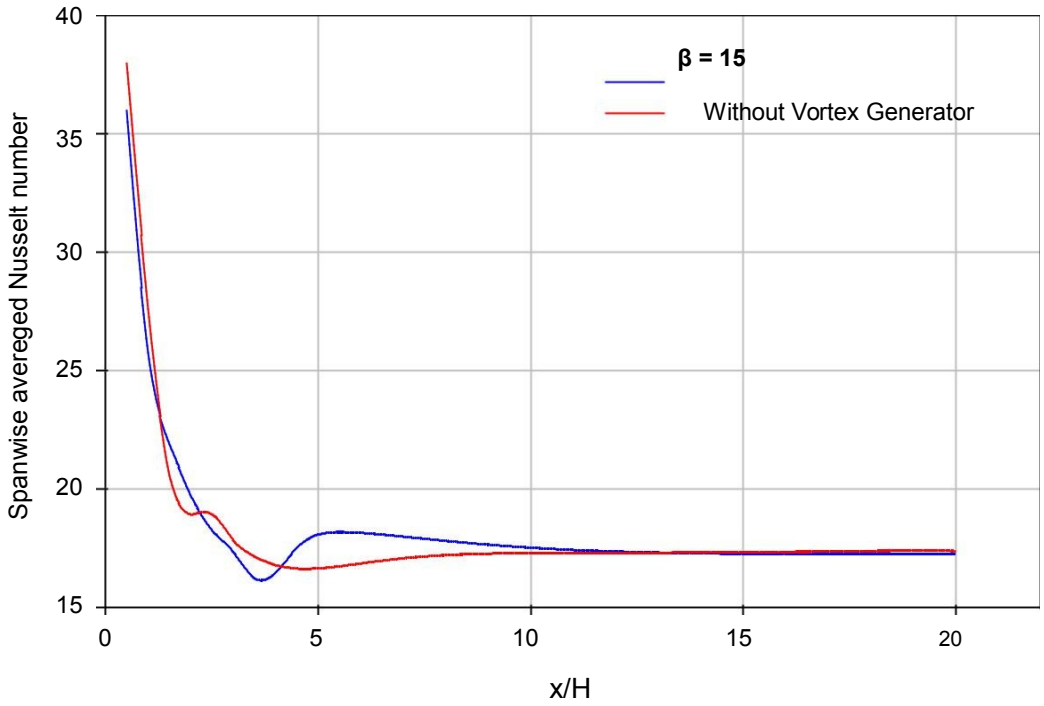

Fig 5.28 Variation of spanwise avereged Nusselt number at Reynold No. 1600

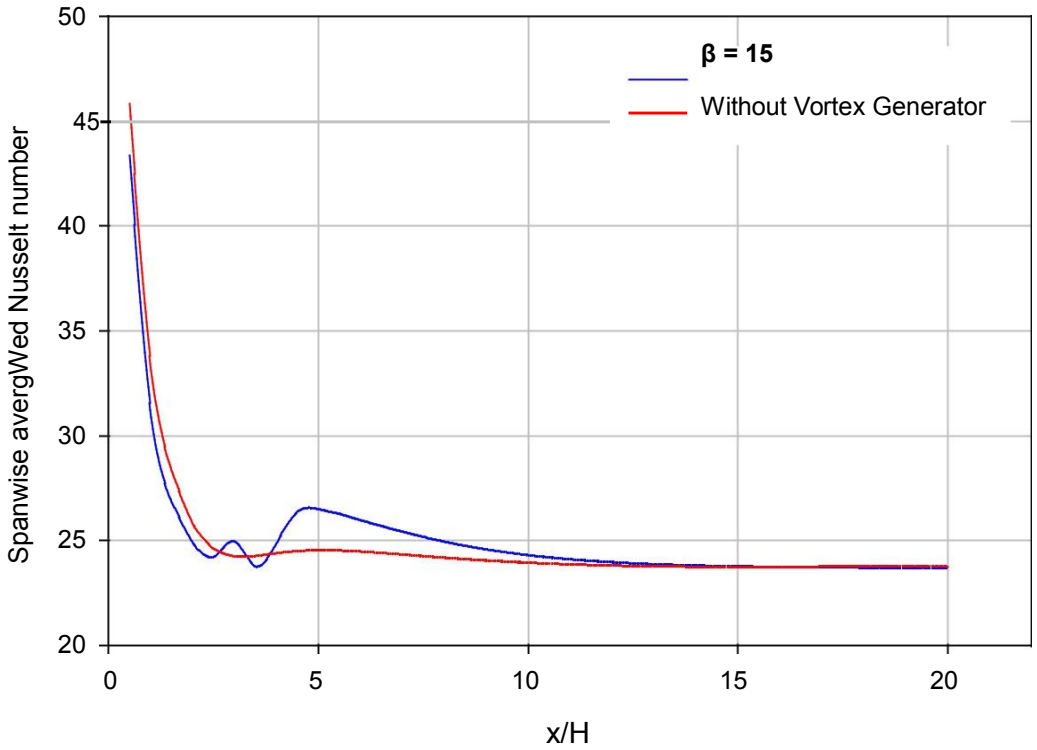

Fig 5.29 Variation of spanwise avereged Nusselt number at Reynold No. 2400

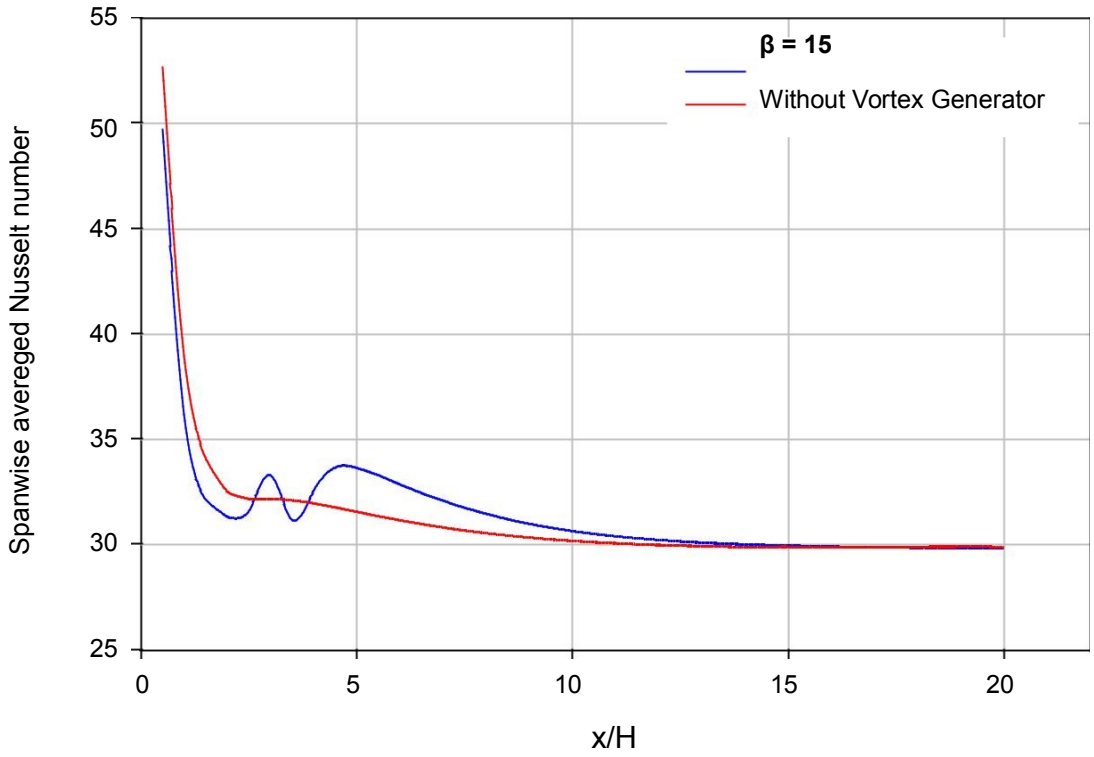

Fig 5.30 Variation of spanwise avereged Nusselt number at Reynold No. 3400

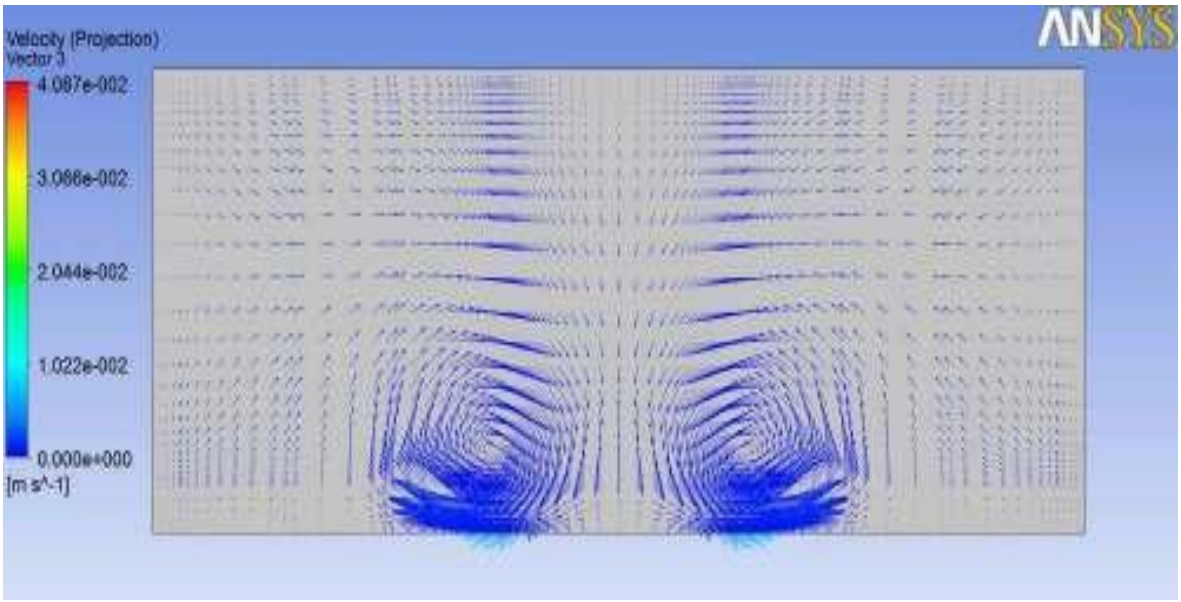

Fig. 5.31 Vortices Formation on a plane at **x/H of 3.5, Re 3200, β** = 15°

Fig 5.31 shows that due to vortex generators the formation of vortices takes place in which the clockwise and counterclockwise vortex is generated. The magnitude of velocity is greater towards the bottom wall. These opposite vortex generator cause the mixing of the fluid due to

which the convection coefficient at the bottom wall increases and hence the Nusselt number increases. With increase in Reynolds no. the strength of the vortex are increased which cause greater increase in the Nusselt number. The vortex formation also prevents the thickening of velocity boundary layer on the bottom wall that cause enhanced heat transfer.

Fig 5.32 shows that strength of the vortex is maximum near the vortex generators region and gradually decreases in the stream wise direction. With increase in Reynolds no. for the same geometry the vortex effect is seen up to much greater distance in the stream wise direction. That is why the difference between the span wise averaged Nusselt number with and without vortex generators is greater at higher Reynolds number than that of at low Reynolds number.

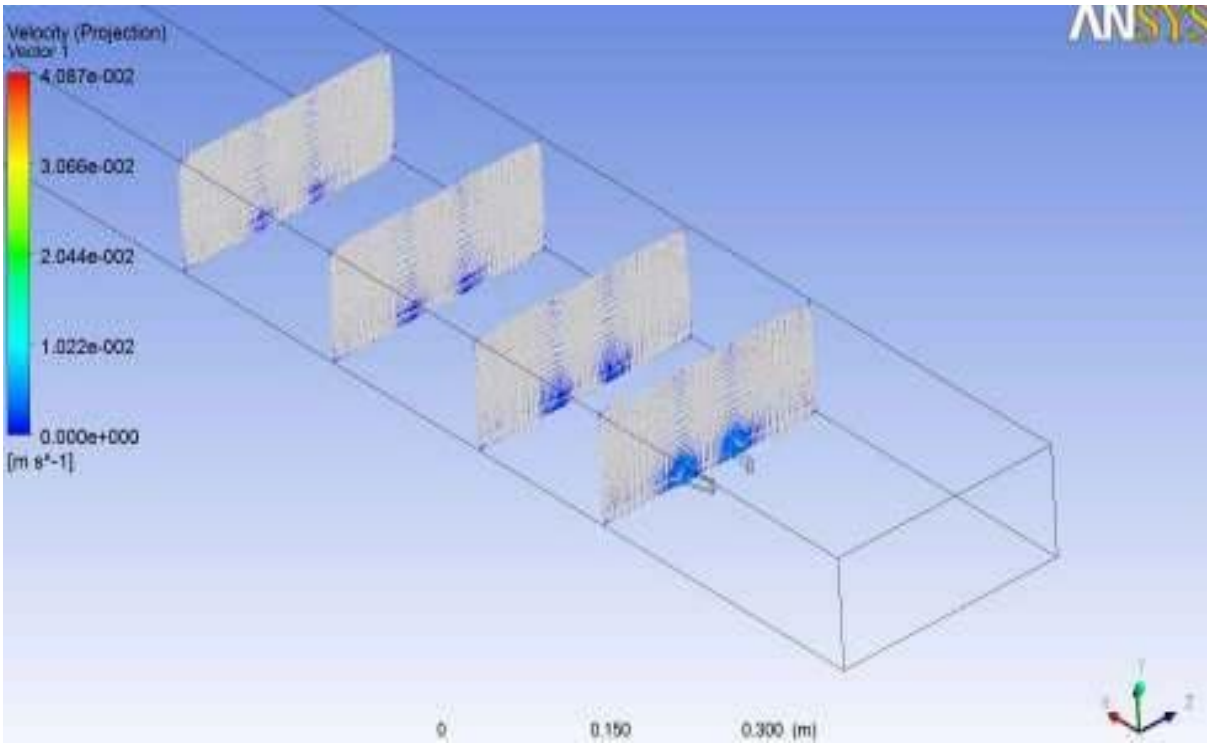

Fig. 5.32 Formation of vortices at di**fferent planes in x direction, Re= 3200, β**=15°

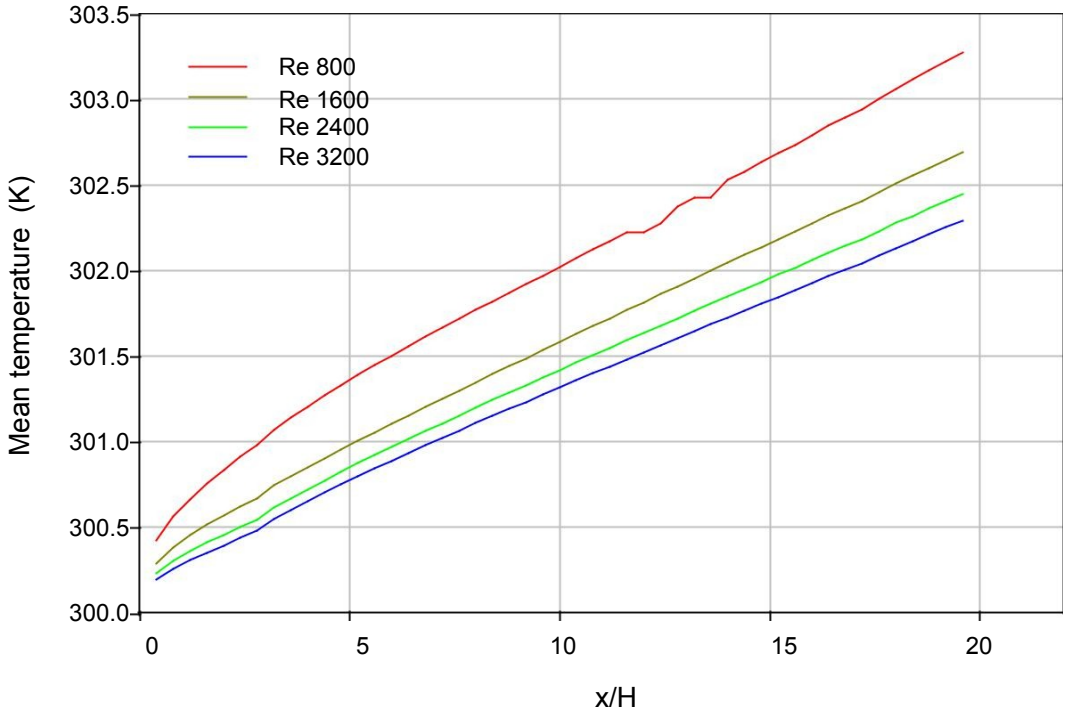

Fig. 5.33 Variation of mean temperature along x/H, **β = 15**

Fig. 5.33 shows that the mean temperature along the direction of the flow increases continuously. As the mixing is enhanced just after the vortex generators, the heat is distributed in the bulk fluid that causes the increment in the bulk fluid temperature because fluid is able to take more heat from the bottom wall as compared to the case of the heat transfer in the channel without vortex generators where the temperature of the fluid along the bottom wall is more compared to the temperature of the fluid away from the bottom wall. Also the mean temperature become less as we increase the Reynolds no. The mean temperature at particular cross section in the channel is more at Re 800 and decreases as we increases the Reynolds number to 1600, 2400 and 3200. This is because at high less time to gain the heat flux so the mean temperature less at higher Reynolds no.

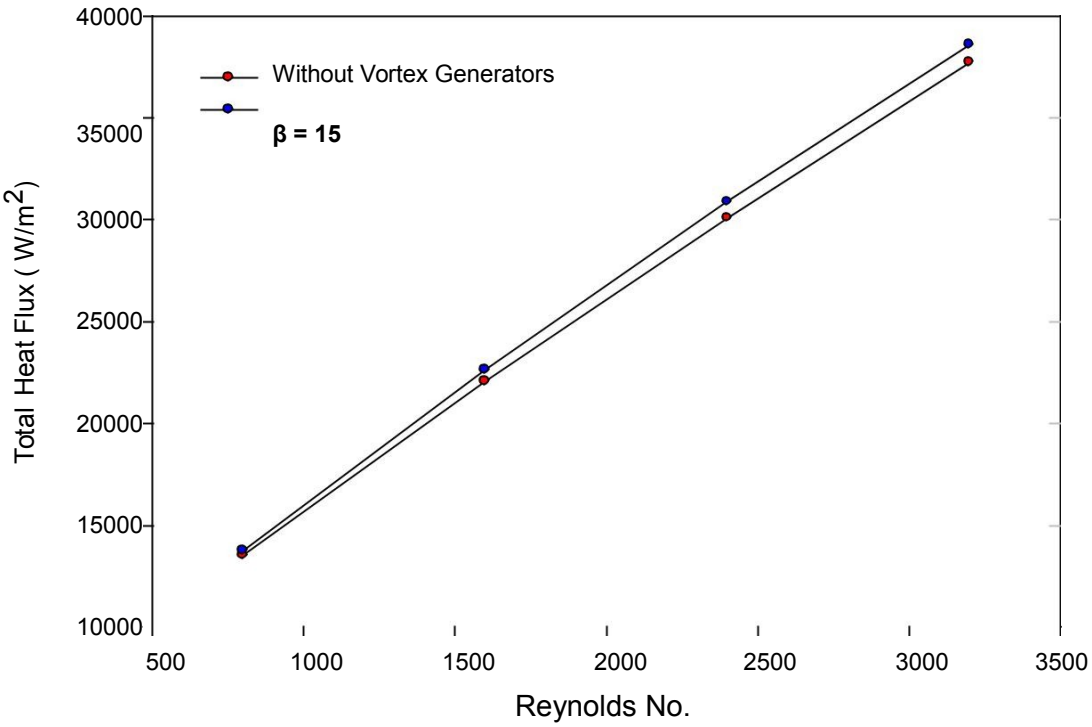

Fig. 5.34 Varition of Total Heat Flux from bottomwal with Reynolds no., **β = 15**

Fig. 5.34 shows the effect of vortex generators that enhance the total heat flux from the bottom wall. As we increase the Reynolds no. the heat transfer performance of the vortex generators increase. The difference between the total heat flux in the cases of without vortex generators and with vortex generators is higher at higher Reynolds no. and less at lower Reynolds number.

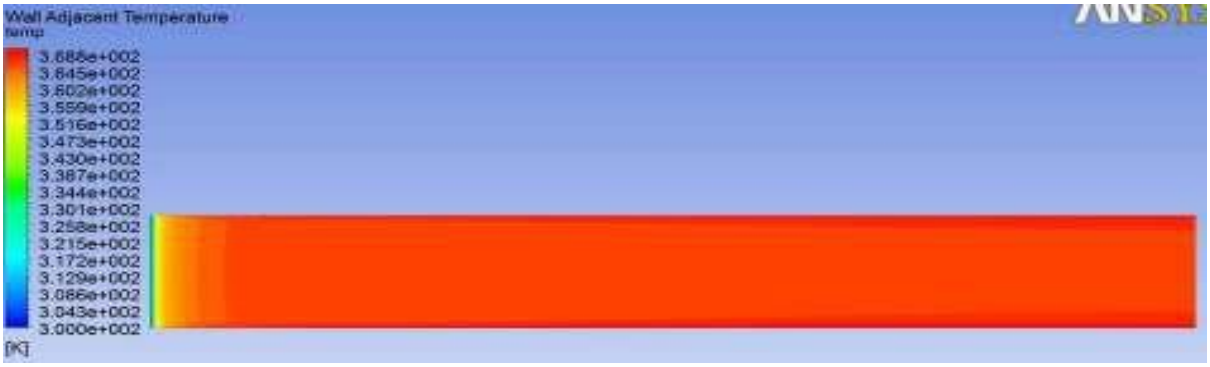

Fig. 5.35 Contours of wall adjacent temperature, Re 2400, without vortex generators

Fig. 5.36 Contours **of wall adjacent temperature, Re 2400, β = 15°**

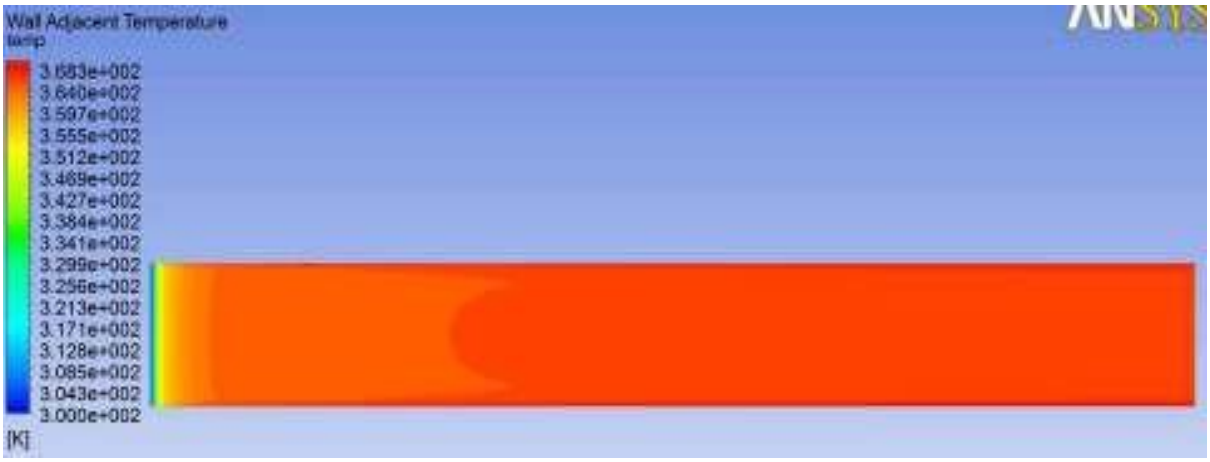

Fig.5.37 Contours of wall adjacent temperature, Re 3200, without vortex generators

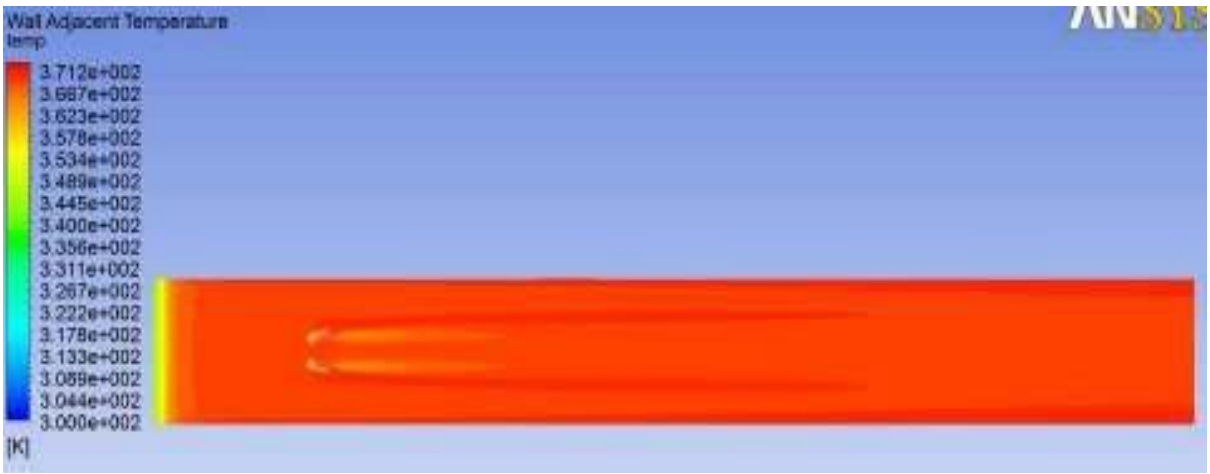

Fig. 5.38 Contours of wall adjacen**t temperature, Re 3200, β = 15°**

Fig. 5.35 to fig. 5.38 show the comparison of the bottom wall adjacent temperature at Re 2400 and 3200 with and without vortex generators. The use of vortex generators causes the

wall adjacent temperature near the bottom wall decrease. The decrease in the wall adjacent temperature cause the larger temperature gradient near the bottom wall which cause the increase in the heat flux, so improved heat transfer and increase in the Nusselt no. in that region. With increase in Reynolds no. the wall adjacent temperature near the bottom wall decrease so at higher Reynolds no. performance increase.

5.2 Analysis of performance of vortex generator with 30° blade angle at Reynolds number 800, 1600, 2400, 3200.

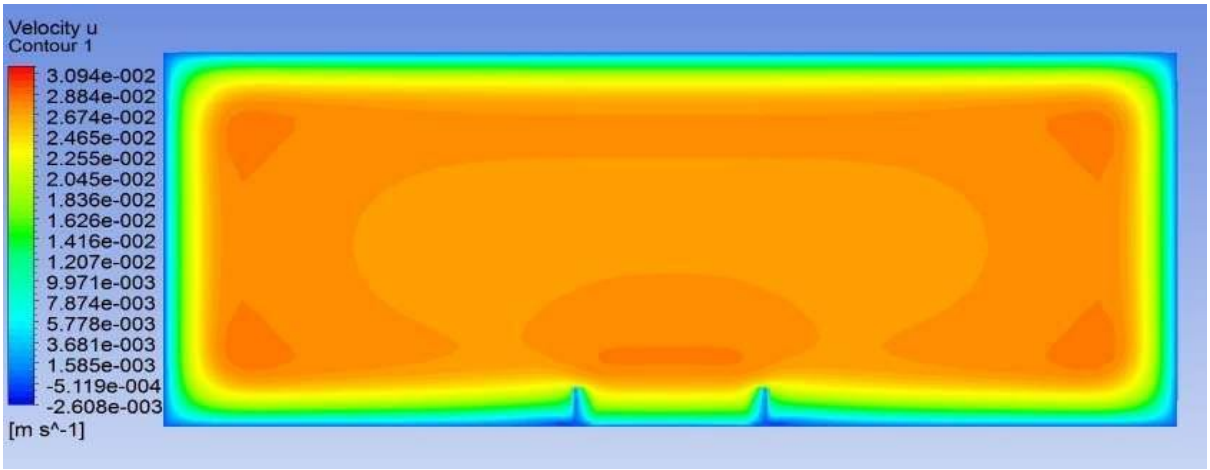

Fig. 5.39 Contours **of u velocity, Re 2400, β** = 30° (yz plane, x=30 cm)

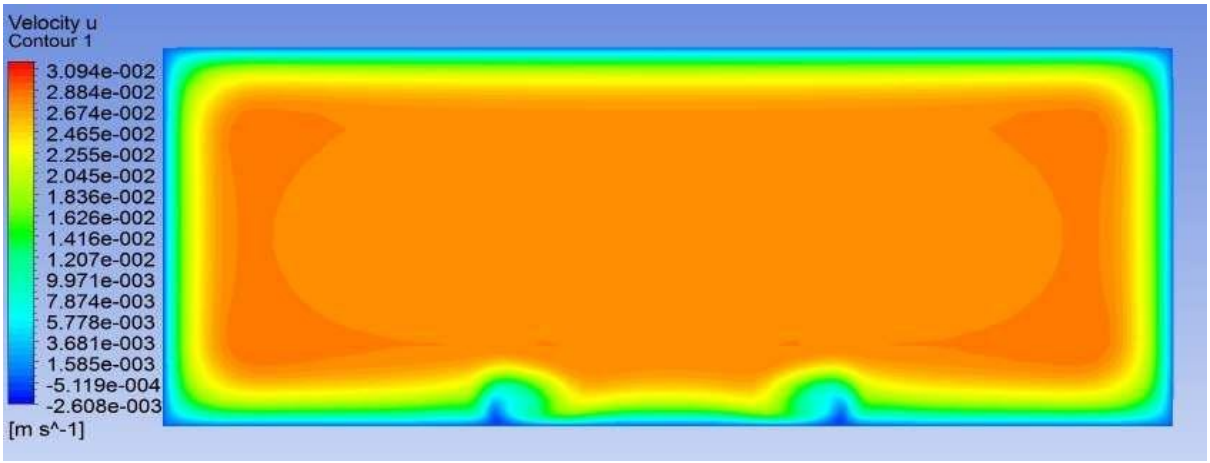

Fig. 5.40 Contours **of u velocity, Re 2400, β** = 30° (yz plane, x=35 cm)

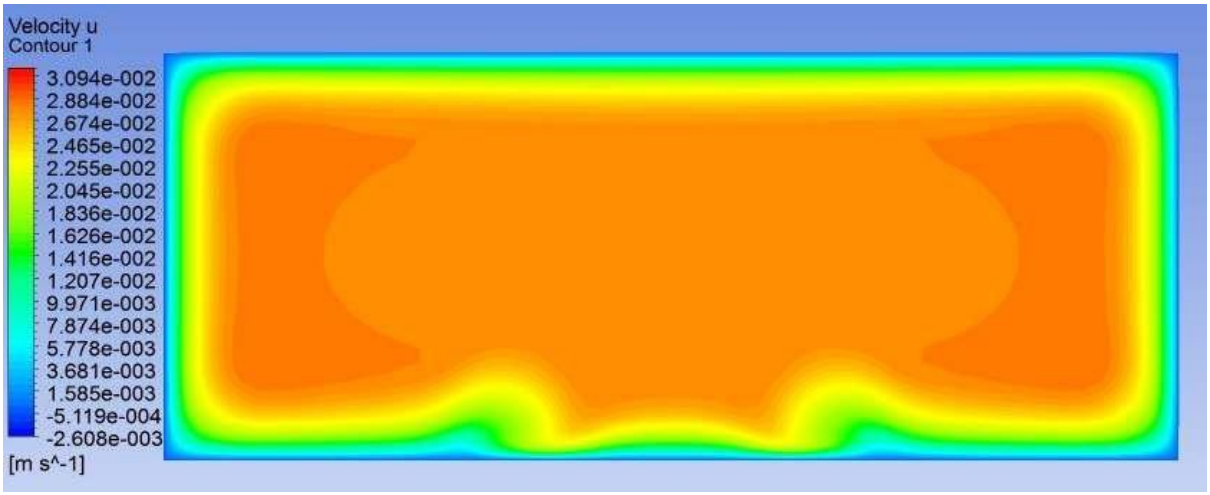

Fig. 5.41 Contours **of u velocity, Re 2400, β** = 30° (yz plane, x=4 0 cm)

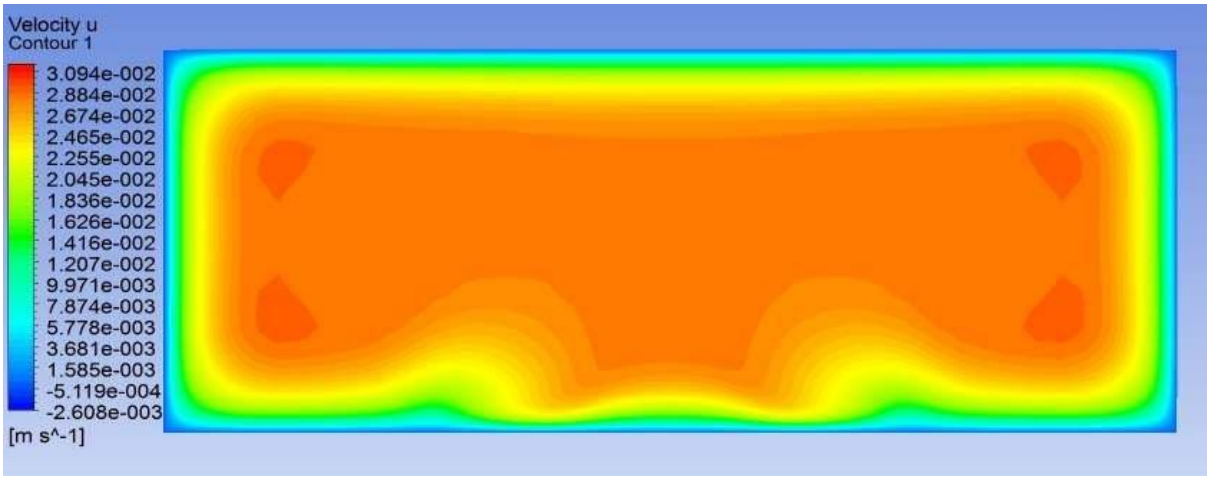

Fig. 5.42 Contours **of u velocity, Re 2400, β** = 30 ° (yz plane, x=50 cm)

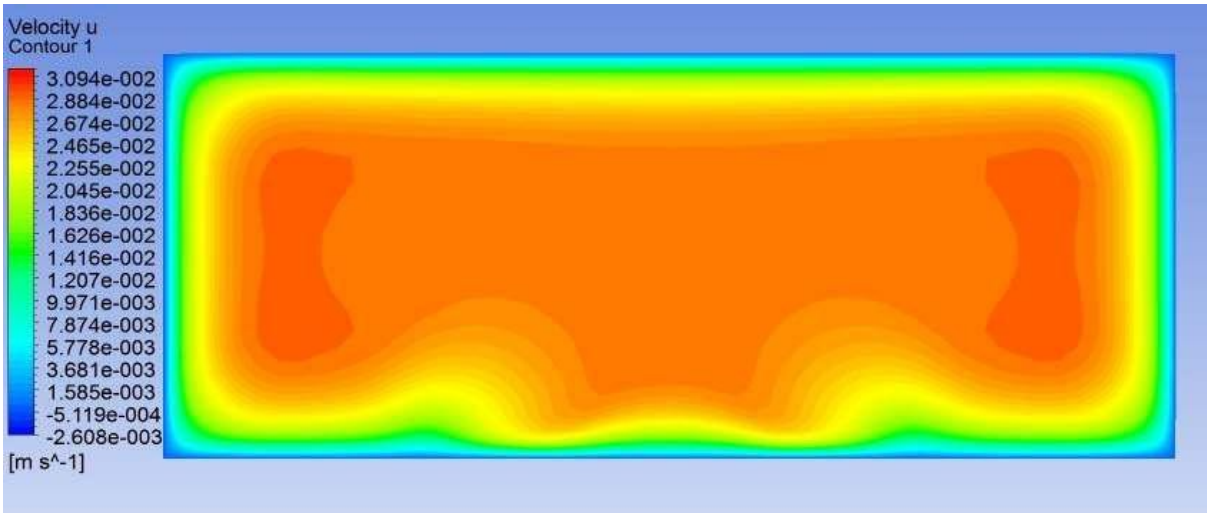

Fig. 5.43 Contours **of u velocity, Re 2400, β** = 30° (yz plane, x=55 cm)

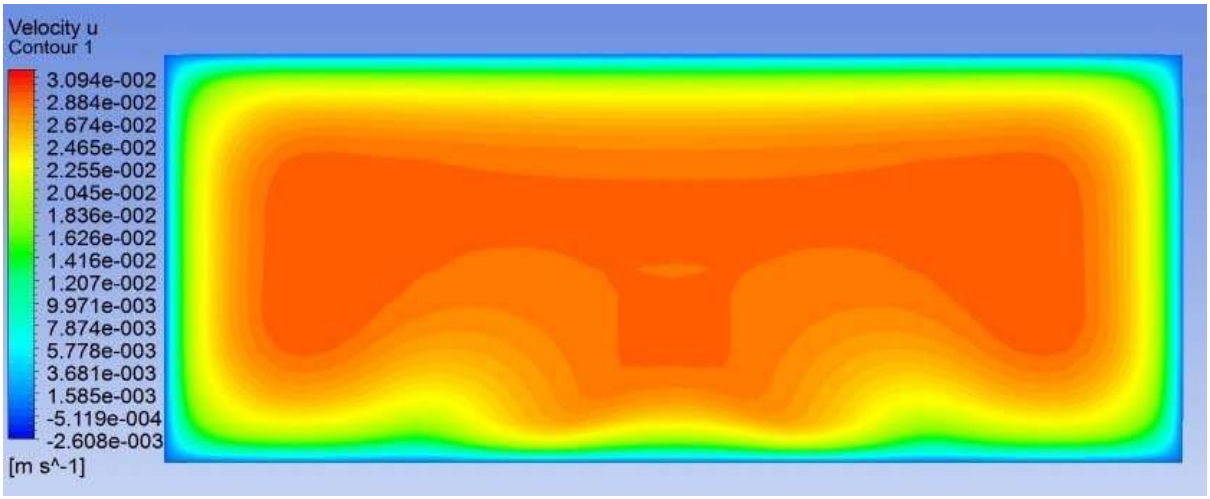

Fig. 5.44 Contours **of u velocity, Re 2400, β** = 30° (yz plane, x=65 cm)

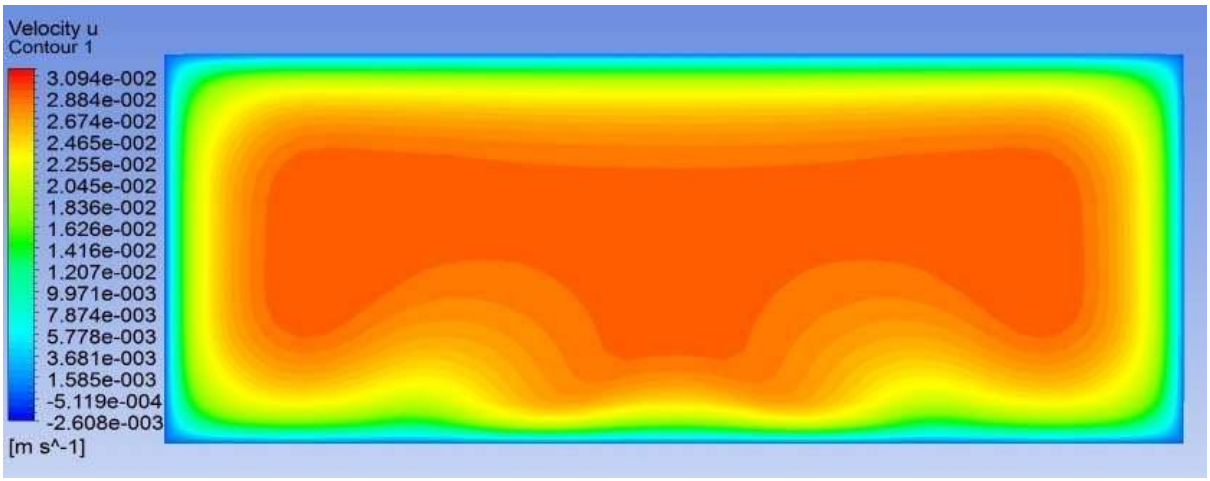

Fig. 5.45 Contours **of u velocity, Re 2400, β** = 30° (yz plane, x=7 0 cm)

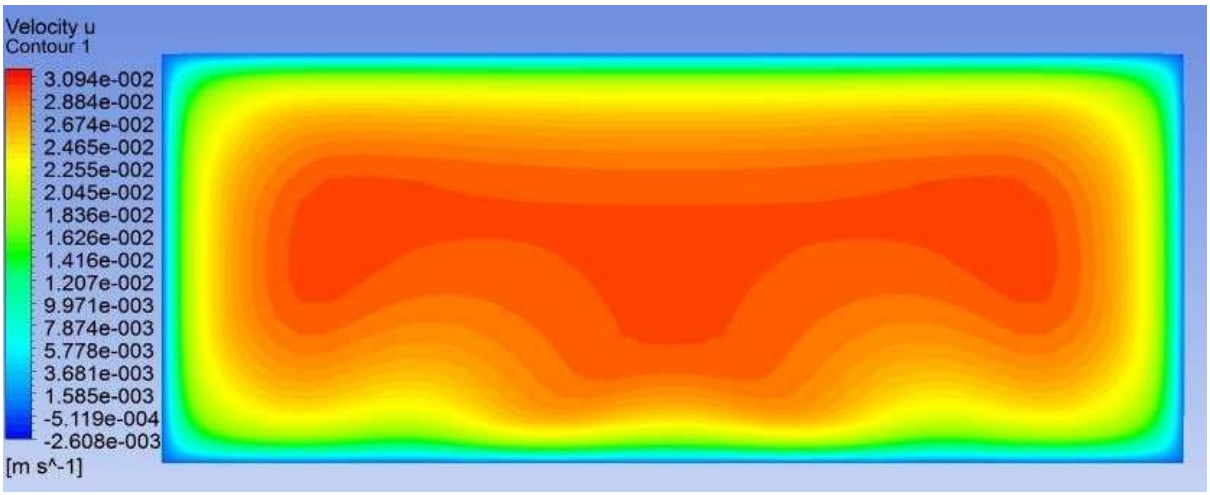

Fig. 5.46 Contours **of u velocity, Re 2400, β** = 30° (yz plane, x=85 cm)

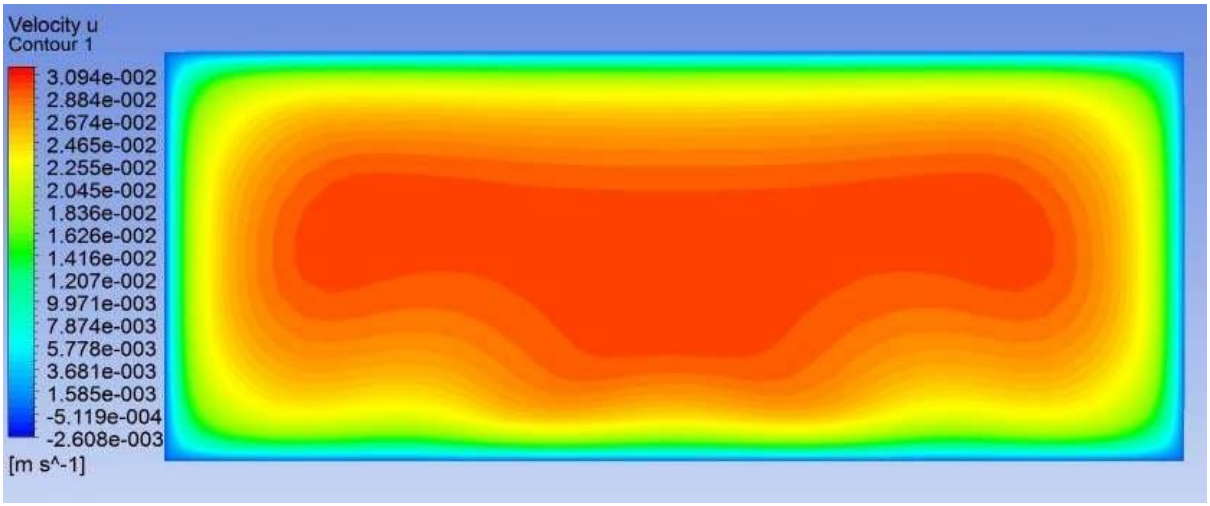

Fig. 5.47 Contours **of u velocity, Re 2400, β** = 30° (yz plane, x=10 0 cm)

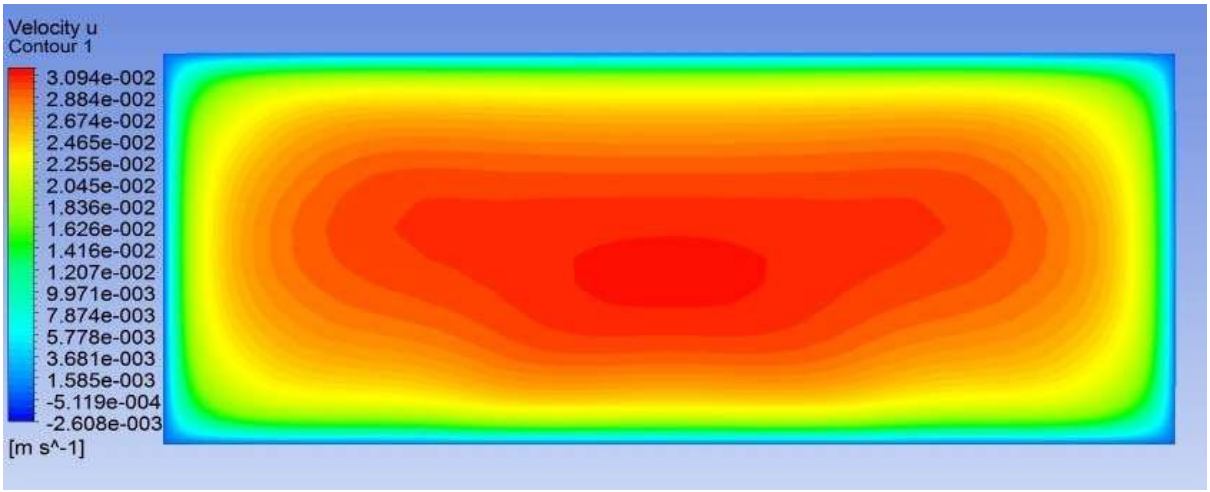

Fig. 5.48 Contours **of u velocity, Re 2400, β** = 30° (yz plane, x=140 cm)

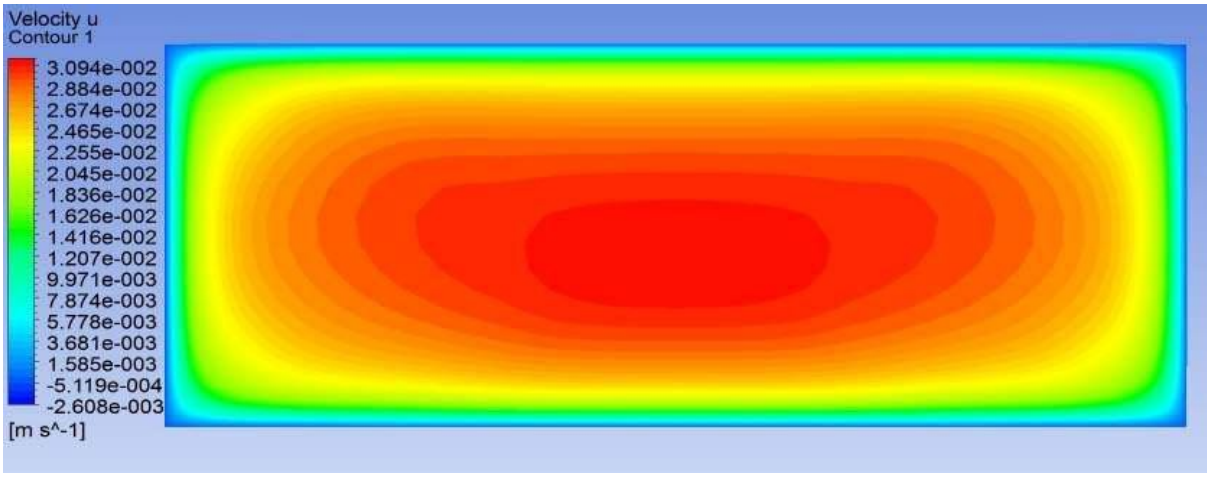

Fig. 5.49 Contours **of u velocity, Re 2400, β** = 30° (yz plane, x=180 cm)

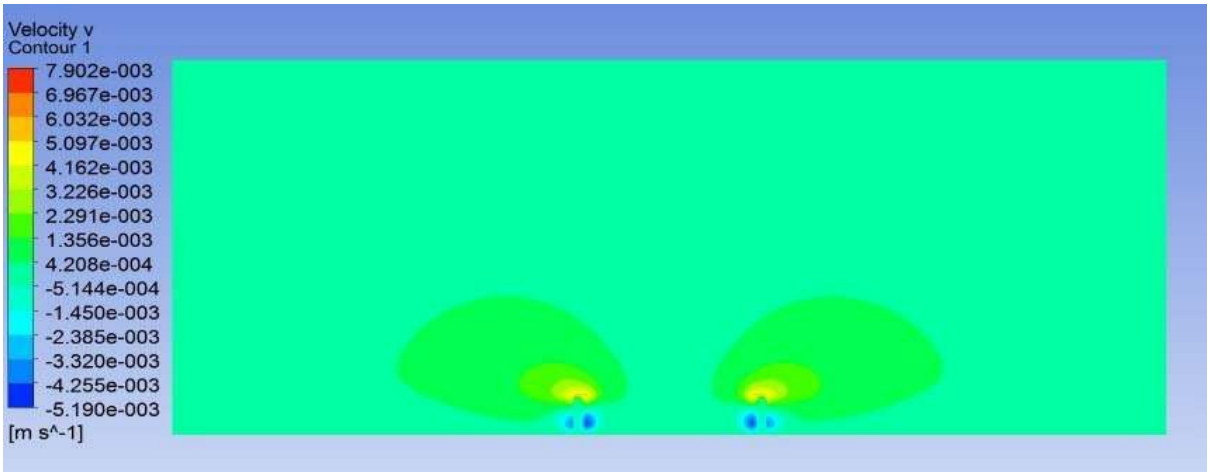

Fig. 5.50 Contours of v **velocity, Re 2400, β = 30 °(** yz plane, x=30 cm)

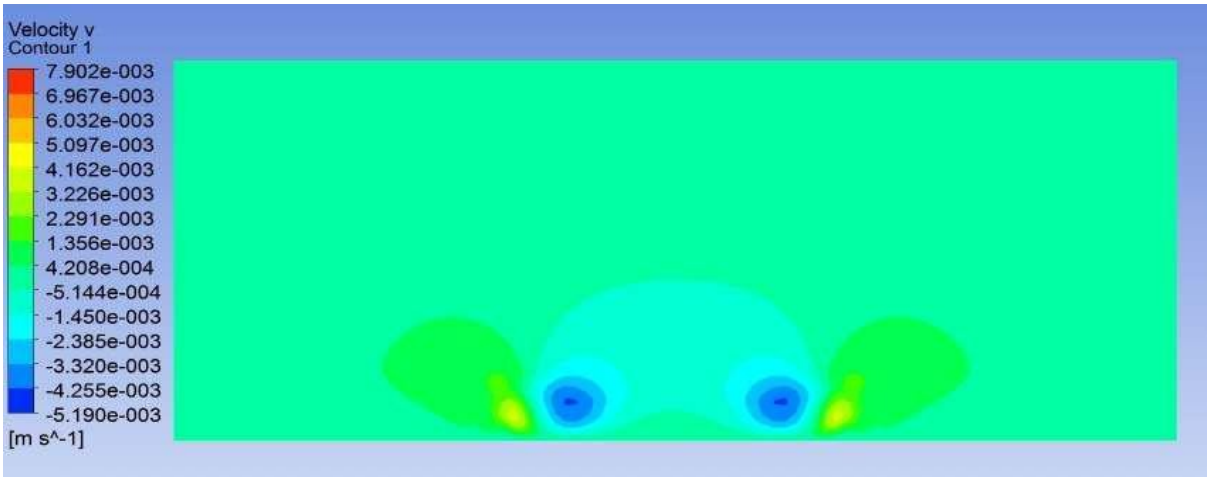

Fig. 5.51 Contours of v **velocity, Re 2400, β = 30 °(** yz plane, x=35 cm)

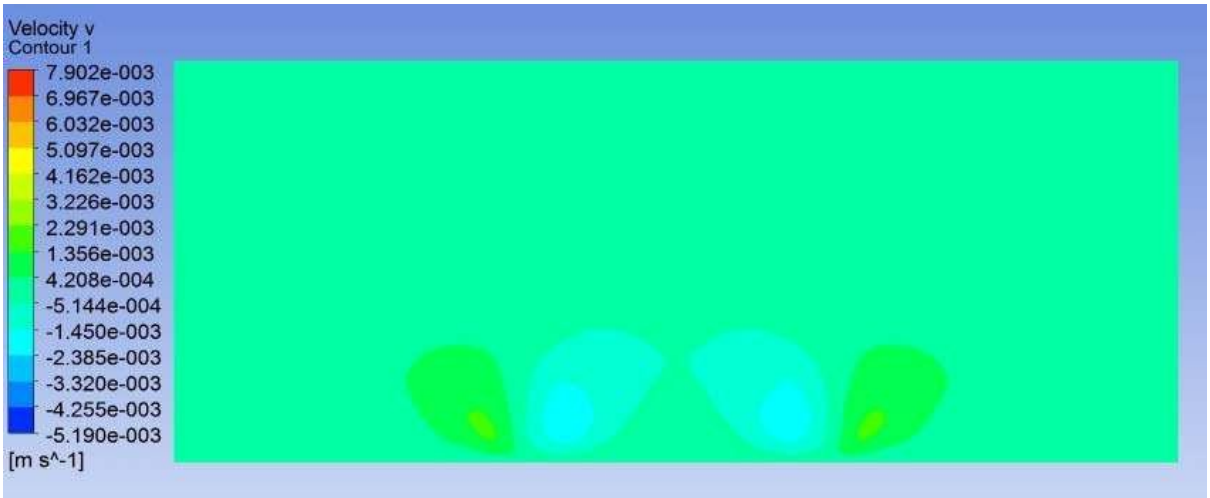

Fig. 5.52 Contours of v **velocity, Re 2400, β** = 30° (yz plane, x=35 cm)

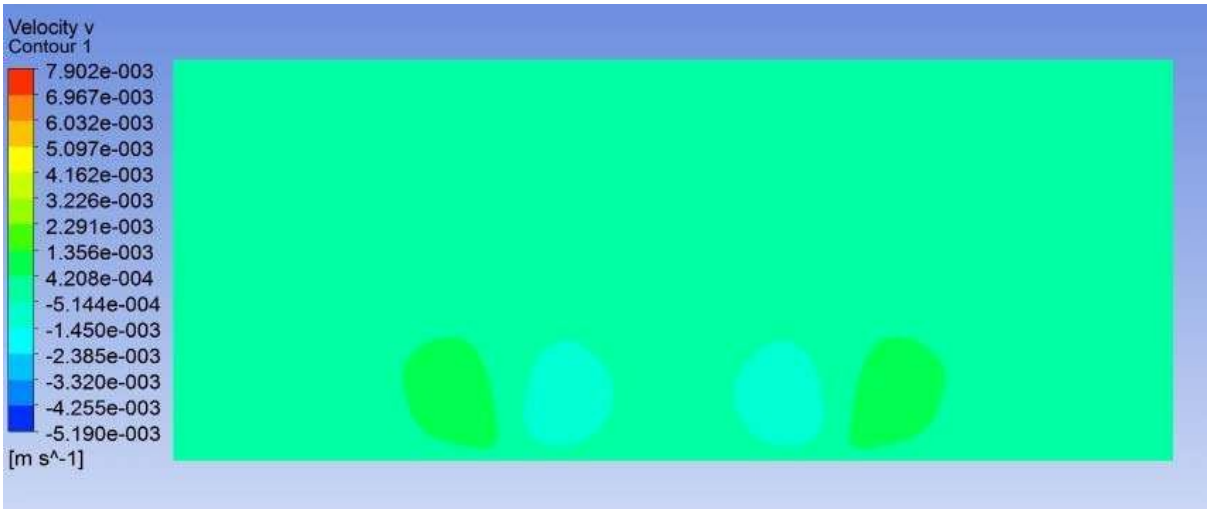

Fig. 5.53 Contours of v **velocity, Re 2400, β** = 30° (yz plane, x=45 cm)

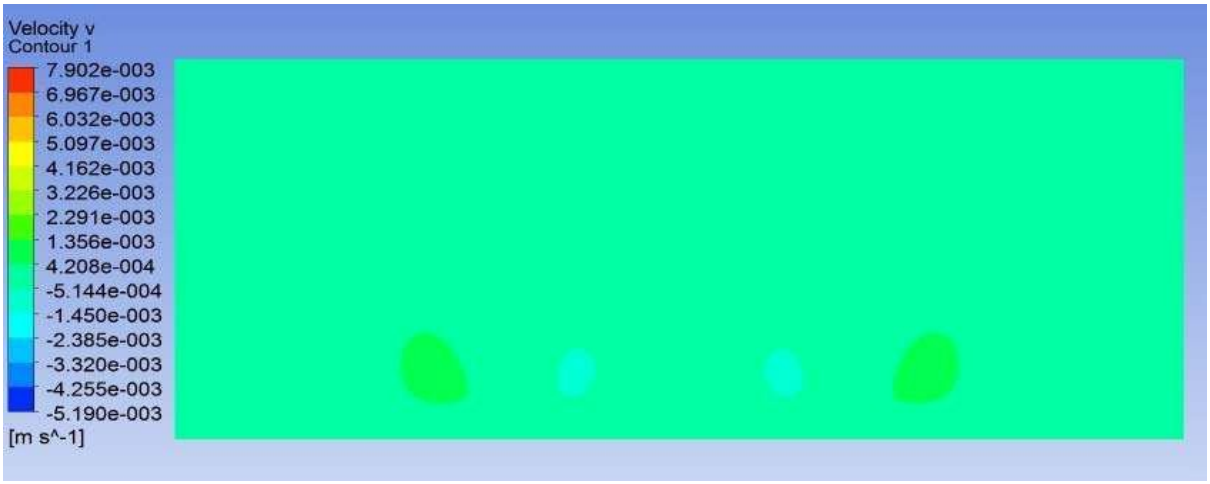

Fig.5.54 Contours of v **velocity, Re 2400, β** = 30° (yz plane, x=60 cm)

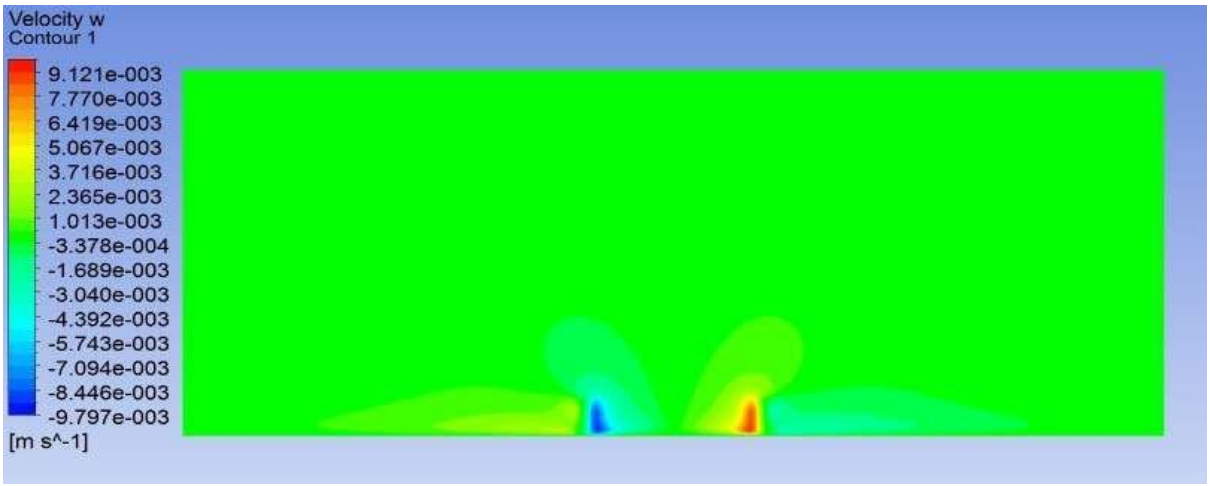

Fig. 5.55 Contours **of w velocity, Re 2400, β = 30 °(** yz plane, x=30 cm)

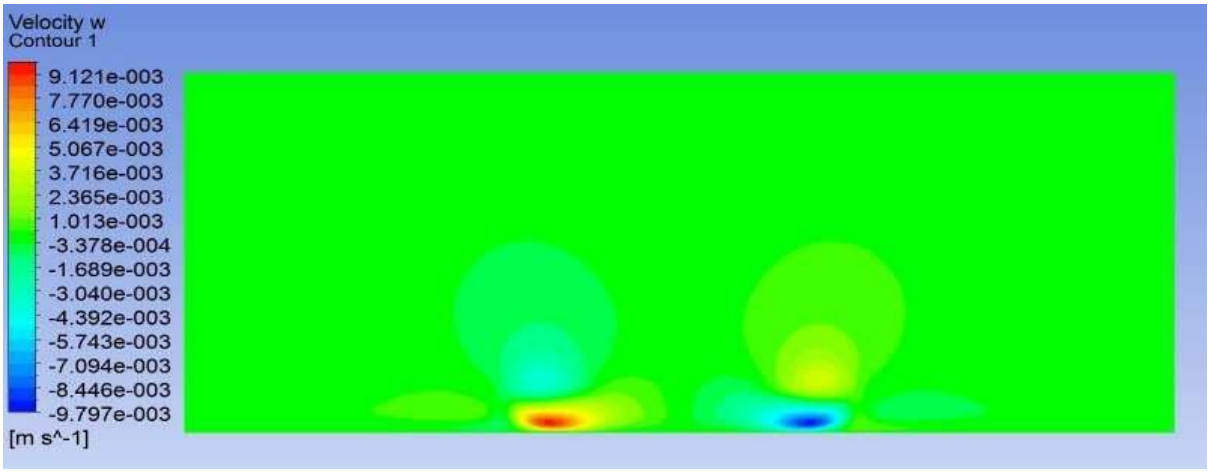

Fig. 5.56 Contours **of w velocity, Re 2400, β = 30 °(** yz plane, x=35 cm)

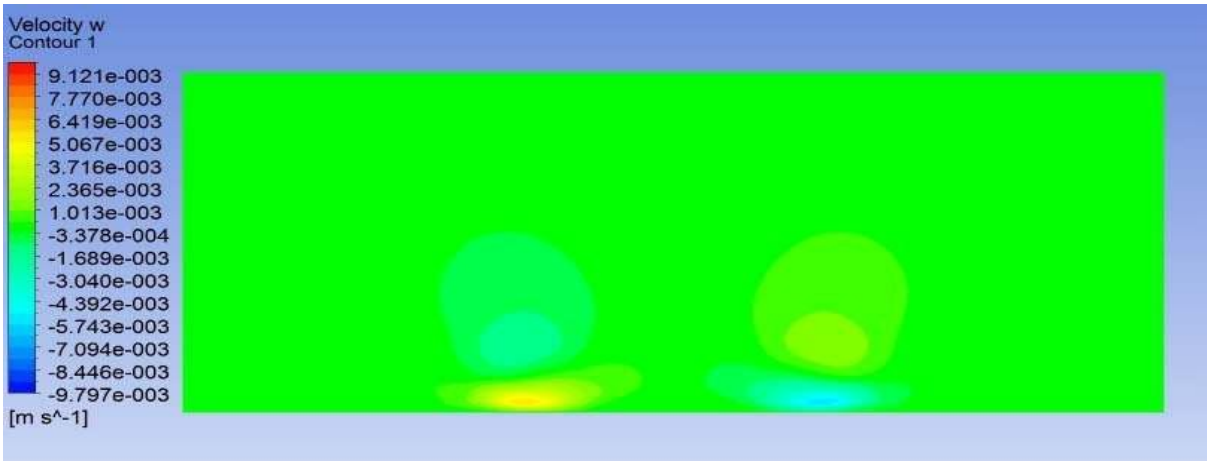

Fig. 5.57 Contours **of w velocity, Re 2400, β = 30 °(** yz plane, x=40 cm)

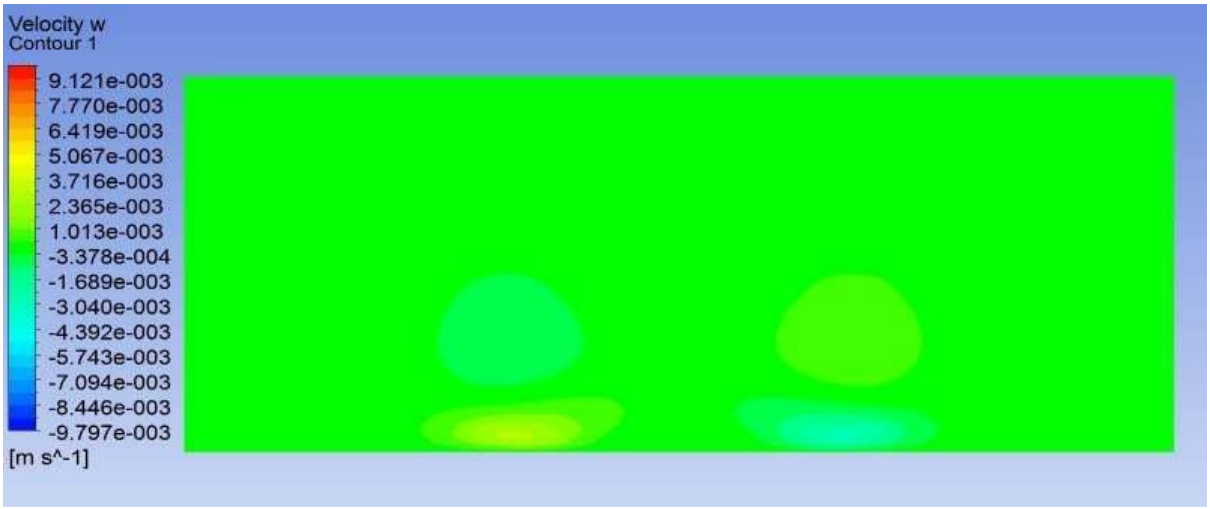

Fig. 5.58 Contours **of w velocity, Re 2400, β = 30 °(** yz plane, x=50 cm)

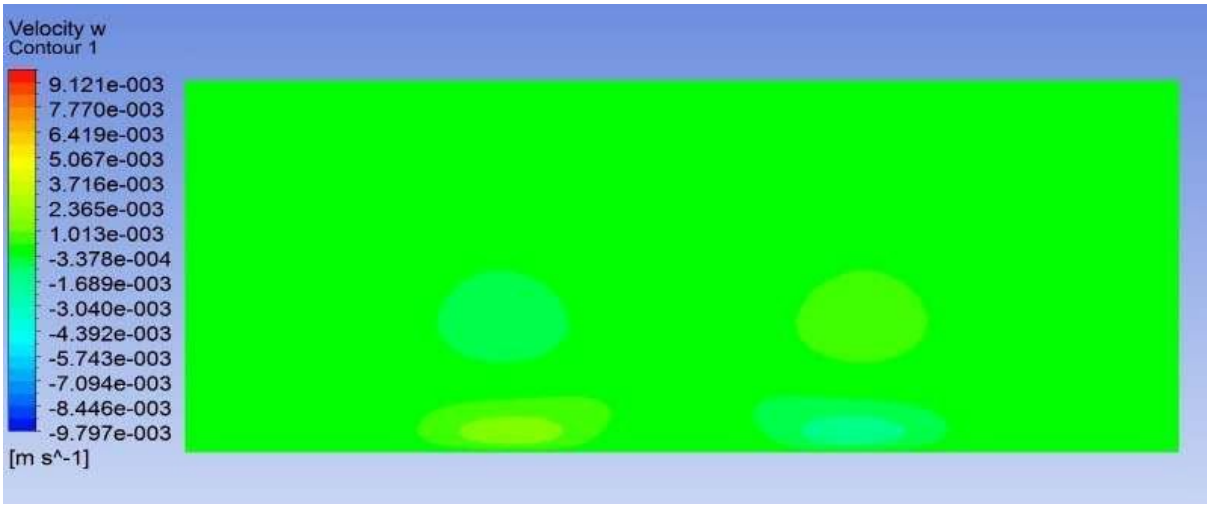

Fig. 5.59 Contours **of w velocity, Re 2400, β** = 30° (yz plane, x=60 cm)

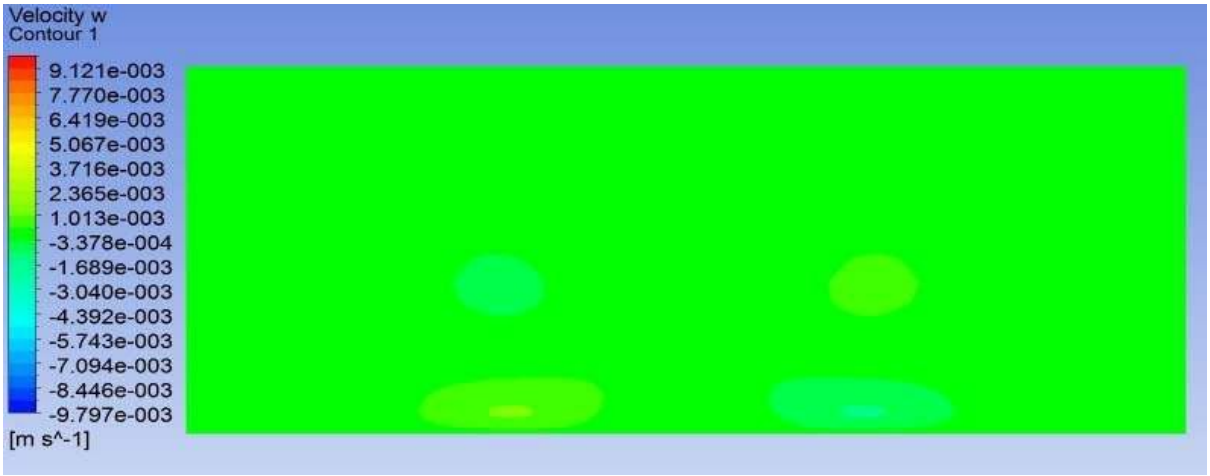

Fig. 5.60 Contours **of v velocity, Re 2400, β** = 30° (yz plane, x=70 cm)

Fig. 5.61 Contours **of v velocity, Re 2400, β = 30 °(yz plane, x=60 cm)**

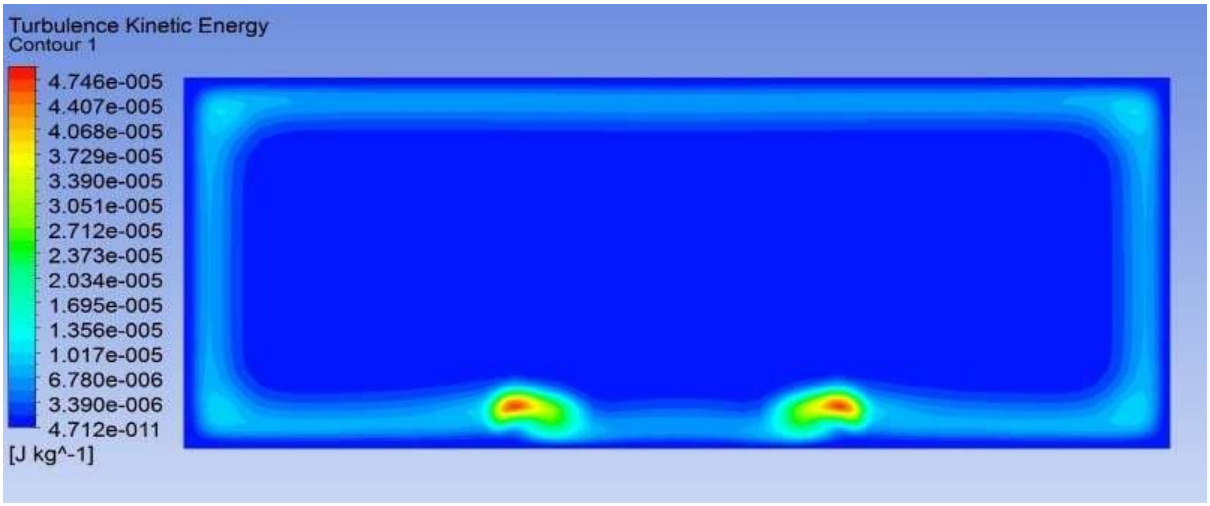

Fig. 5.62 Contours **of turbulent kinetic energy, Re 2400, , β = 30 °(** yz plane, x=35 cm)

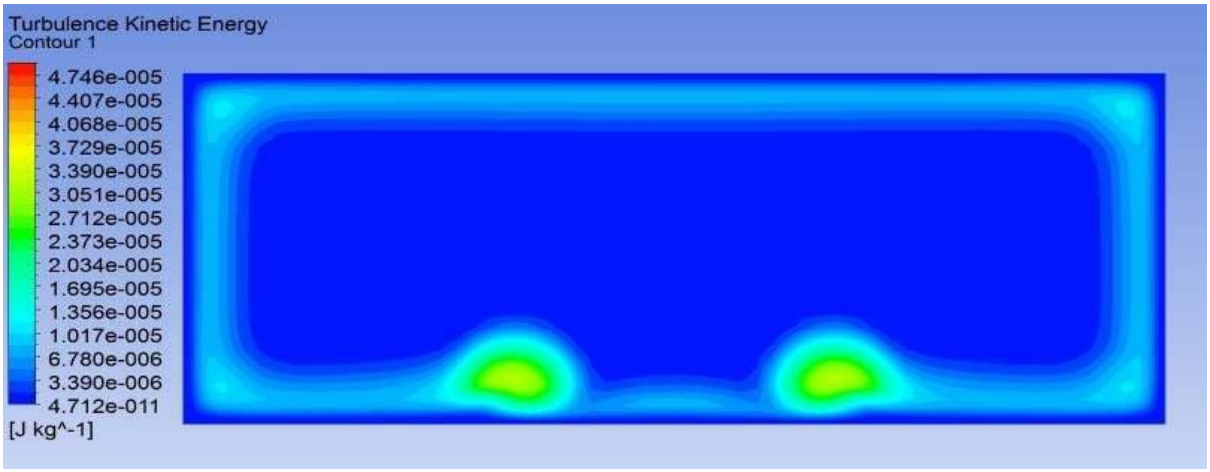

Fig. 5.63 Contours **of turbulent kinetic energy, Re 2400, , β = 30 °(** yz plane, x=40 cm)

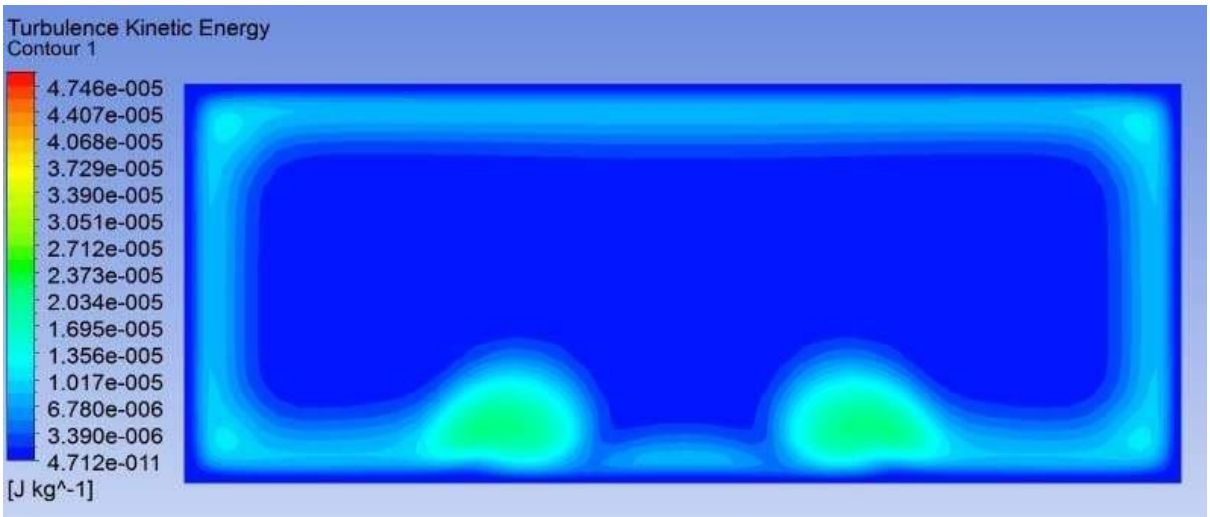

Fig. 5.64 Contours **of turbulent kinetic energy, Re 2400, , β = 30 °(** yz plane, x=45 cm)

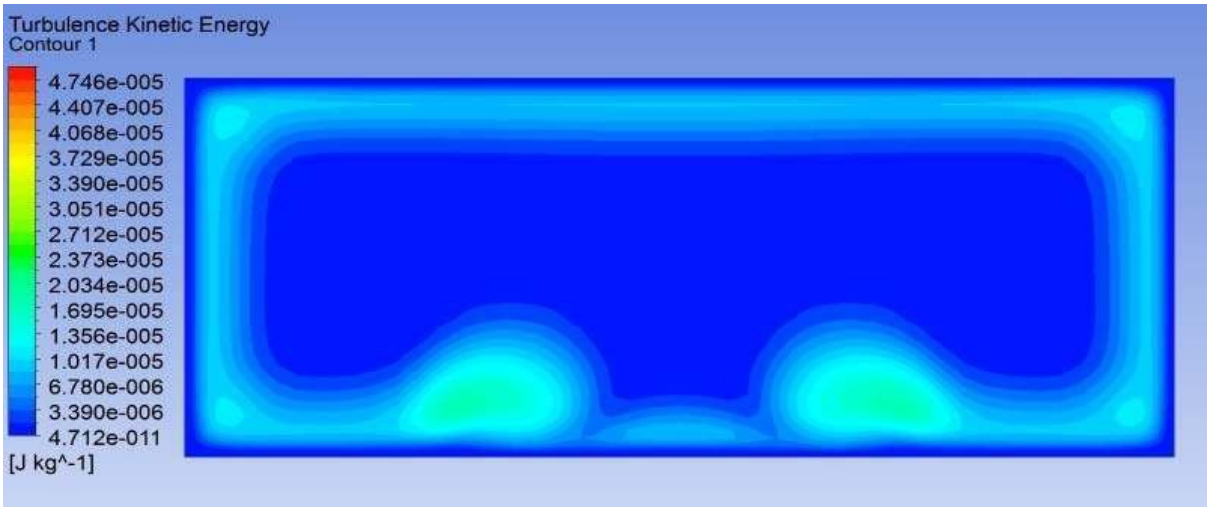

Fig. 5.65 Contours **of turbulent kinetic energy, Re 2400, , β = 30 °(** yz plane, x=50 cm)

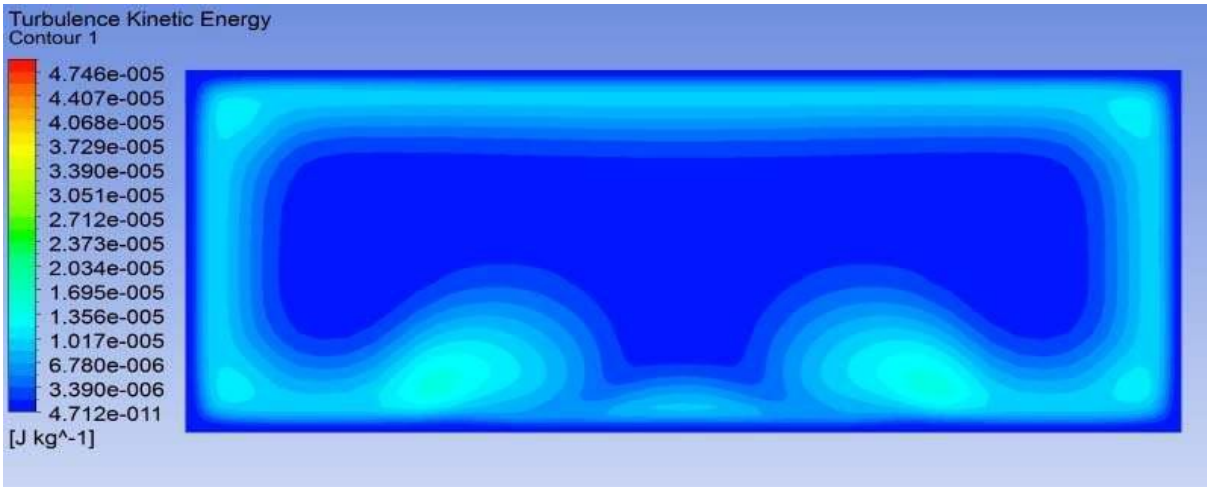

Fig. 5.66 Contours **of turbulent kinetic energy, Re 2400, , β = 30 °(** yz plane, x=60 cm)

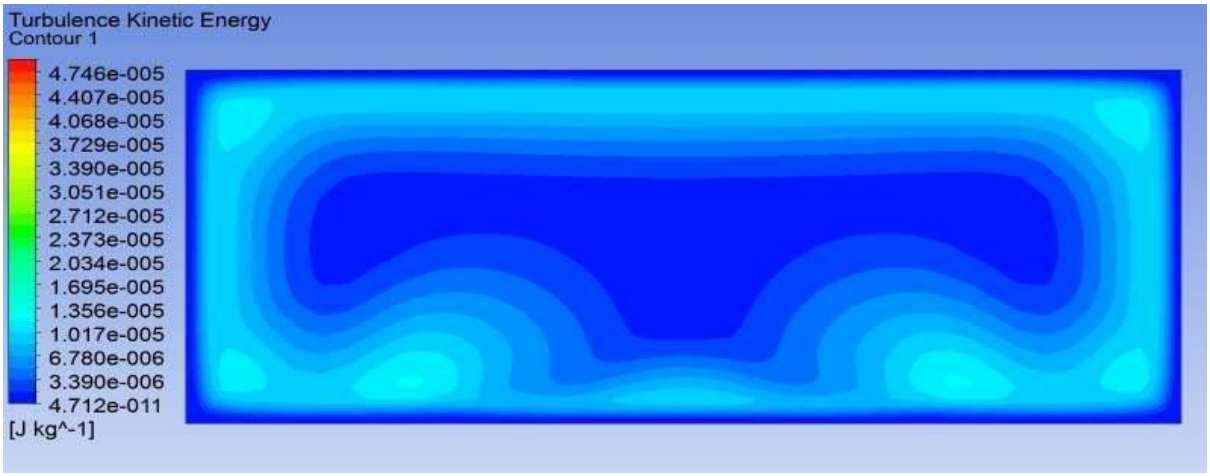

Fig. 5.67 Contours **of turbulent kinetic energy, Re 2400, , β = 30 °(** yz plane, x=80 cm)

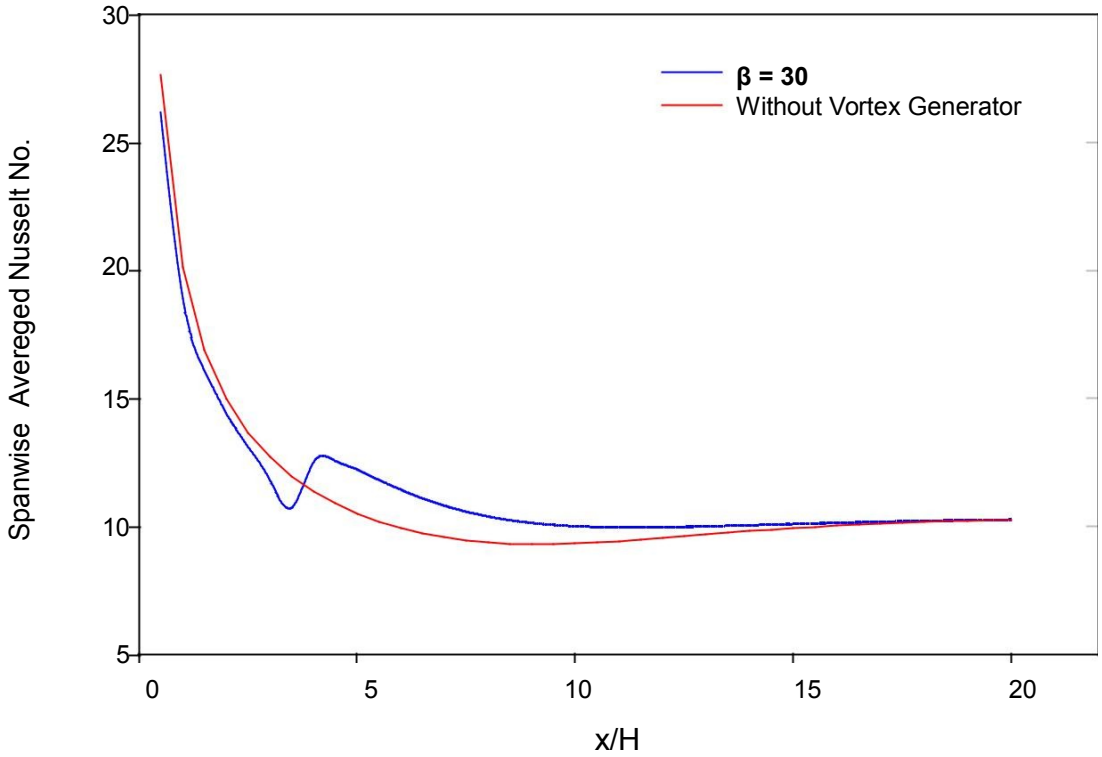

Fig. 5.68 Variation of Spanwise Avereged Nusselt No. at Re 800, **β = 30**

Fig 5.68 to fig. 4.71 show the variation of span wise averaged Nusselt number at Reynolds **no. 800, 1600, 2400, 3200 with β = 30°**. Comparison between the case of 15° and 30° shows that the increase in span wise averaged Nusselt number is greater in case of 30° than the case of 15°. The 30° blade angle cause the greater mixing because the vortices formed are larger than the case of 15°. L arger vortices formed cause the thinning of the thermal boundary layer at the bottom wall than the case of the 15°. This increases the heat transfer from the bottom wall.

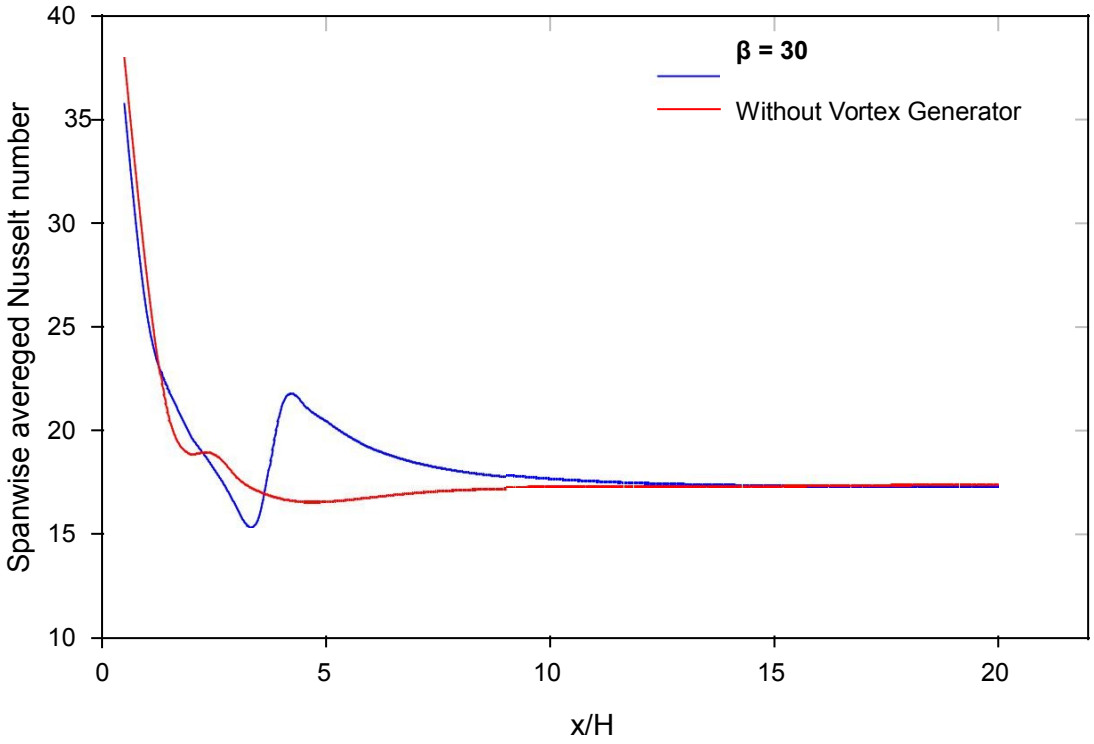

Fig. 5.69 Variation of spanwise avereged Nusselt number at Re 1600, **β = 30**

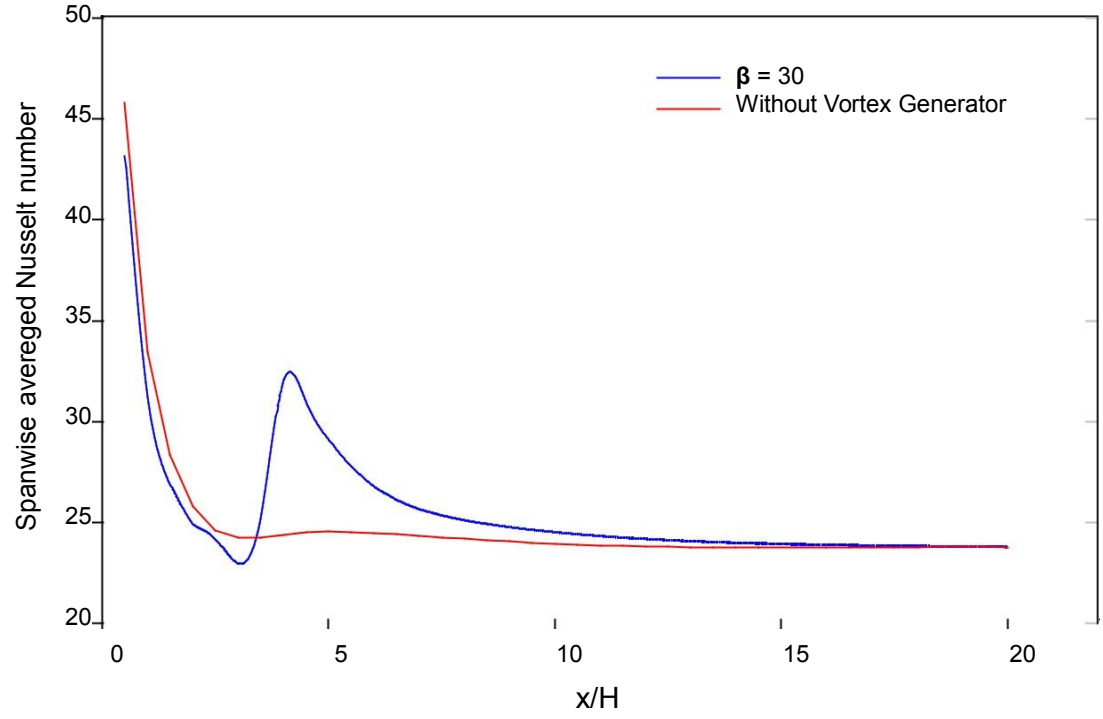

Fig. 5. 70 Variation of spanwise avereged Nusselt number at Re 2400, **β = 30**

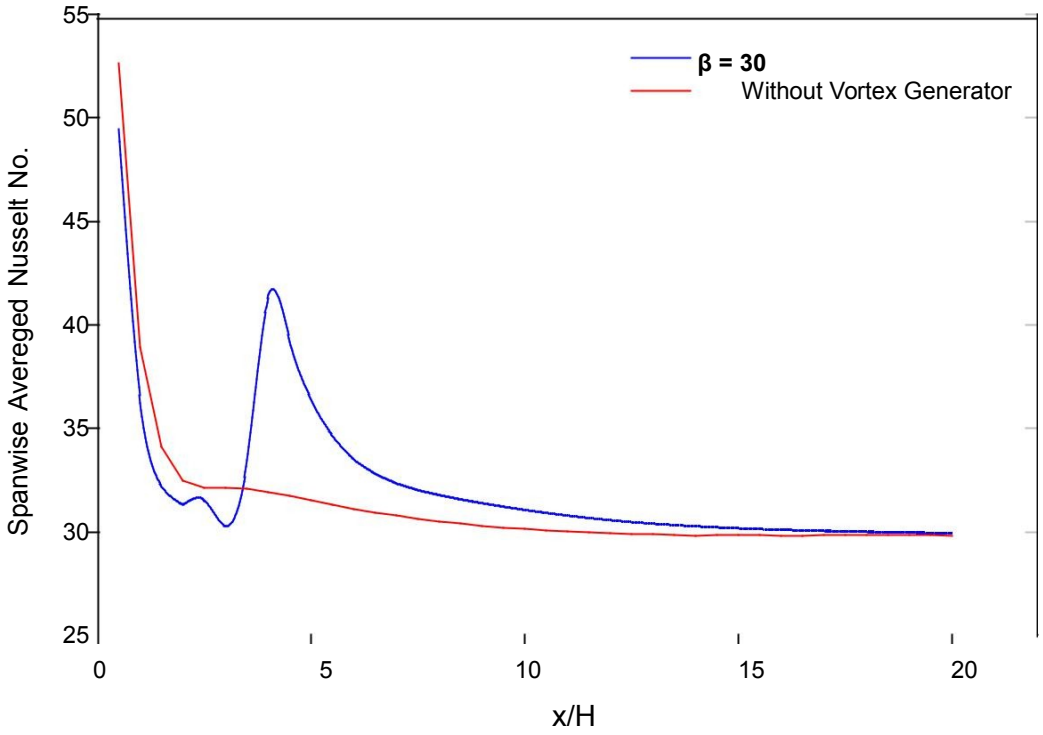

Fig. 5.71 Variation of Spanwise Avereged Nusselt No. at Re 3200, **β = 30**

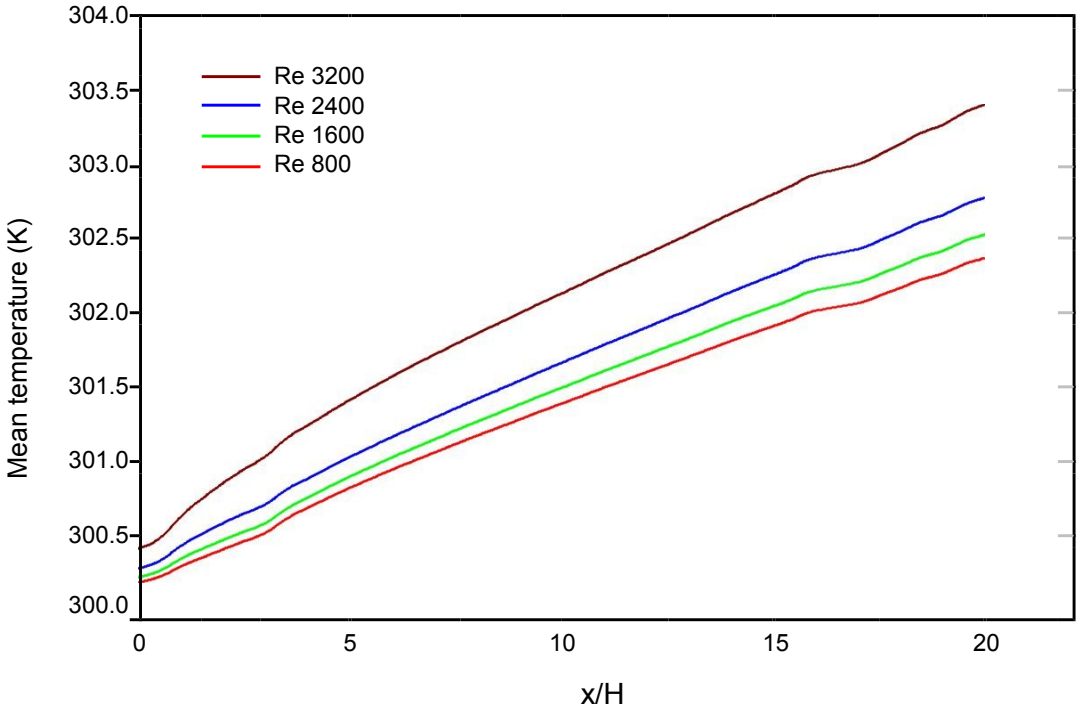

Fig. 5.72 Variation of mean temperature, **β = 30**

Fig.5.72 shows the mean temperature variation along the x/H at Reynolds number of 800, 1600, 2400, and 3200 with 30° blade angle. Just after the vortex generators the increase in mean temperature at these Reynolds number is found greater than the case of 15° blade angle between at the same Reynolds number.

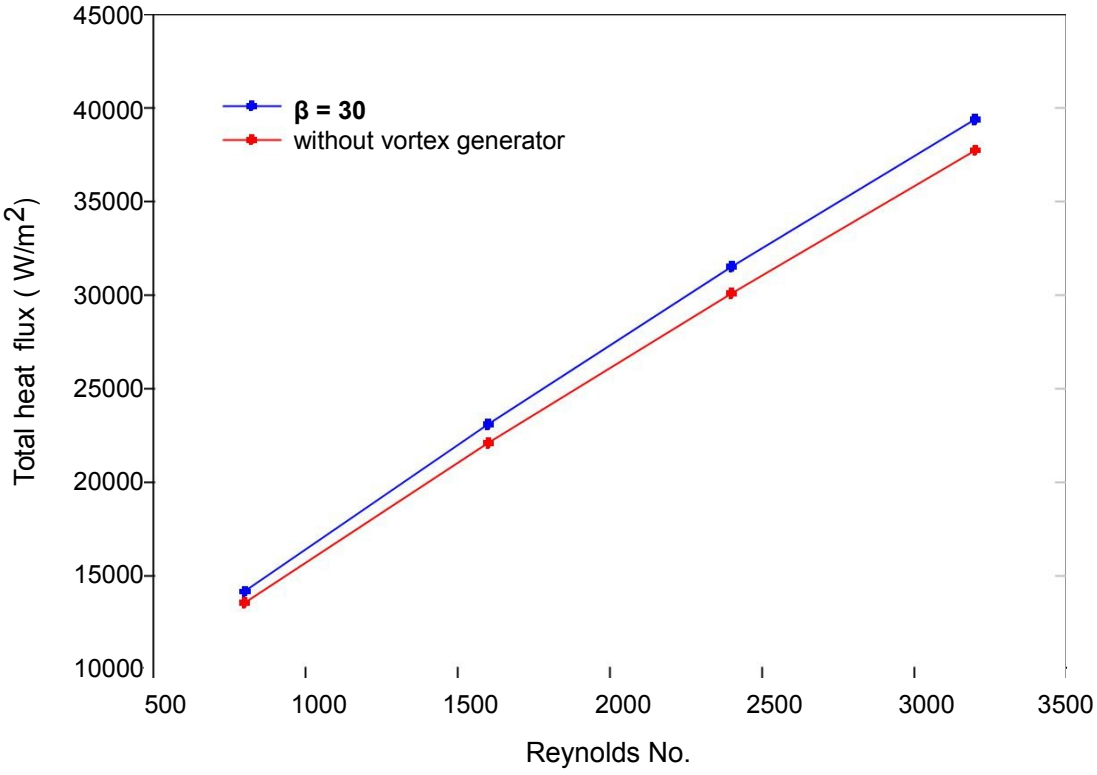

Fig. 5.73 Variaton of wall heat flux with reynolds no., **β = 30**

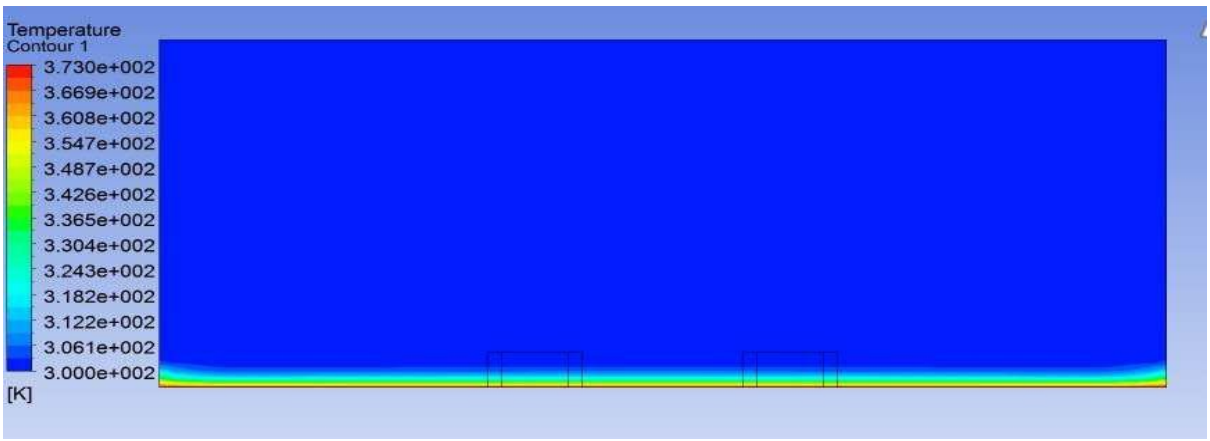

Fig. 5.74 Contours of temperature at R**e 3200,β = 30°** (yz plane, x = 20cm)

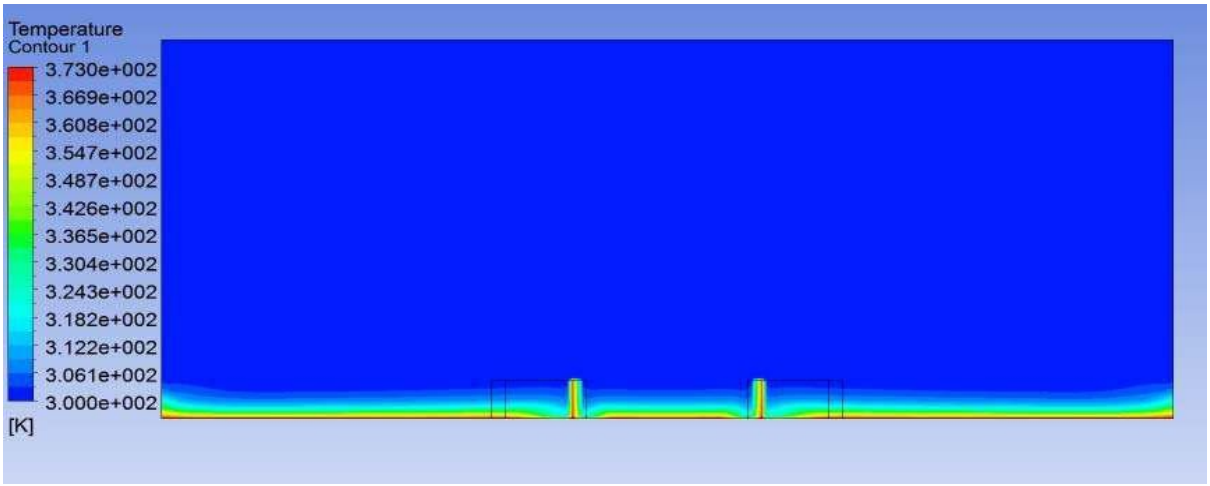

.Fig. 5.75 Contours of temperature at R**e 3200,β = 30°** (yz plane, x = 30cm)

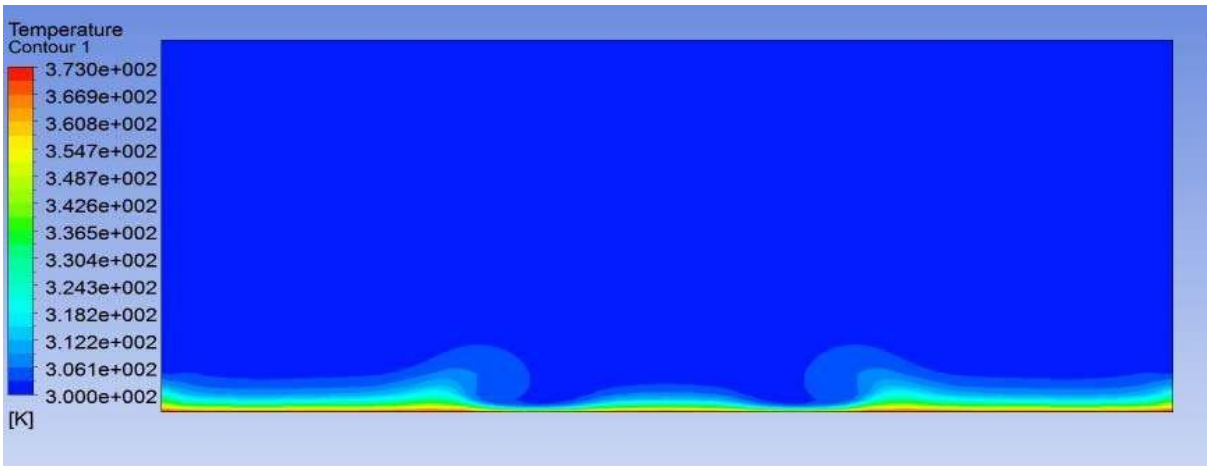

Fig. 5.76 Contours of temperature at R**e 3200,β = 30°** (yz plane, x = 40cm)

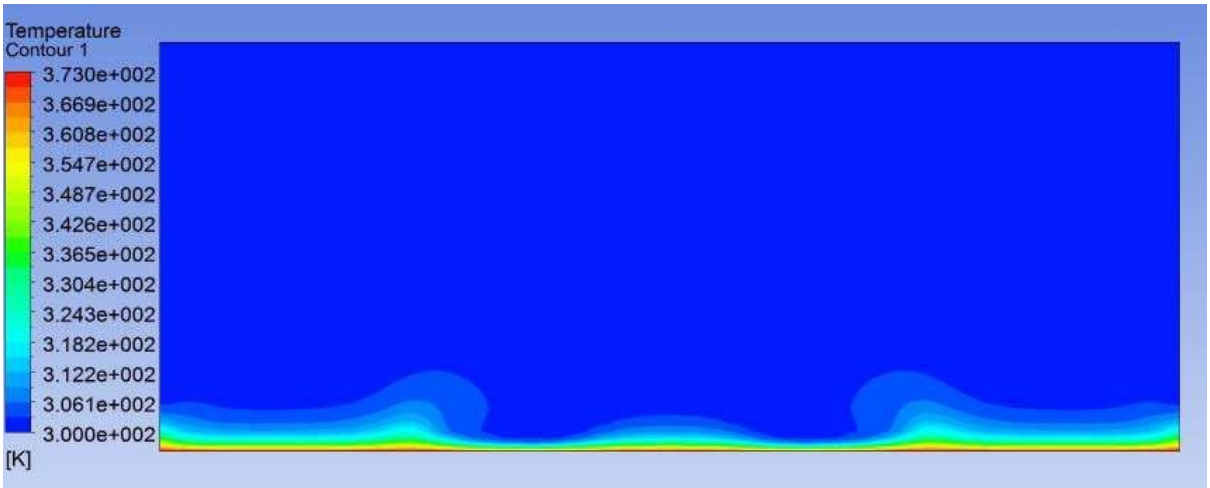

. Fig. 5.77 Contours of temperature at Re 3200, **β = 30°** (yz plane, x = 50cm)

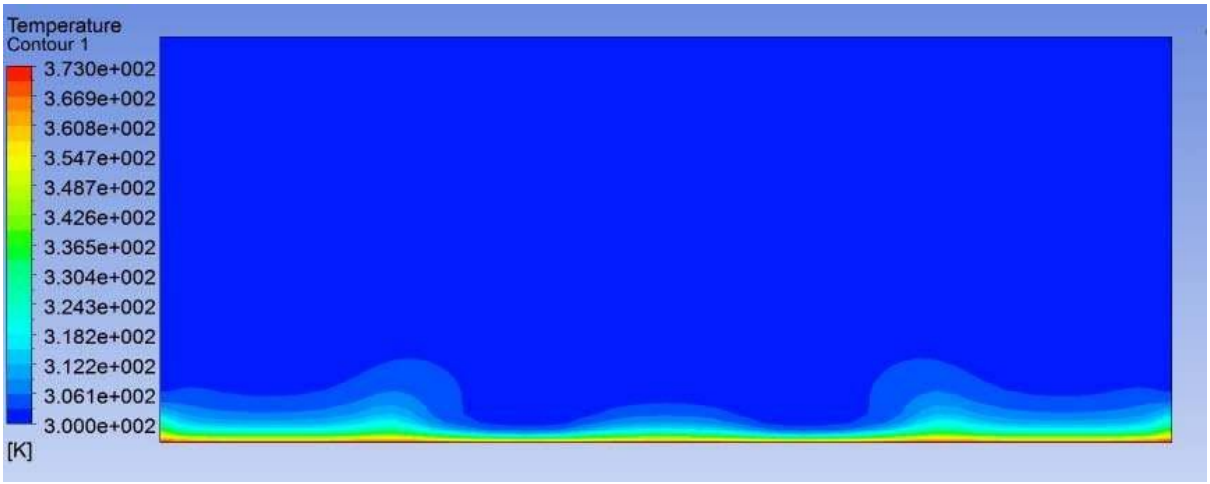

. Fig. 5.78 Contours of temperature at Re 3200, **β = 30°** (yz plane, x = 60cm)

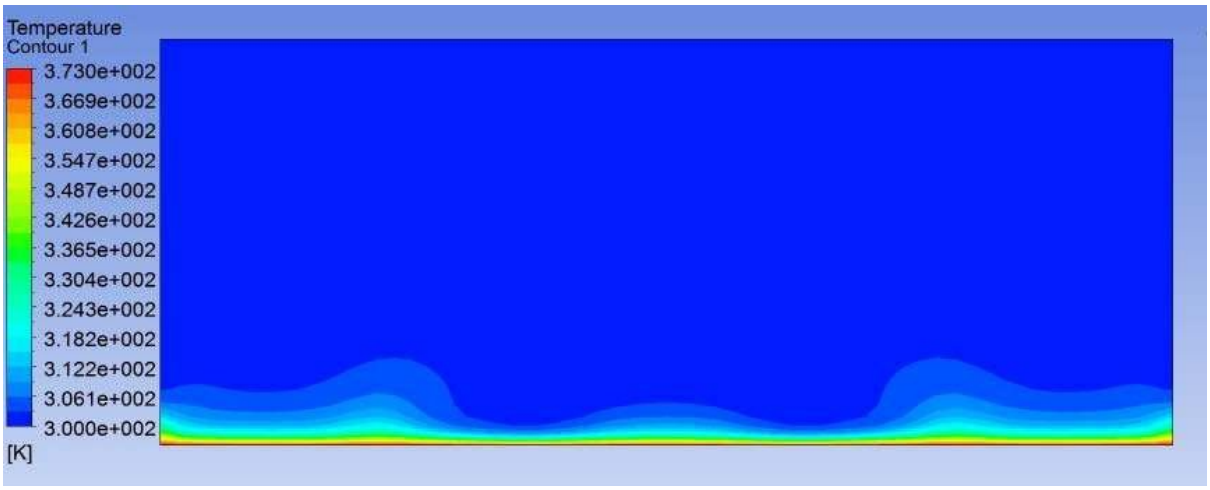

Fig. 5.79 Contours of temperature at R**e 3200,β = 30°** (yz plane, x = 70cm)

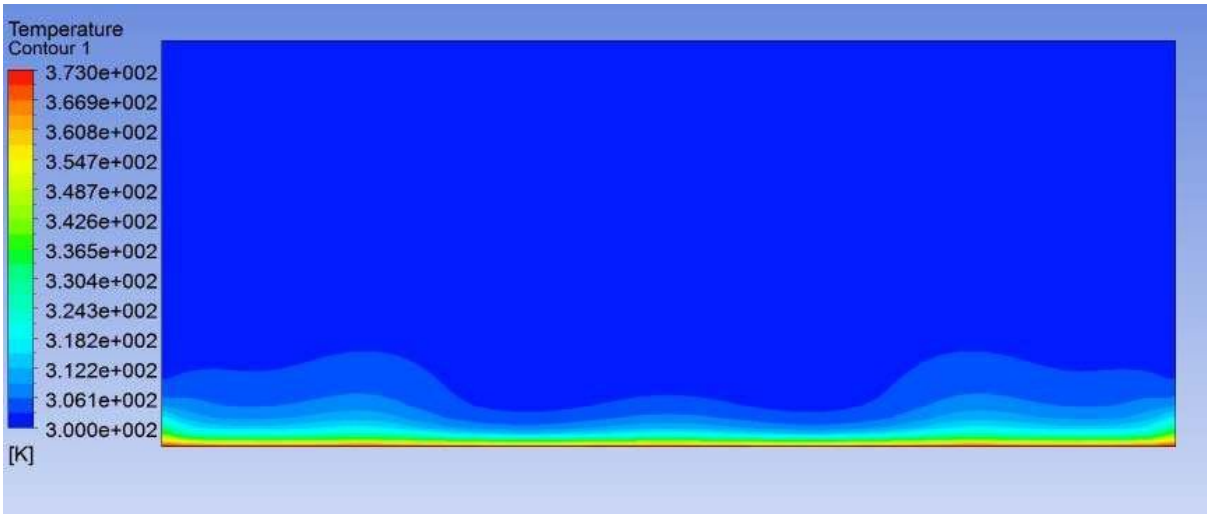

Fig. 5.80 Contours of temperature at R**e 3200,β = 30°** (yz plane, x = 80cm)

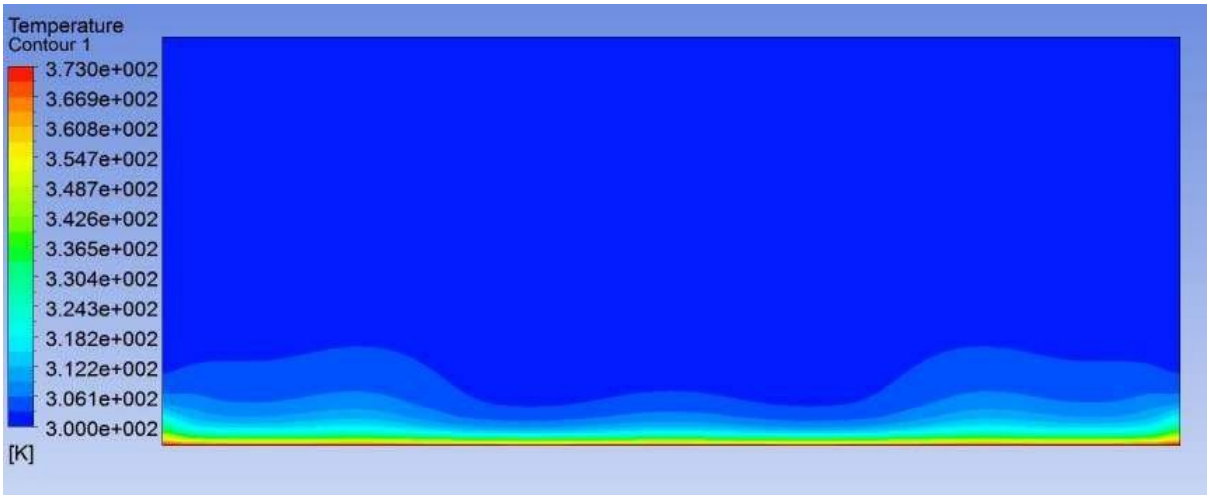

. Fig. 5.81 Contours of temperature at R**e 3200,β = 30°** (yz plane, x = 90cm)

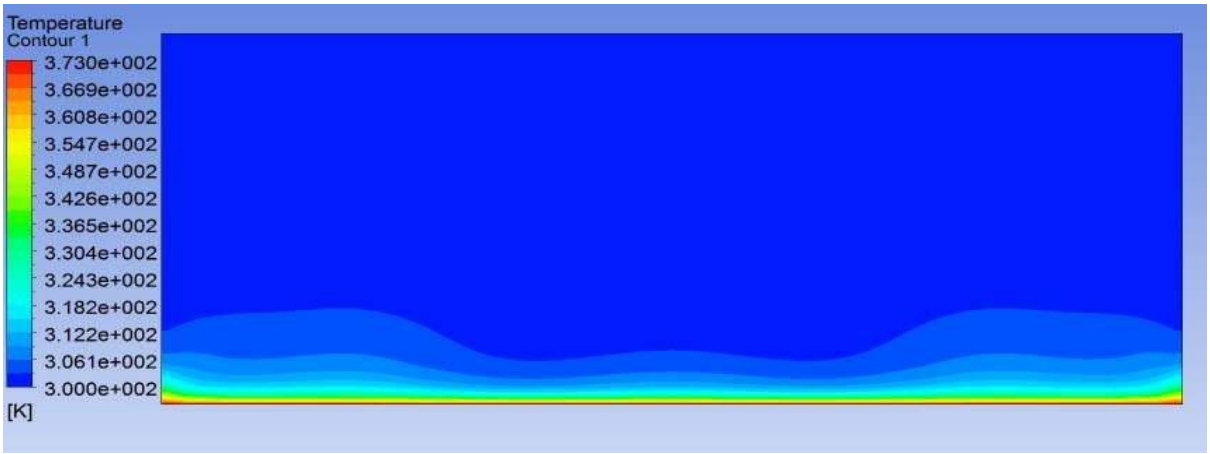

Fig. 5.82 Contours of temperature at Re 3200, **β = 30°** (yz plane, x = 110cm)

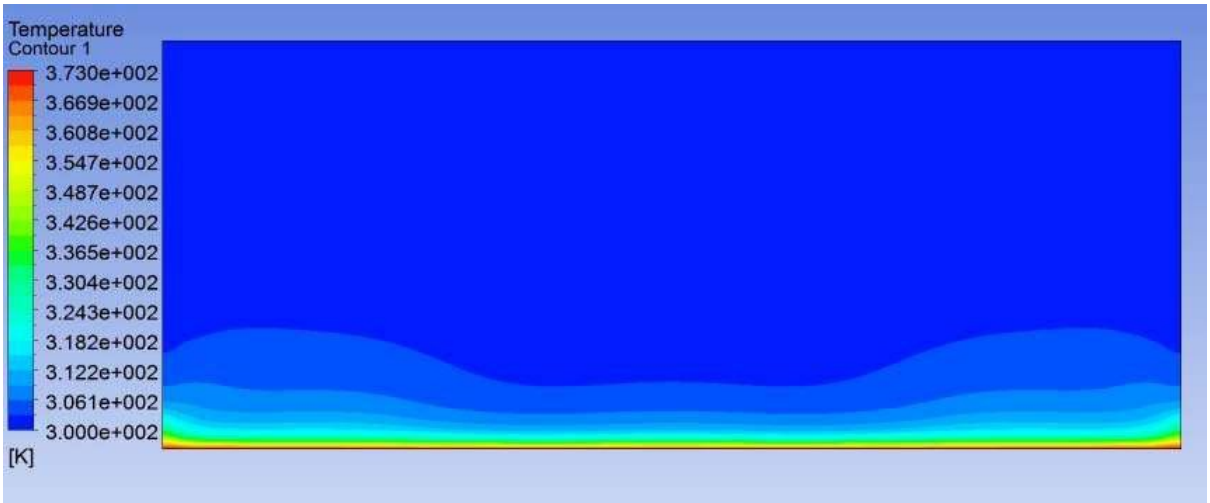

Fig. 5.83 Contours of temperature at Re 3200, **β = 30°** (yz plane, x = 110cm)

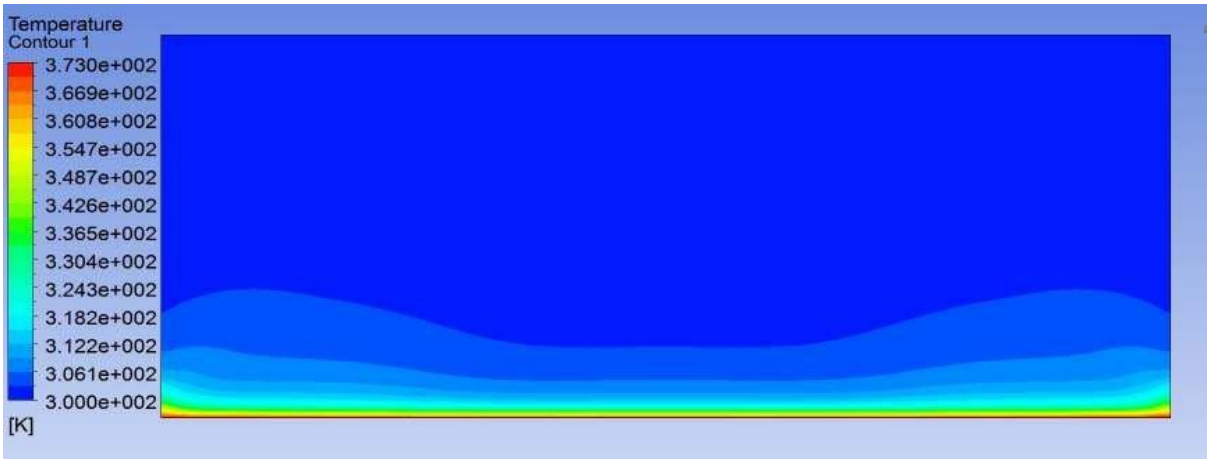

Fig. 5.84 Contours of temperature at R**e 3200,β = 30°** (yz plane, x =190cm)

Fig. 5.74 to fig. 5.84 show the effect of vortex generators on the temperature distribution along the x. the vortex formation causes the heat from the bottom wall to distribute in the bulk fluid and hence increase the temperature of the fluid away from the bottom wall. But when the vortex strength decreases after a certain distance of x, the temperature contours show that the temperature near the bottom wall is much higher than the bulk fluid away from the wall. So the temperature gradient near the bottom wall decrease that is way the span wise averaged Nusselt no. decrease after that certain distance of x and is higher where the vortex strength is higher

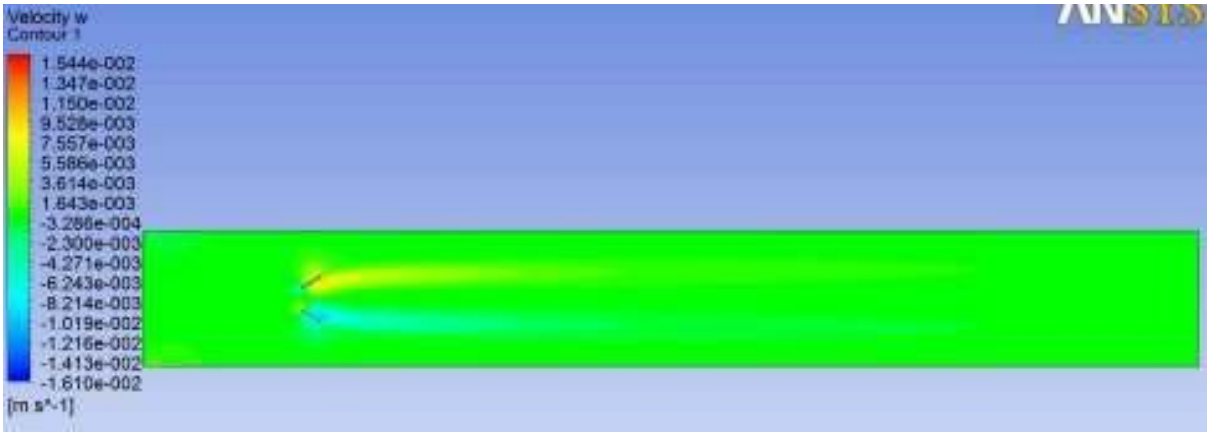

Fig. 5.85 Contours of w velocity (xz plane, y = .5 cm**) at Re 3200, β = 30°**

Fig. 5.85 **shows that the strength of the vortices is greater in the case of β = 30° than the case of β =** 15° as the contour of w velocity shows at both sides of the vortex generators the strength of w velocity is higher than the case of 15°.

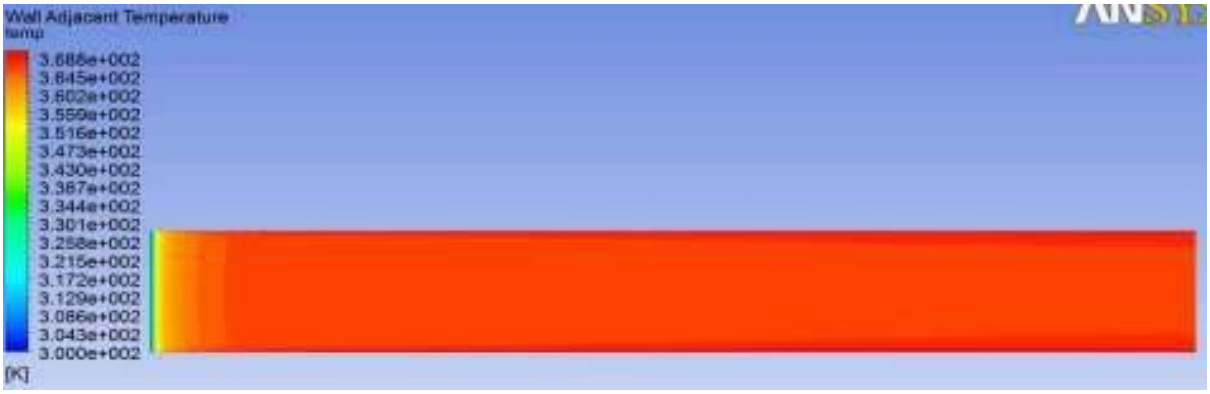

Fig. 5.86 Contours of wall adjacent temperature, Re 2400, without vortex generators

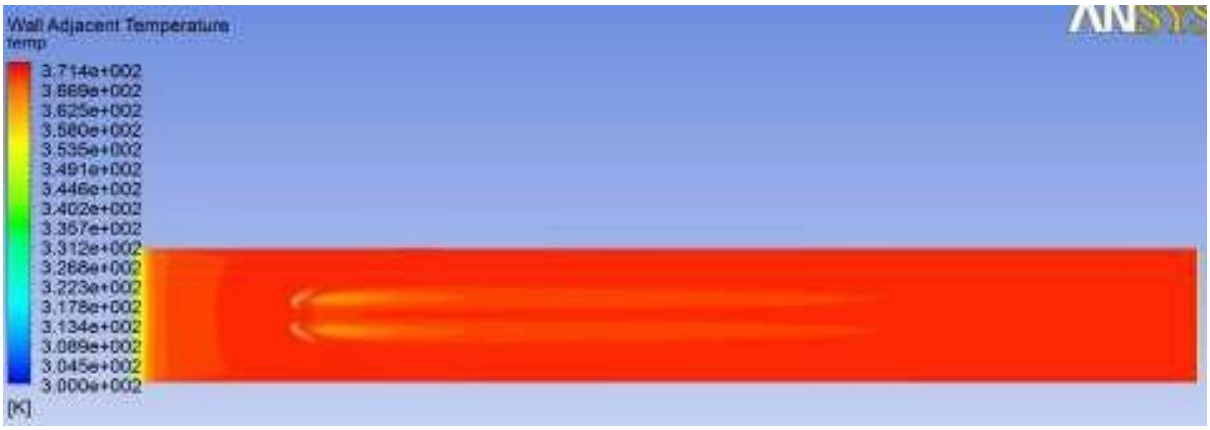

Fig. 5.87 Contours **of wall adjacent temperature, Re 2400, β = 30°**

Fig. 5.88 Contours of wall adjacent temperature, Re 3200, without vortex generators

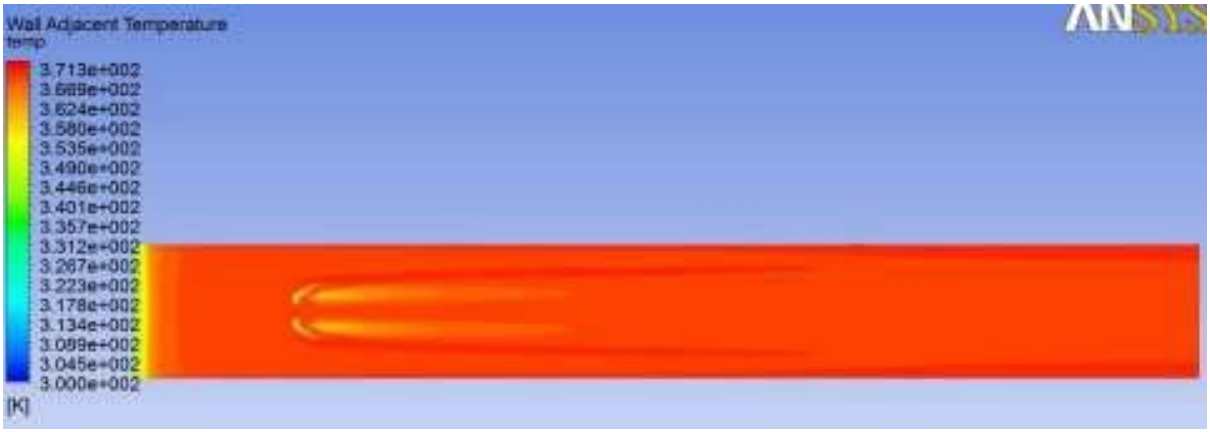

Fig. 5.89 Contours of wall adjacent t**emperature, Re 3200, β = 30°**

Fig 5.86 to Fig. 5.89 show the comparison of the wall adjacent temperature at Reynolds no of 2400 and 3200 with vortex generators at 30° and without vortex generators. This case of 30° is more effective than the previous case of 15°. The 30° blade angle is more able to reduce the bottom wall adjacent temperature. So the heat flux from the bottom wall is more than the case of 15°.

5.3 Analysis of performance of vortex generator with 45° blade angle at Reynolds number 800, 1600, 2400 and 3200.

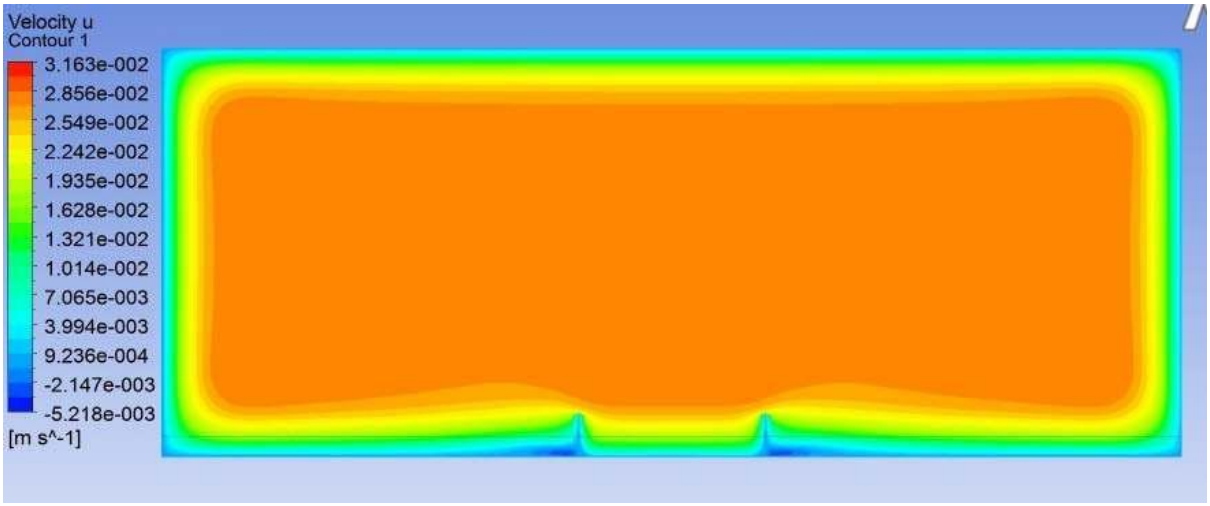

Fig. 5.90 Contours **of u velocity, Re 2400, β = 45°** (yz plane, x=30cm)

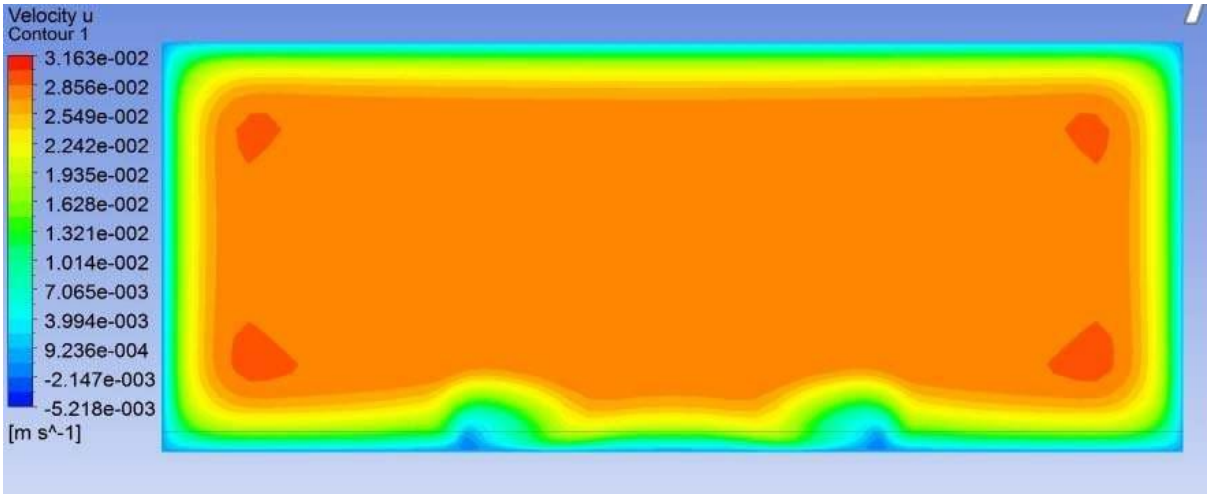

Fig. 5.91 Contours **of u velocity, Re 2400, β = 45°** (yz plane, x=35cm)

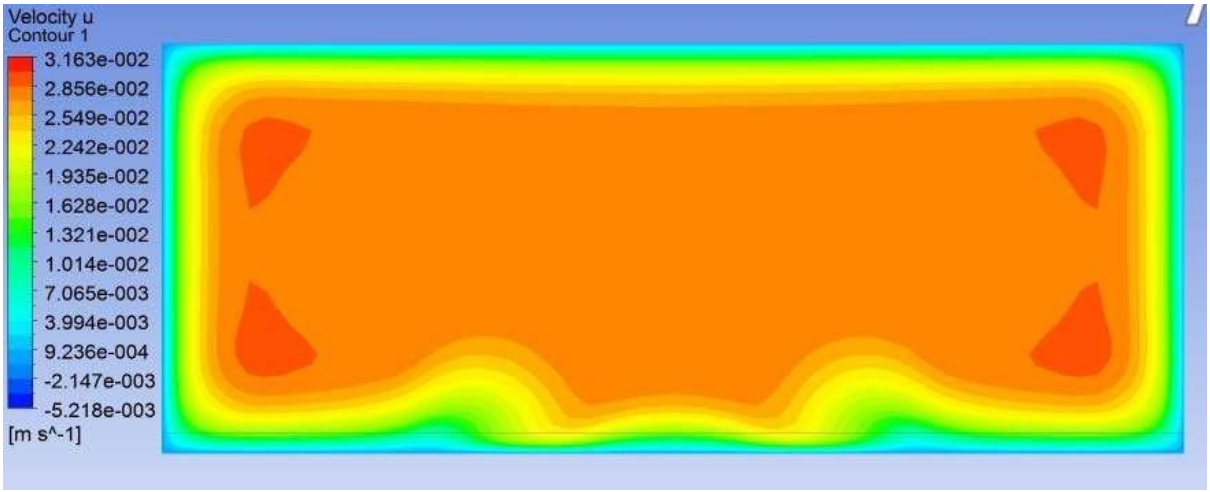

Fig. 5.92 Contours **of u velocity, Re 2400, β = 45°** (yz plane, x=40cm)

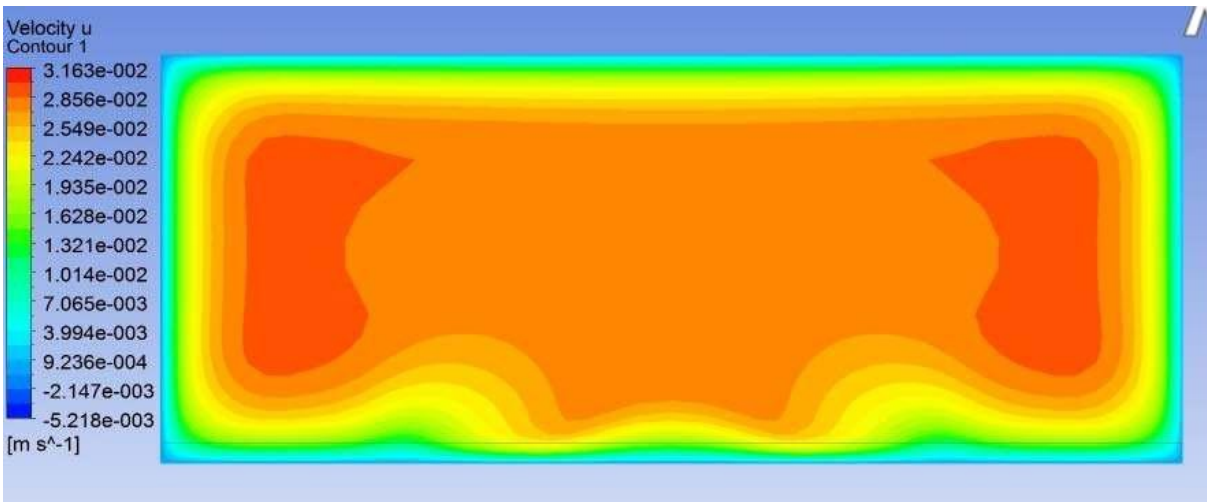

Fig. 5.93 Contours **of u velocity, Re 2400, β = 45°** (yz plane, x=50cm)

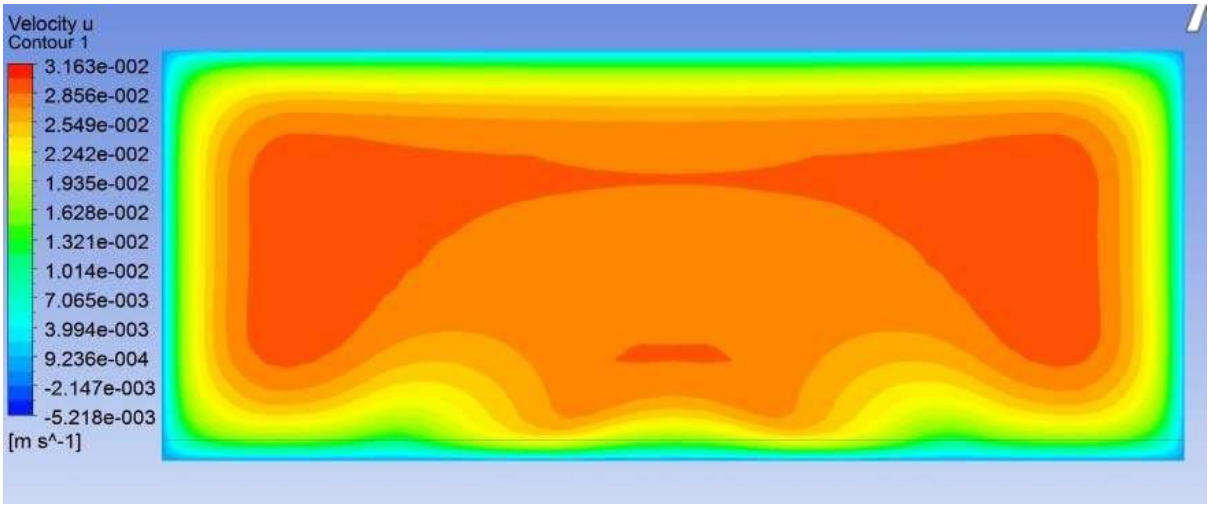

Fig. 5.94 Contours **of u velocity, Re 2400, β = 45°** (yz plane, x=55cm)

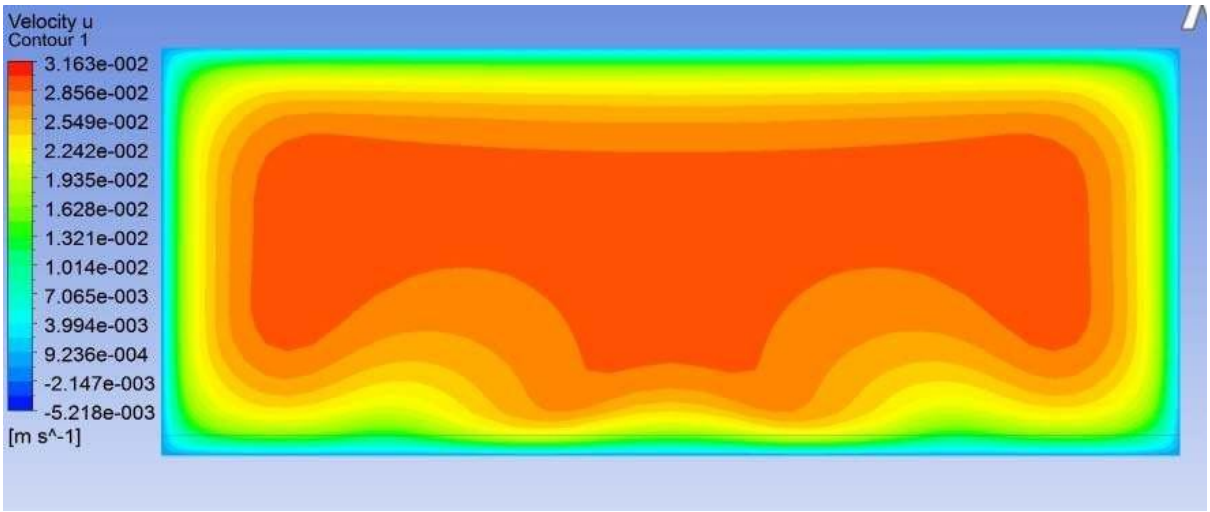

Fig. 5.95 Contours **of u velocity, Re 2400, β = 45°** (yz plane, x=65cm)

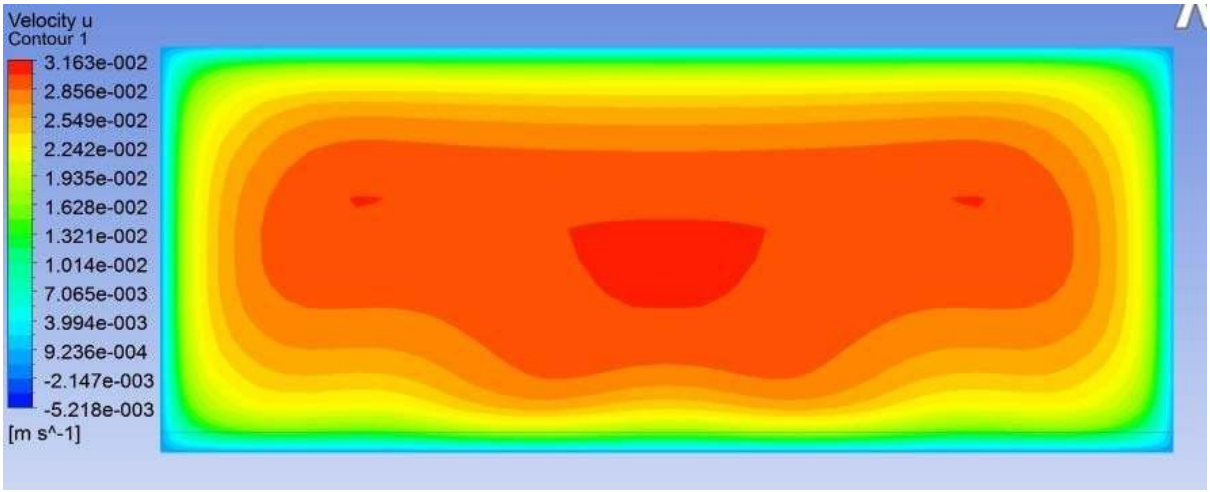

Fig. 5.96 Contours **of u velocity, Re 2400, β = 45°** (yz plane, x=100cm)

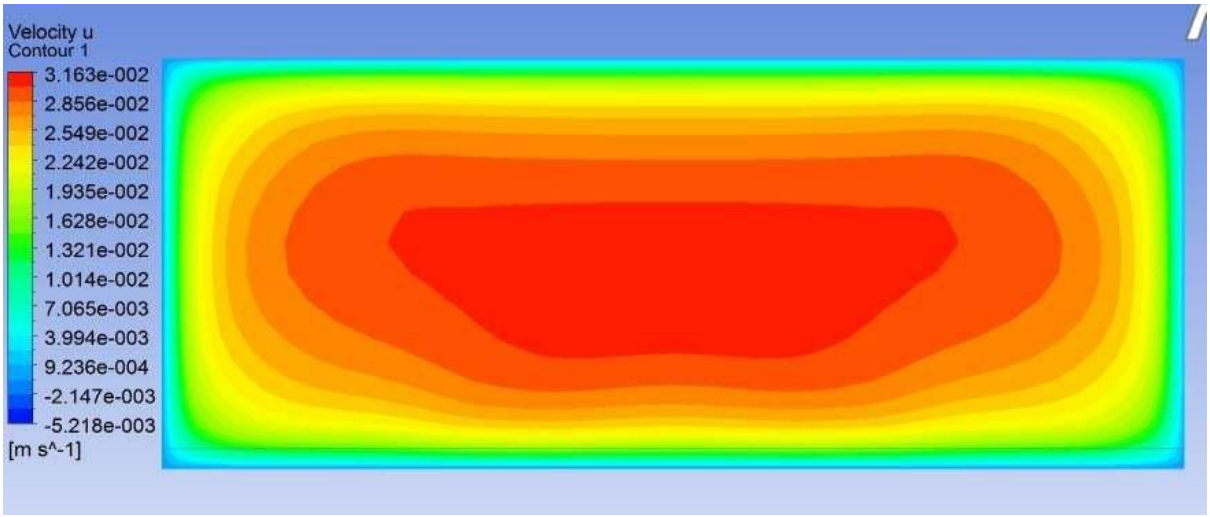

Fig. 5.97 Contours **of u velocity, Re 2400, β = 45°** (yz plane, x=140cm)

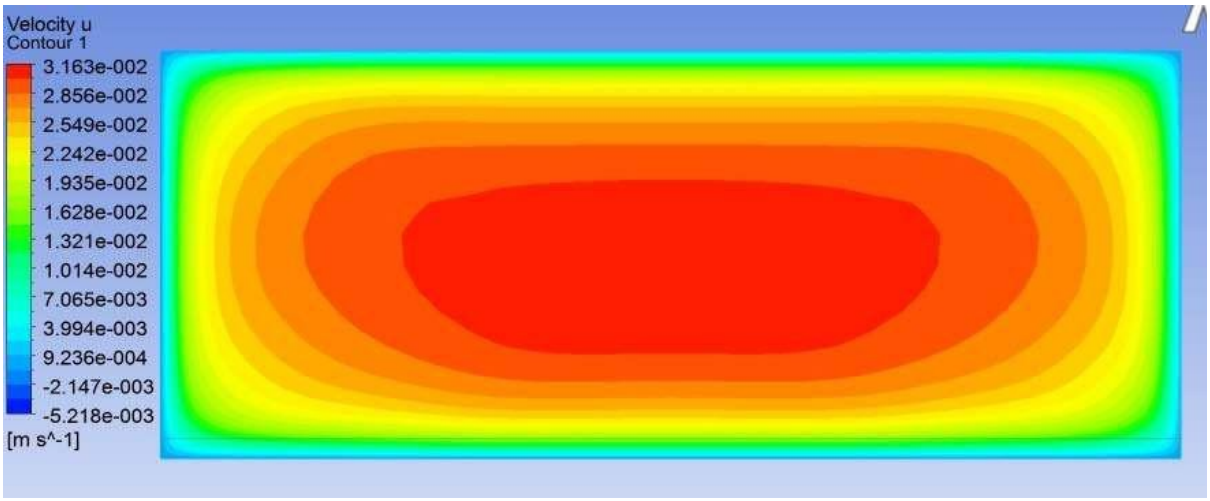

Fig. 5.98 Contours **of u velocity, Re 2400, β** = 45° (yz plane, x=180 cm)

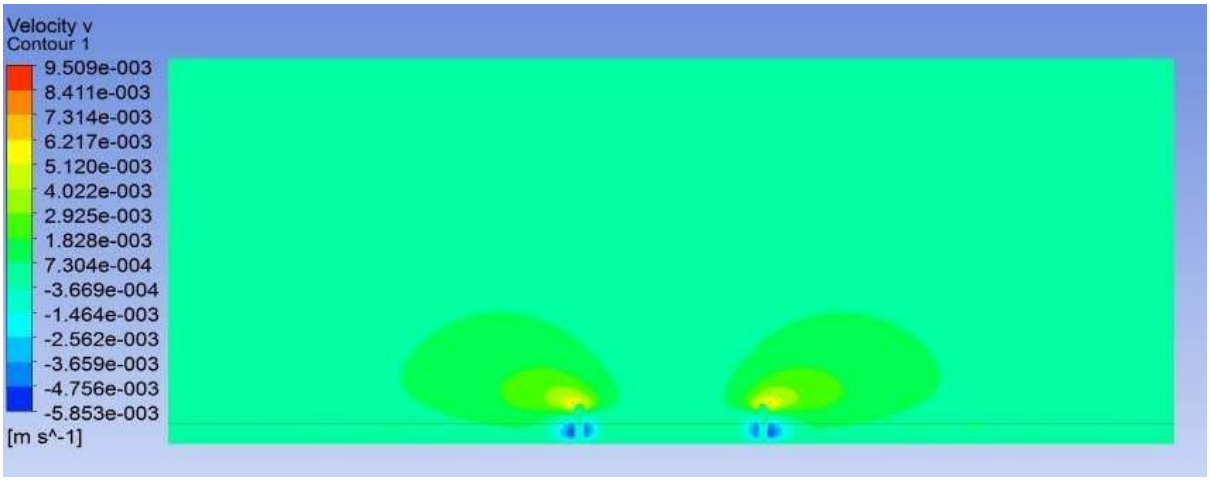

5.99 Contours **of v velocity, Re 2400, β** = 45° (yz plane, x=30 cm)

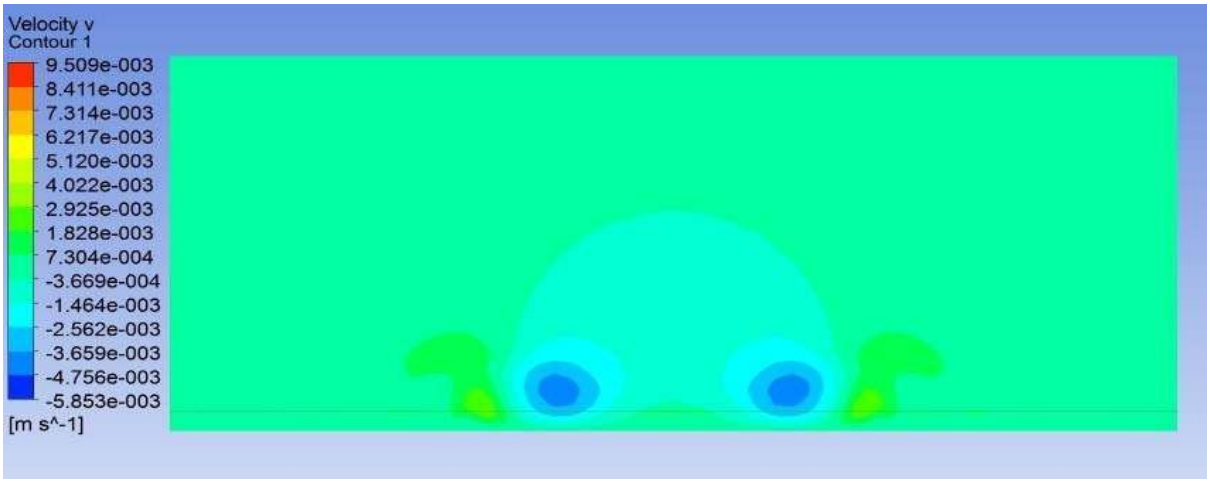

5.100 Contours **of v velocity, Re 2400, β** = 45° (yz plane, x=35 cm)

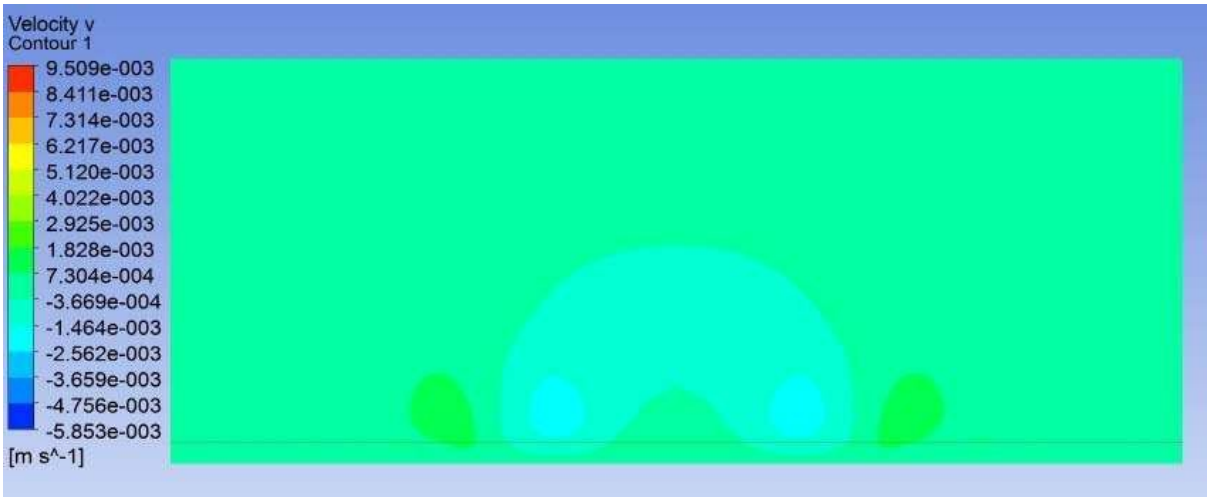

5.101 Contours **of v velocity, Re 2400, β** = 45° (yz plane, x=40 cm)

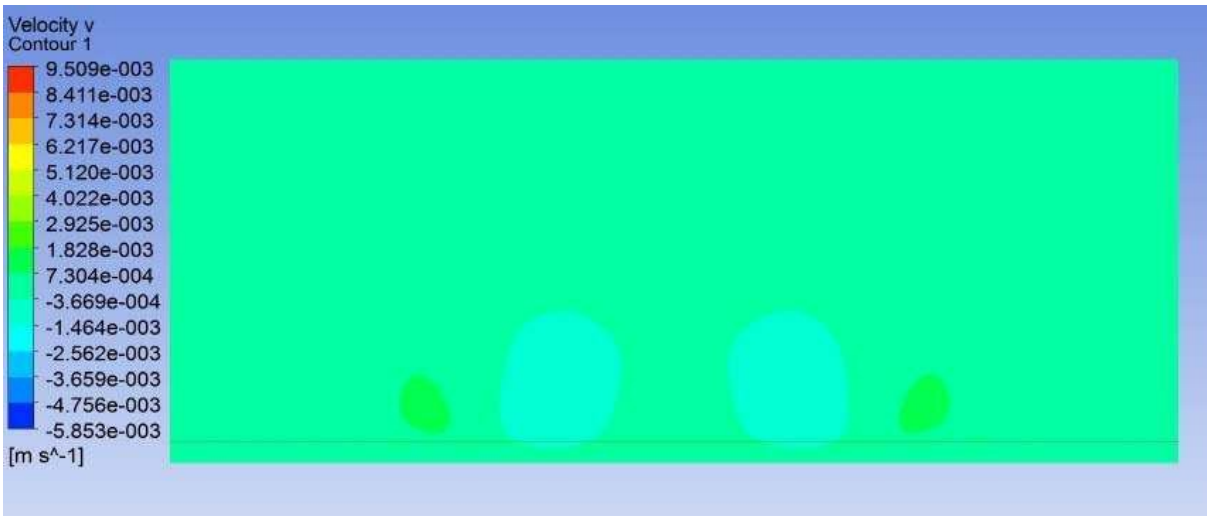

5.102 **Contour of v velocity, Re 2400, β** = 45° (yz plane, x=45 cm)

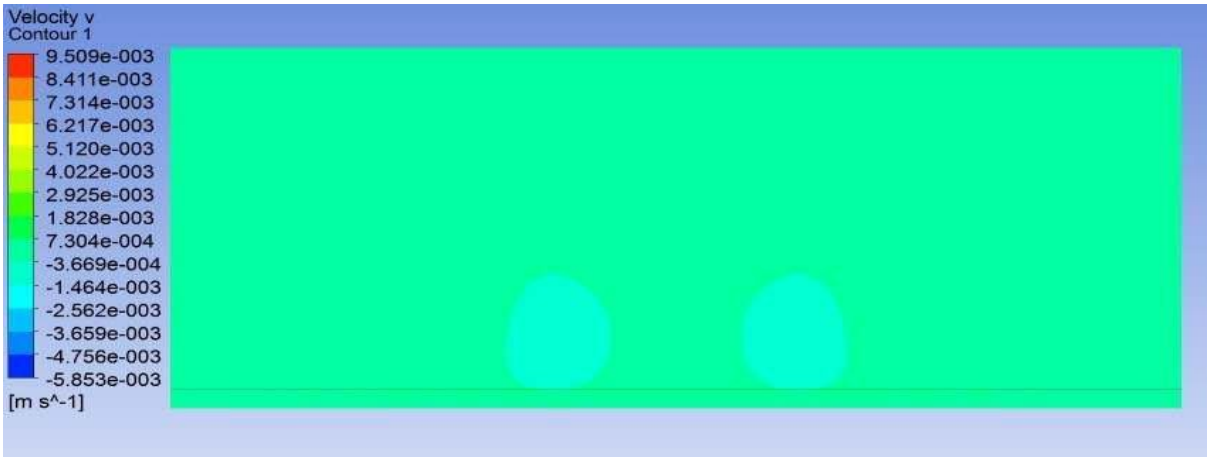

5.103 Contours **of v velocity, Re 2400, β** = 45° (yz plane, x=50 cm)

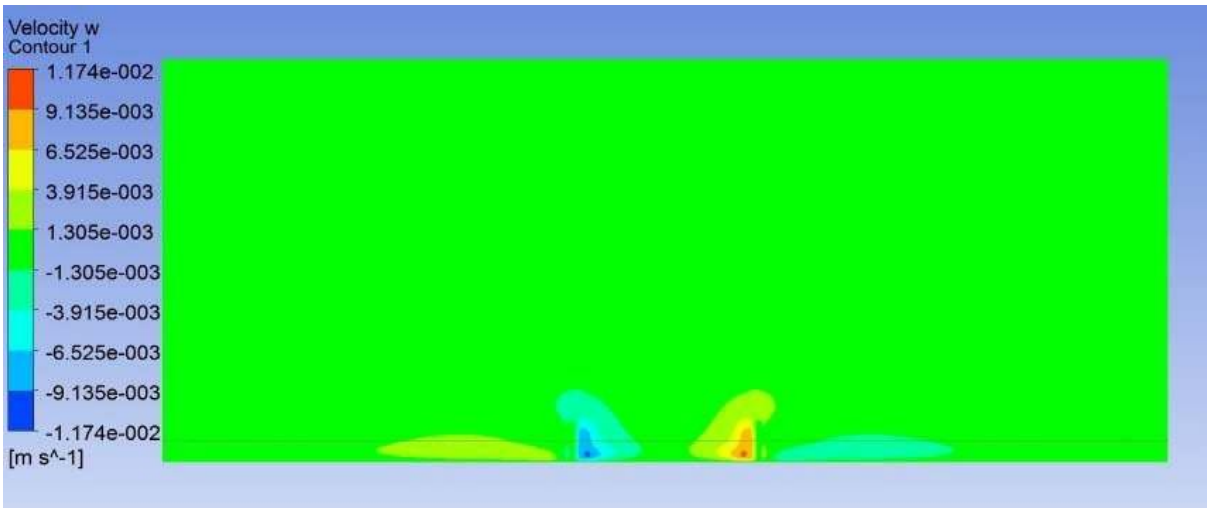

5.104 Contours **of w velocity, Re 2400, β** = 45° (yz plane, x=30 cm)

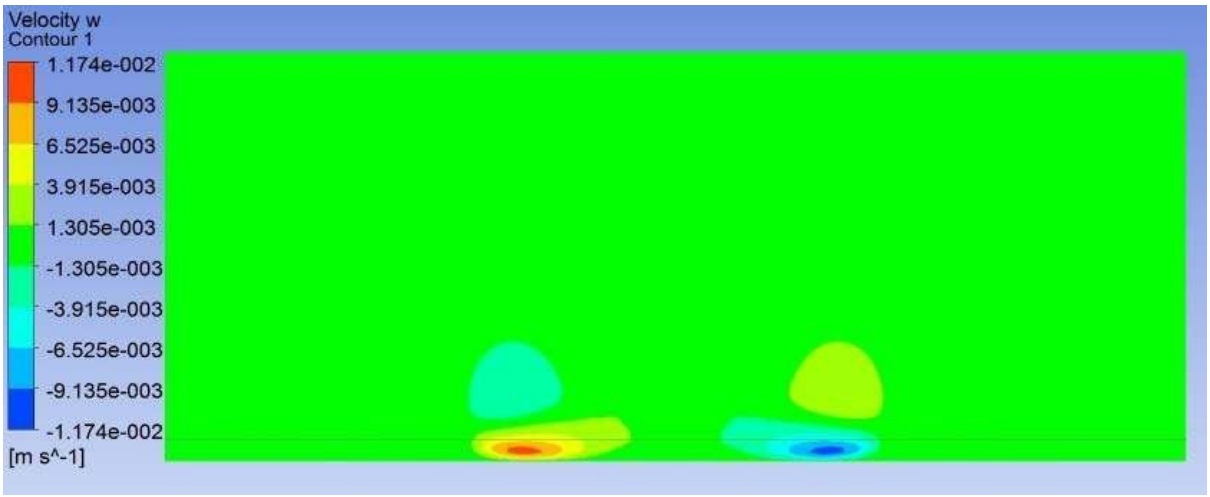

5.105 Contours **of w velocity, Re 2400, β** = 45° (yz plane, x=50 cm)

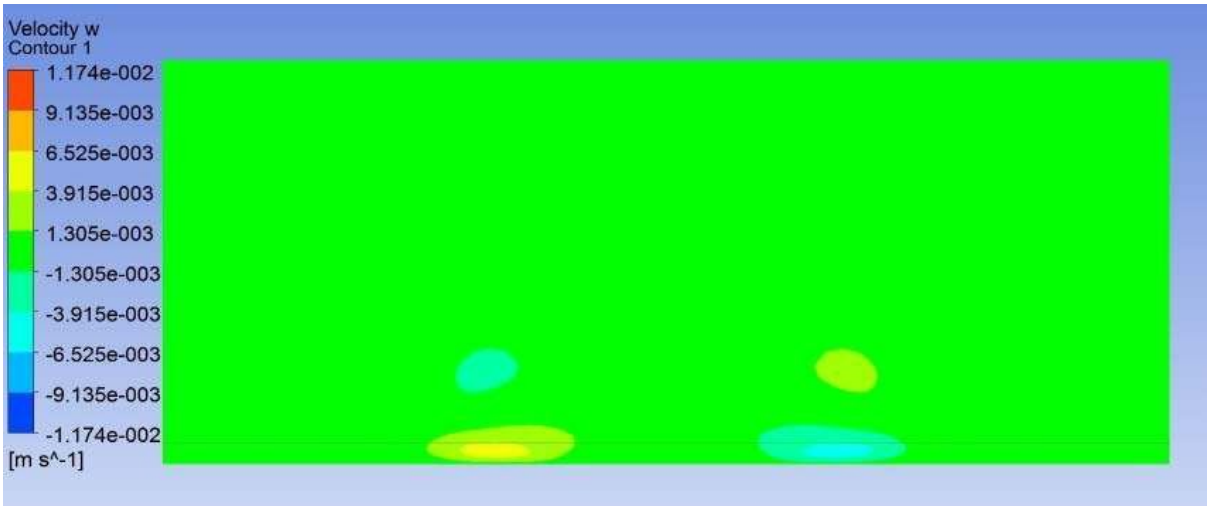

5.106 Contours **of w velocity, Re 2400, β** = 45° (yz plane, x=40 cm)

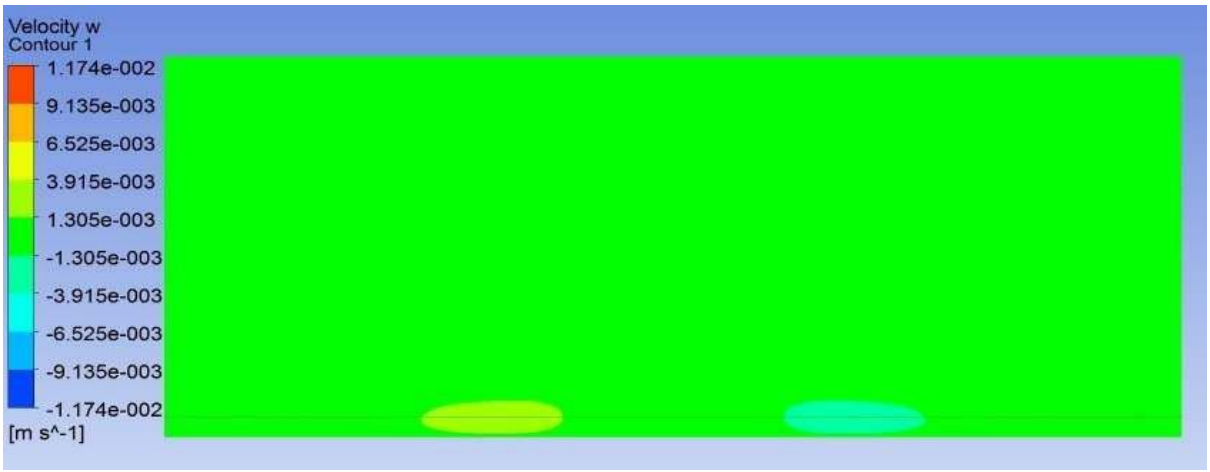

5.107 Contours **of w velocity, Re 2400, β** = 45° (yz plane, x=45cm)

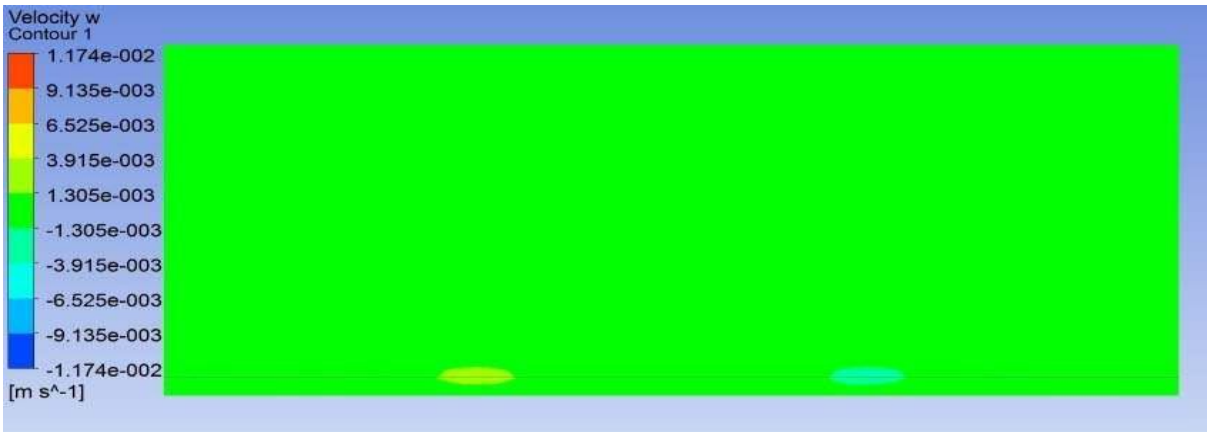

5.108 Contours **of w velocity, Re 2400, β** = 45° (yz plane, x=50 cm)

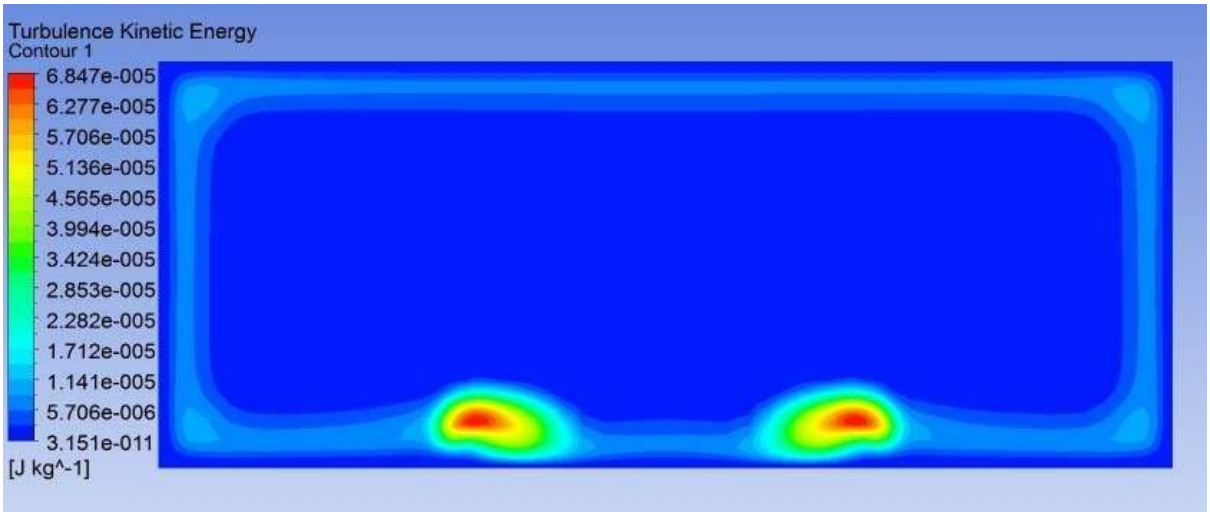

5.109 Contours of turbulent kinetic energy, Re 2400**, β** = 45° (yz plane, x=35 cm)

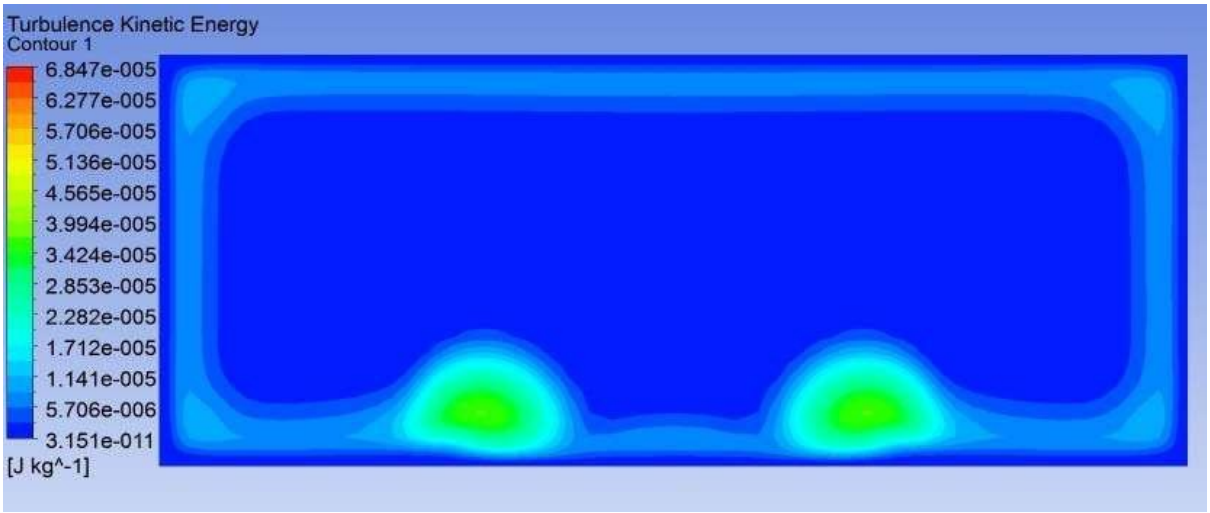

5.110 Contours of turbulent kinetic energy, Re 2400**, β = 45 °(yz plane, x**=40 cm)

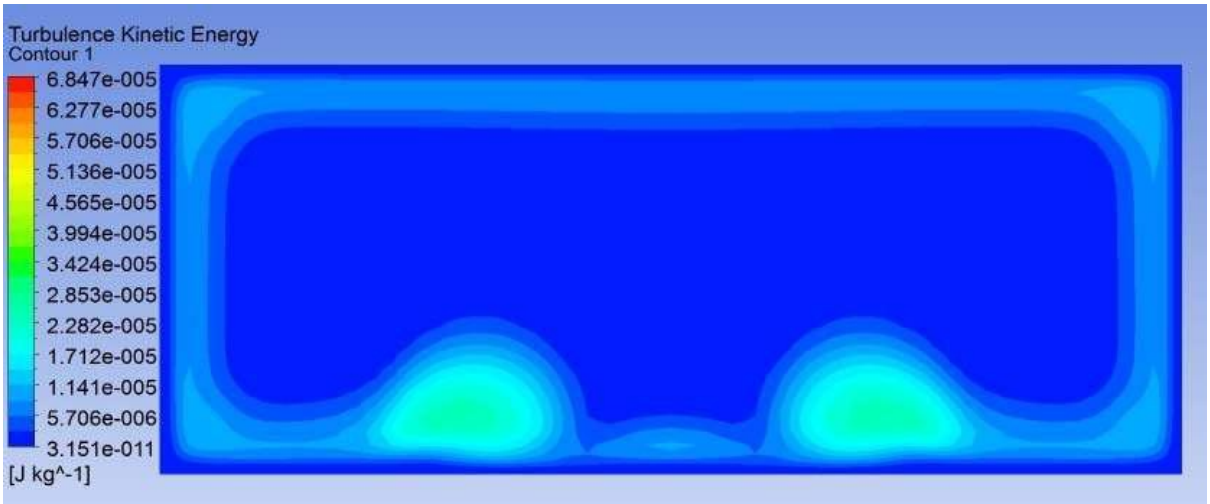

5.111 Contours of turbulent kinetic energy, Re 2400**, β = 45 °(yz plane, x**=45 cm)

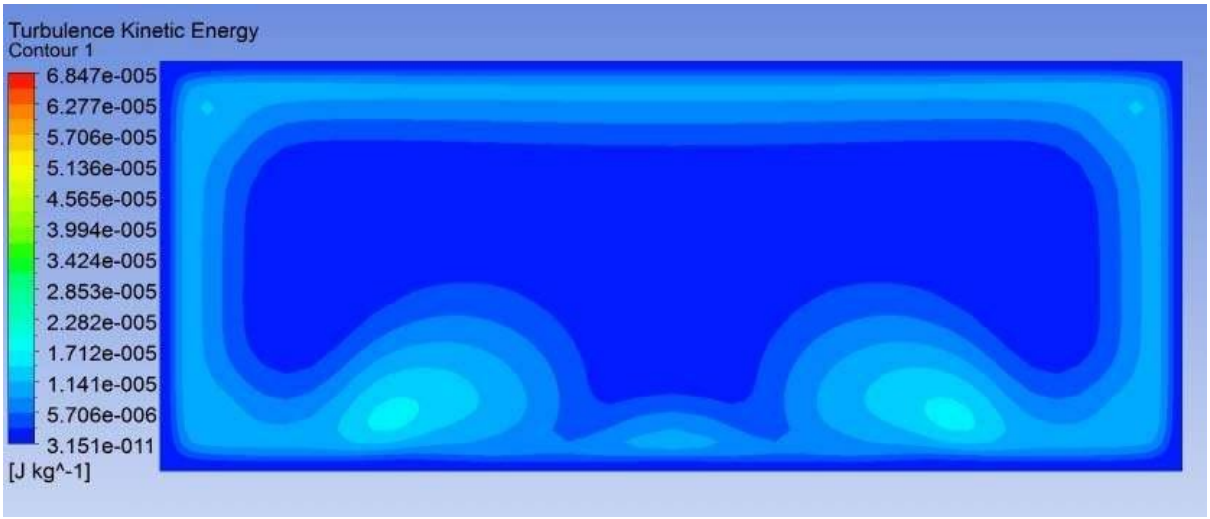

5.112 Contours of turbulent kinetic energy, Re 2400**, β = 45 °(yz plane, x**=60 cm)

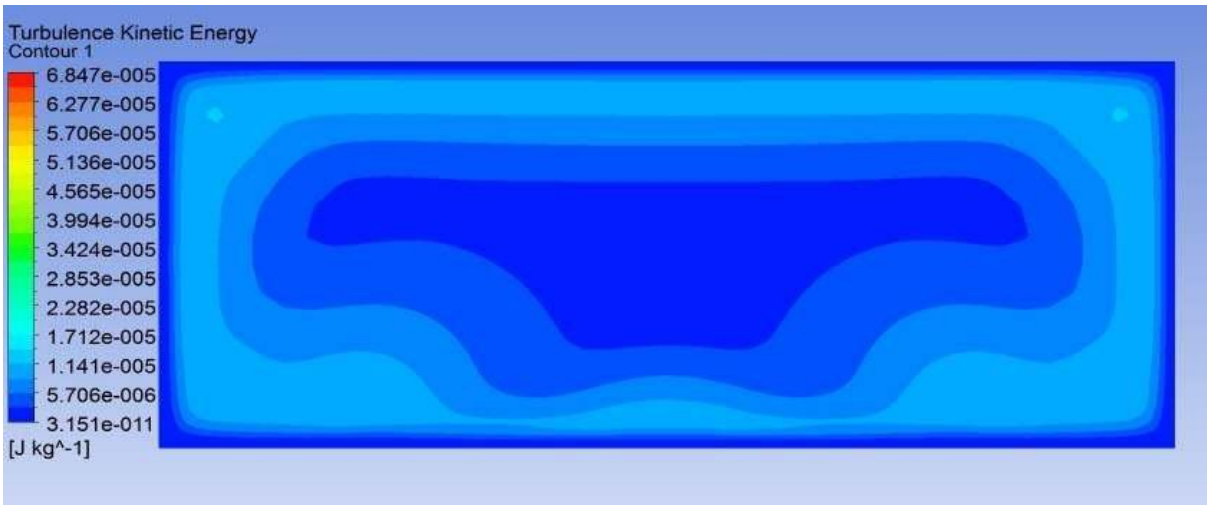

5.113 Contours of turbulent kinetic energy, Re 2400**, β = 45 °(yz plane, x**=100 cm)

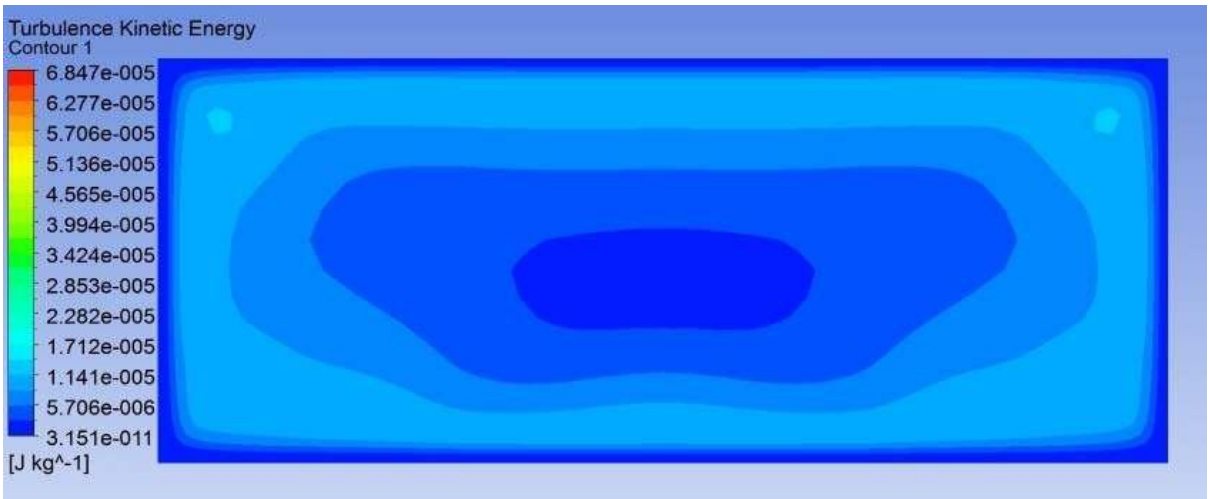

5.114 Contours of turbulent kinetic energy, Re 2400**, β = 45 °(yz plane, x**=140 cm)

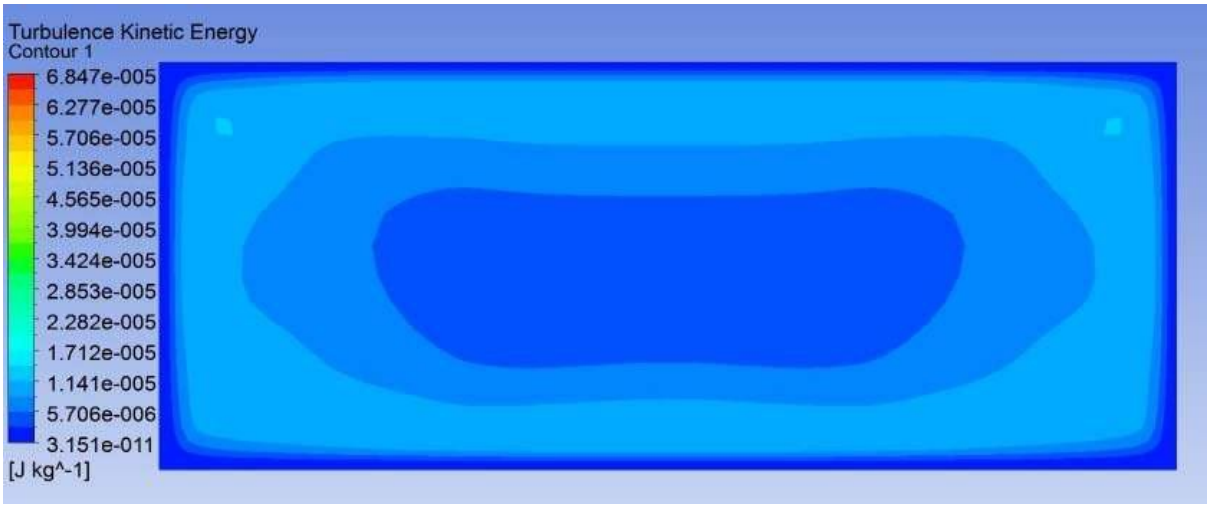

5.115 Contours of turbulent kinetic energy, Re 2400**, β = 45 °(yz plane, x**=180 cm)

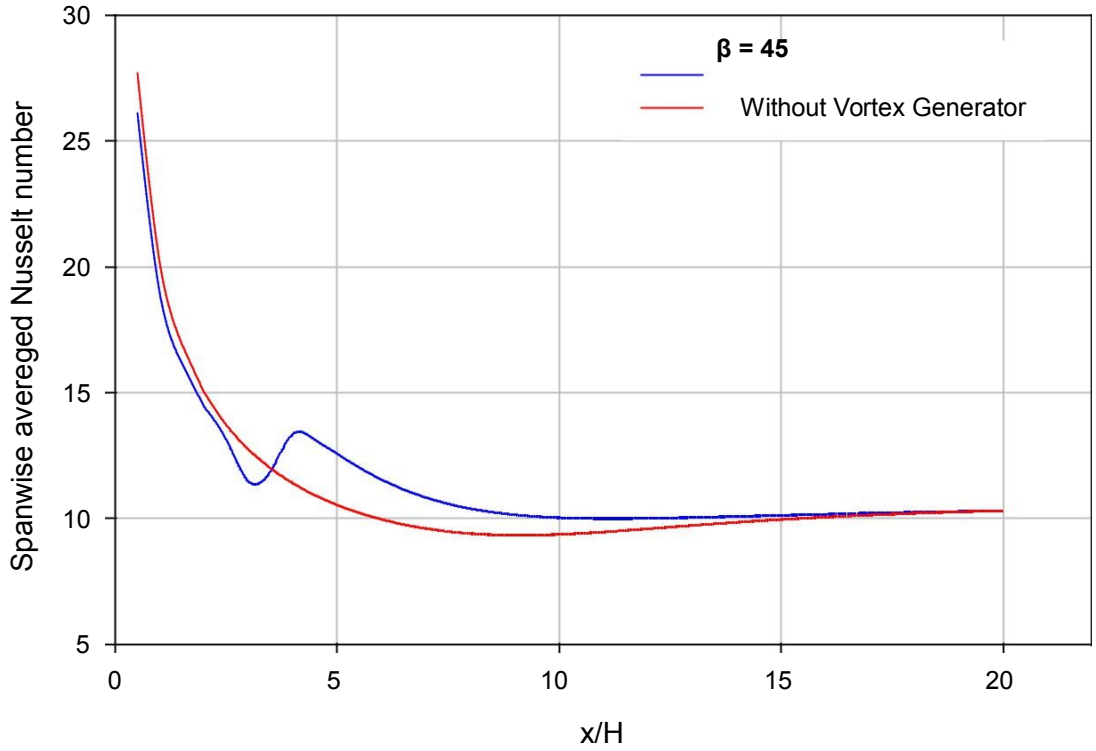

Fig 5.116 Variation of spanwise Nusselt number at Re 800

With 45° blade angle a large increase in performance was found compared to the cases of 15° and 30°. The increase strength of the vortex generated is a ble to hold its strength to a larger distance along x direction. As we look on the fig 5.116 to fig. 5.19, the plots show that there is very larger effect near the region of the vortex generators. With increase in the Reynolds

no. this effect increase and also with increase in Reynolds no. the increase in span wise averaged Nusselt no was observed to be to a greater distance along the flow direction in the channel.

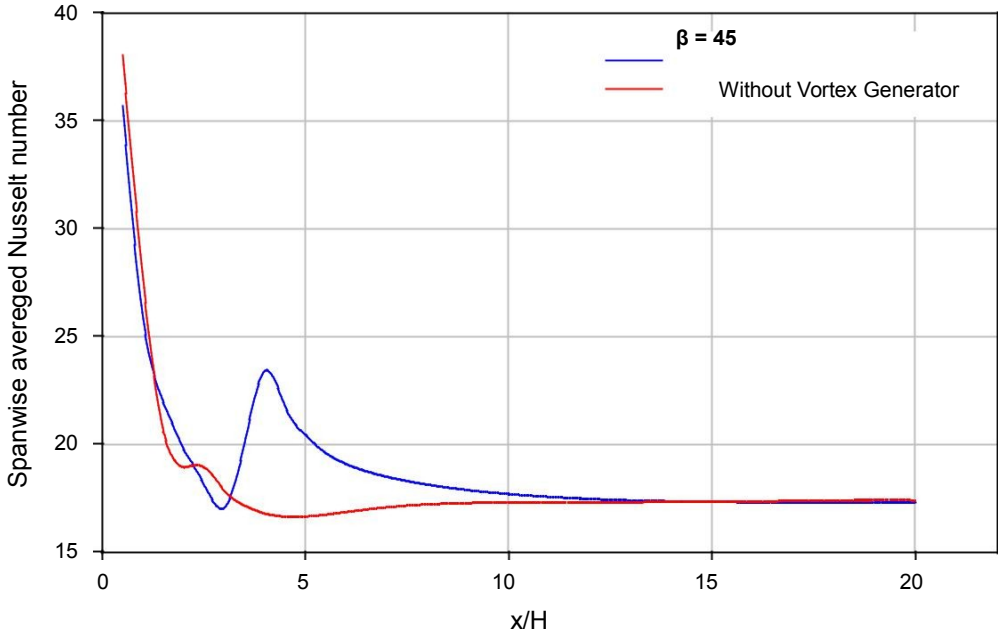

Fig 5.117 Variation of spanwise Nusselt number at Re 1600

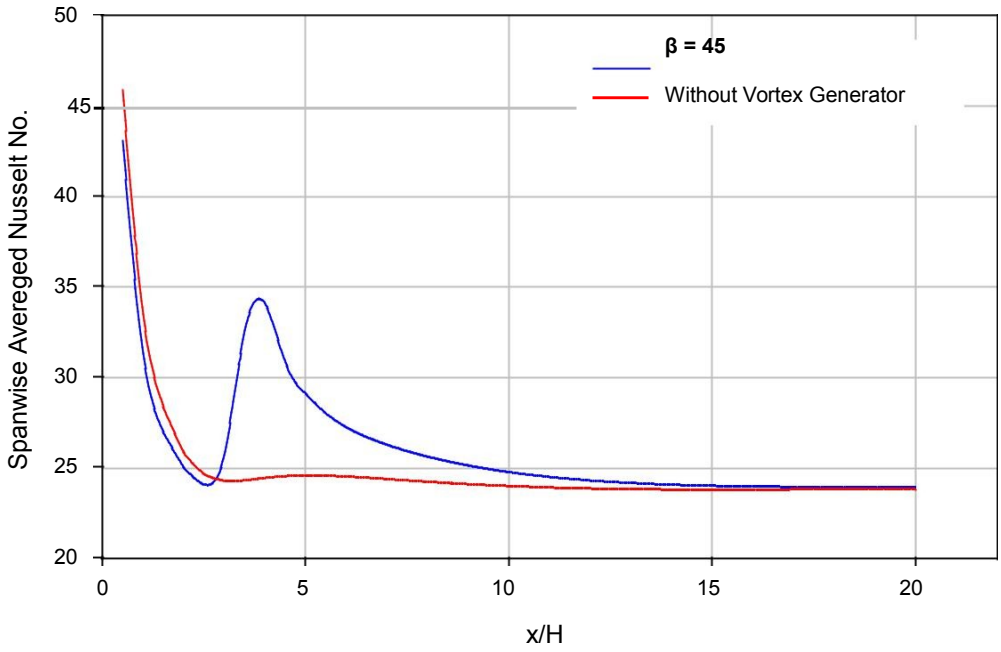

Fig 5.118 Variation of Spanwise Nusselt No. at Re 2400

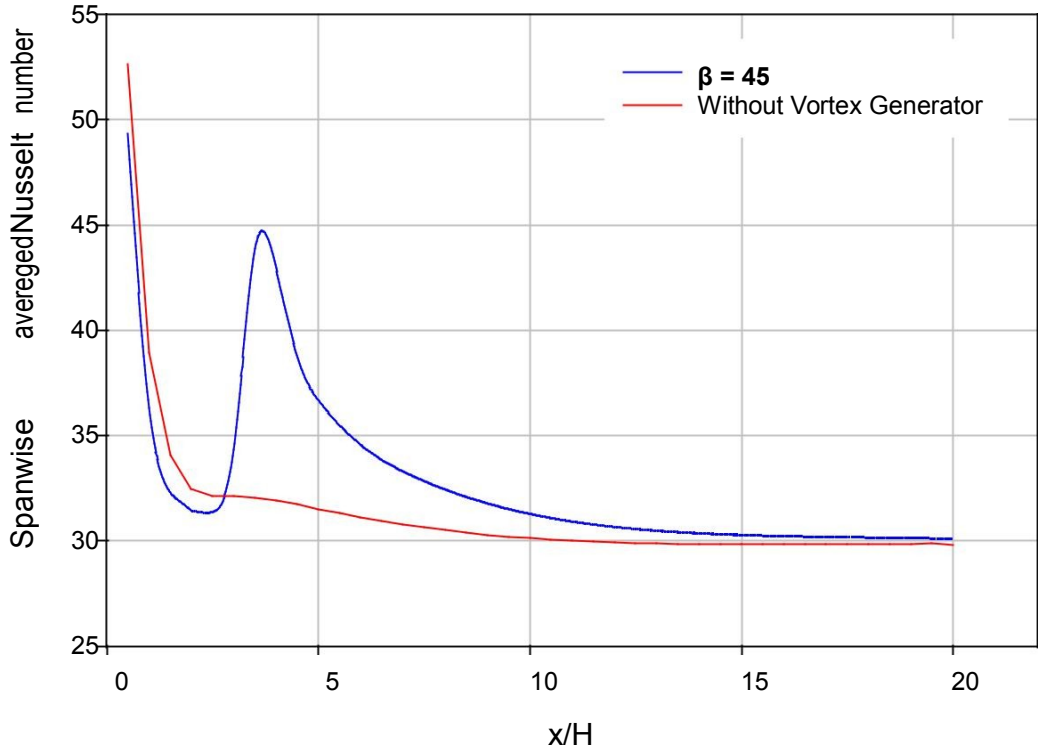

Fig 5.119 Variation of spanwise Nusselt number at Re 3200

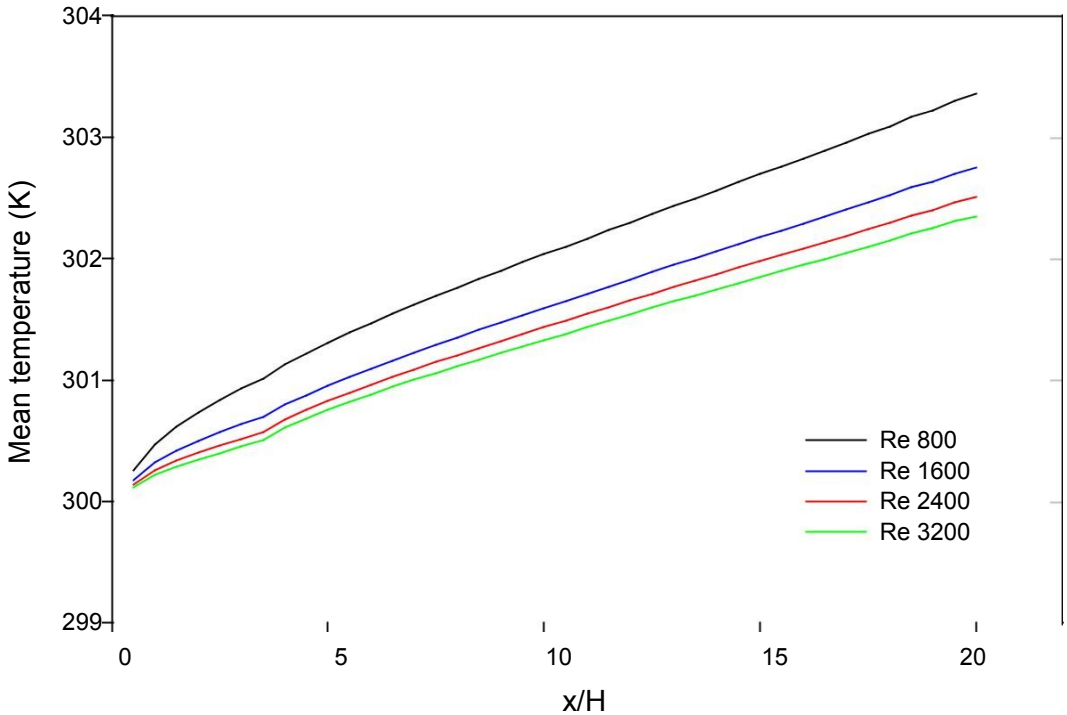

Fig. 5.120 Variation of mean temperature, **β = 45**

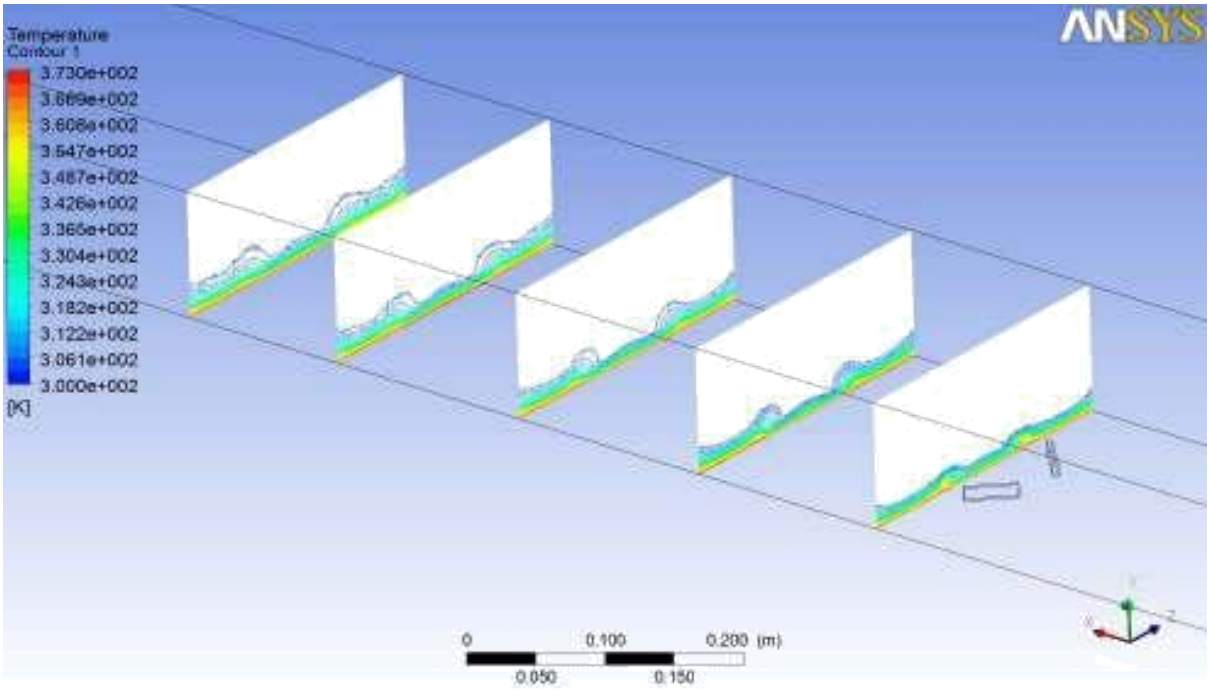

Fig. 5.121 Contours of temperature distribution at Re 800

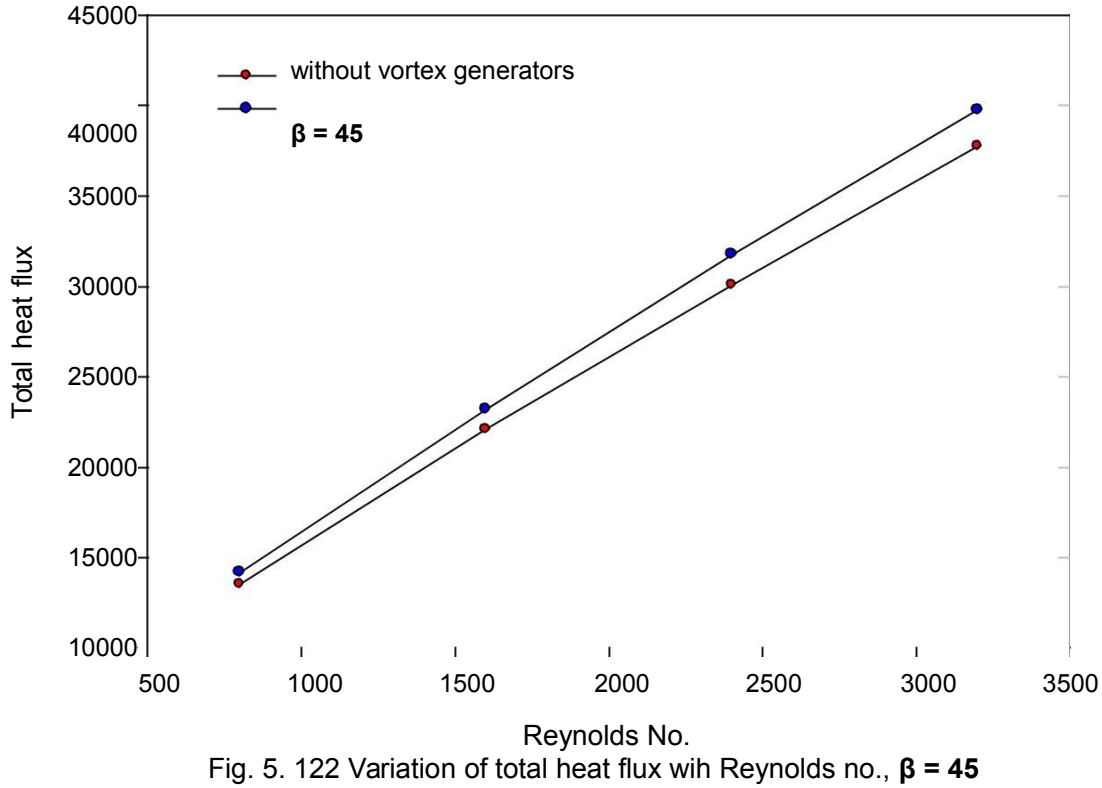

Fig. 5. 122 Variation of total heat flux wih Reynolds no., **β = 45**

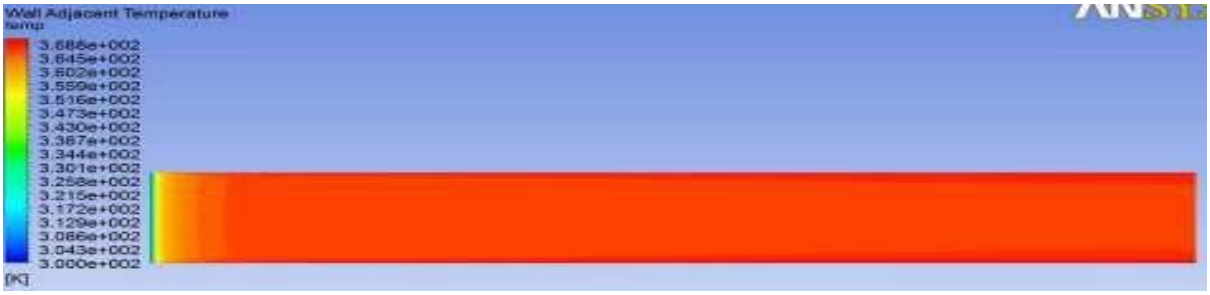

Fig. 5.123 Contours of wall adjacent temperature at Re 2400, without vortex generators

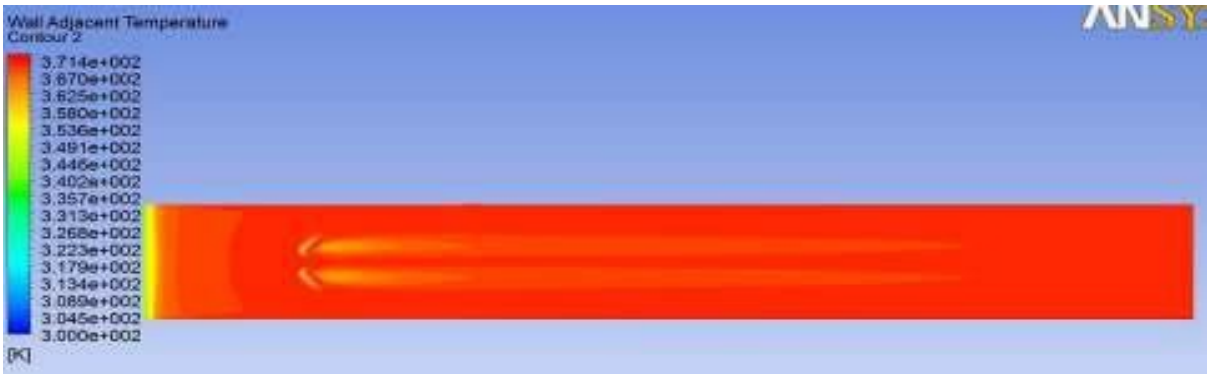

Fig. 5.124 **Contour of wall adjacent temperature at Re 2400, β = 45°**

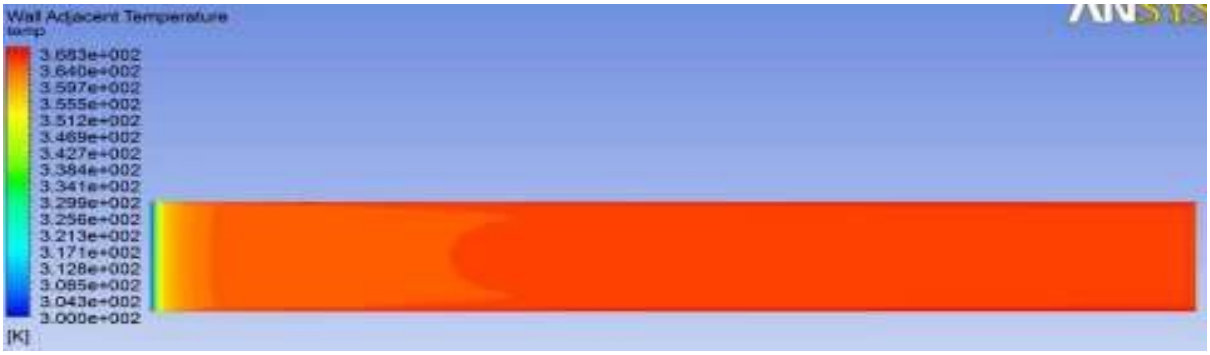

Fig. 5.125 Contours of wall adjacent temperature at Re 3200, without vortex generators

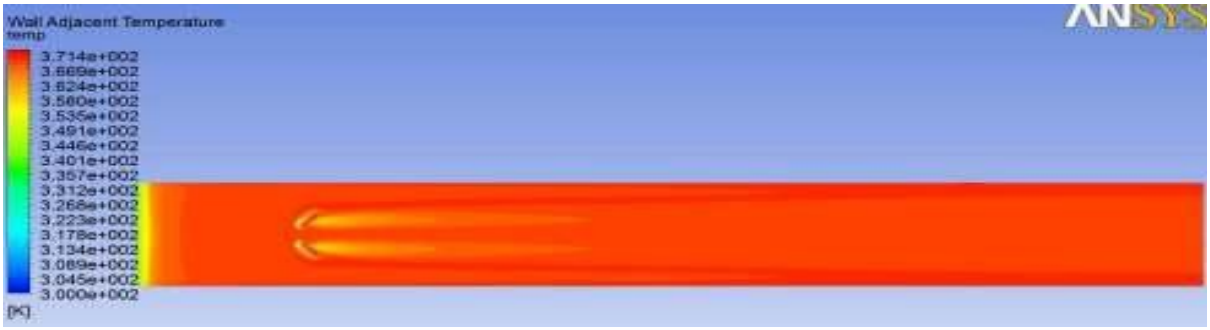

Fig. 5.126 Contours **of wall adjacent temperature at Re 3200, β = 45°**

5.4 Comparison between previous work and present work

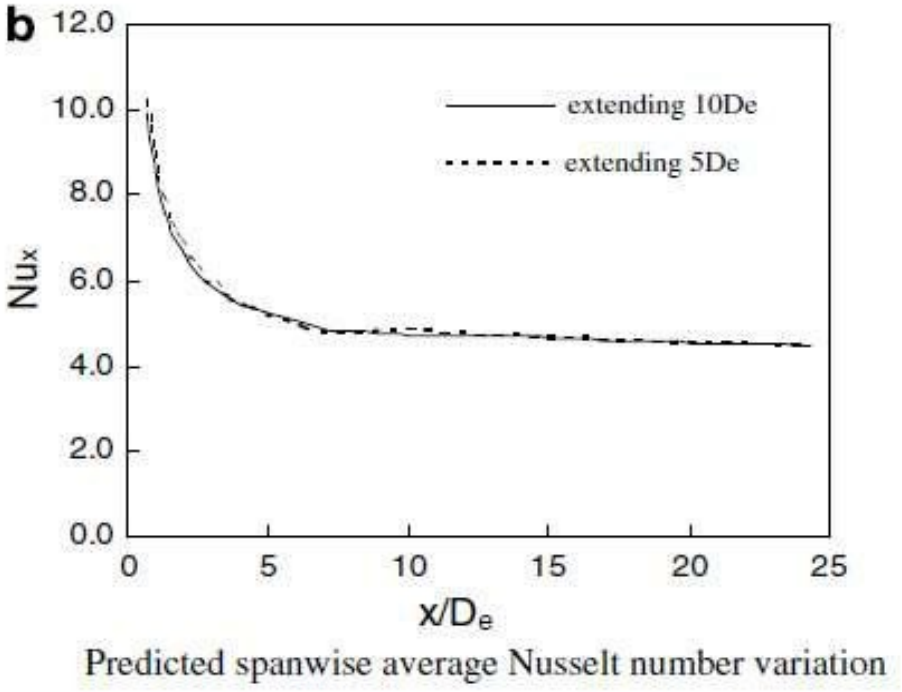

Fig. 5.127 Computational domain of the rectangular duct and the predicted span wise average Nusselt number variation (Wua and Tao [2005])

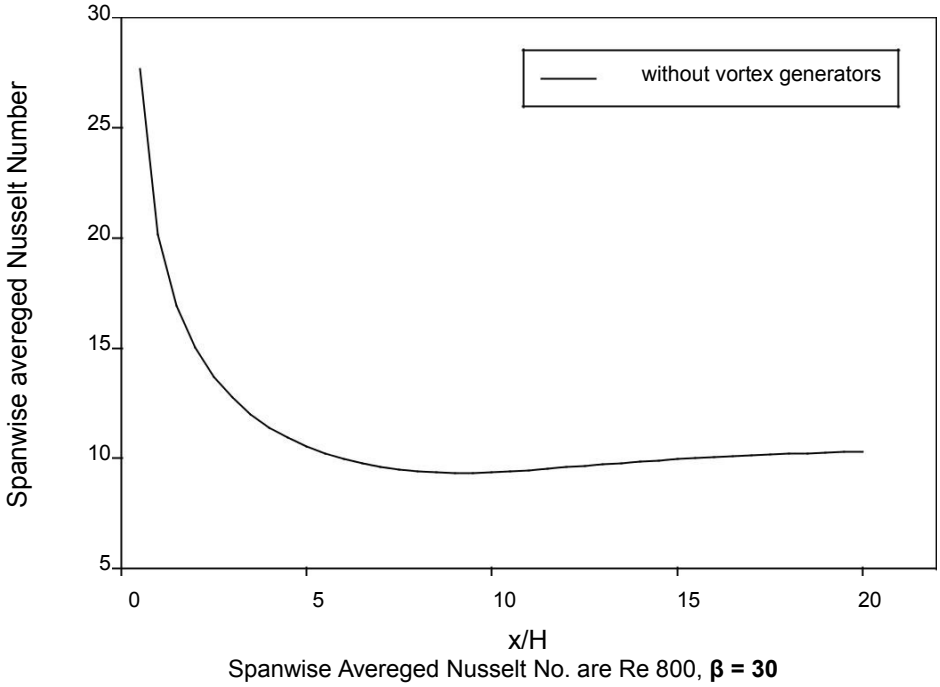

Fig. 5.128 Present work (performed with k ε **model)**

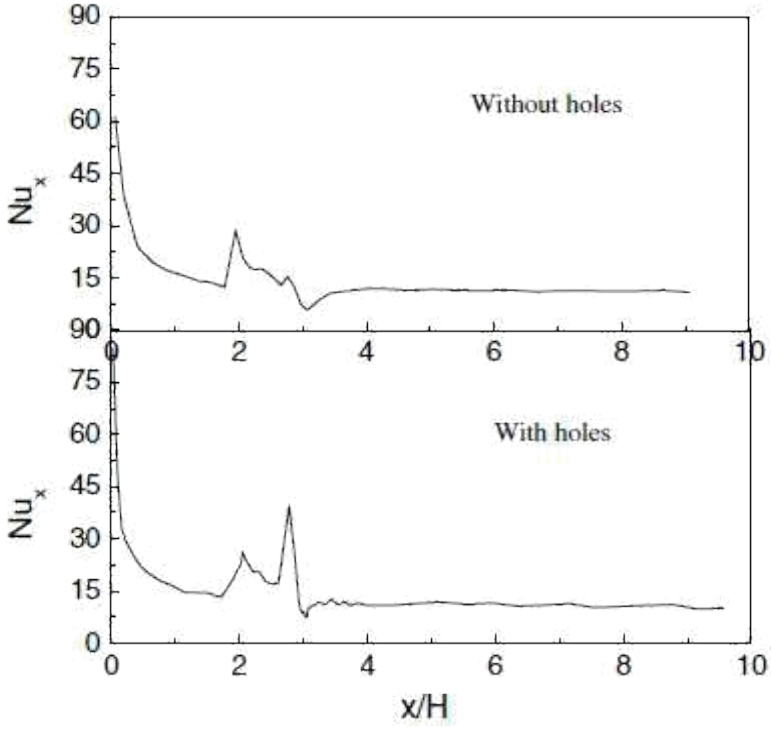

Fig. 5. 129 Effect of vortex generators on the Nusselt number. (Wua and Tao [2005])

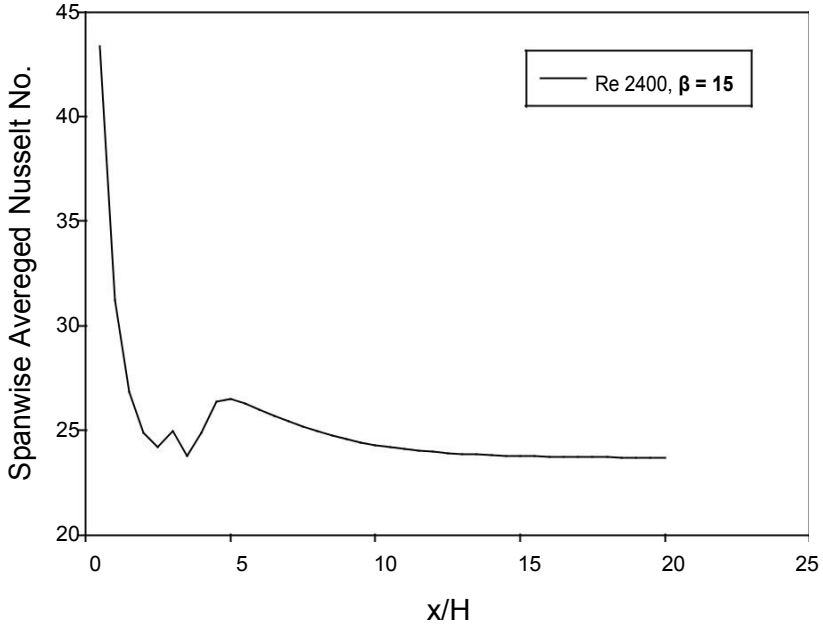

Variation of Spanwise Avereged Nusselt No. at Reynold No. 1600

Fig. 5.130 Present work of without holes in the vortex generators

Fig 5.127 - fig.5.128 and fig. 5.128 - fig. 5.129 show the comparison between the previous work **(Wua and Tao [2005**]) and the present work. The curve trend is observed same. The difference between the values of Nusselt number is due to difference in the channel and vortex generators dimensions.

Table below shows the improvement of heat flux (in percentage) from the bottom wall by the use of vortex generators.

Table 5.1

Reynolds No.	**β = 15°**	**β = 30°**	**β = 45°**
800	1.67	4.48	4.74
1600	2.54	4.45	5.07
2400	2.63	4.70	5.58
3200	2.25	4.40	5.36

Chapter 6

Conclusions and scope for future work

6.1 Conclusions

In this study of augmentation of heat transfer in a rectangular channel with rectangular vortex generators was evaluated. The span wise averaged Nusselt no., mean temperature and total heat flux were compared with and without vortex generators in the channel at blade angle 15°, 30°, and 45° for Reynolds no. of 800, 1600, 2400, and 3200 respectively.

1) The use of vortex generators increases the span wise averaged Nusselt no. than the case of without vortex generators considerably.
2) With increase in the blade angle (15°, 30° and 45°) the span wise averaged Nusselt no. shows an increase at particular Reynolds number.
3) At particular angle, by increasing the Reynolds no. the overall performance increases and span wise averaged Nusselt no. was found to be greater at particular location for larger Reynolds number.
4) The mean temperature of the bulk fluid at particular location in the flow direction was increased by the use of vortex generators.
5) The total heat flux from the bottom wall with vortex generators was found to be greater than the case of without vortex generators [table 5-1]. Also this difference increases with increase in Reynolds number.

6.2 Scope for the future work

Future recommendation based on this study using vortex generator for heat transfer enhancement, a great deal of work can be done in the future. Average surface Nusselt number and to improve the performance enhancement factor, few ways are :

1) The effect of placing more than one pair of vortex generators i. e. an array of VGs along the flow direction at particular distance between them can be studied.
2) The effect of varying the height of the vortex generators on the heat transfer can be studied.
3) Other shapes of vortex generators (triangular, trapezoidal etc.) can be studied.

References

Gentry, M., and Jacobi, A., 1997, "Heat Transfer Enhancement by Delta-Wing Vortex Generators on a Flat Plate: Vortex Interactions with the Boundary Layer," Experimental Thermal and Fluid Science, 14(3) pp. 231-242

M. Fiebig, Vortices and heat transfer, Zeit. Angew. Math. Mech. 77 (1) (1997) 3–18

C.C. Wang, Technical review – a survey of recent patents of fin-andtube heat exchangers, J. Enhanced Heat Transfer 7 (5) (2000) 333– 345.

Anderson, J.D., 2001, "Fundamentals of aerodynamics," McGraw-Hill New York.

Mahmood, G., Hill, M., Nelson, D., 2001, "Local Heat Transfer and Flow Structure on and Above a Dimpled Surface in a Channel," Journal of Turbomachinery, 123(1) pp. 115-123.

J.M. Wua, W.Q. Tao., 2005 Numerical study on laminar convection heat transfer in a rectangular channel with longitudinal vortex generator. Part A: Verification of field synergy principle

Zhu, J., Fiebig, M., and Mitra, N., 1995, "Numerical Investigation of Turbulent Flows and Heat Transfer in a Rib-Roughened Channel with Longitudinal Vortex Generators," International Journal of Heat and Mass Transfer, 38(3) pp. 495-501.

Deb, P., Biswas, G., and Mitra, N., 1995, "Heat Transfer and Flow Structure in Laminar and Turbulent Flows in a Rectangular Channel with Longitudinal Vortices," International Journal of Heat and Mass Transfer, 38(13) pp. 2427-2444.

Kakaç, S., Bergles, A.E., Mayinger, F., 1999, "Heat transfer enhancement of heat exchangers," Springer,.